TBMCE2023

6th International Conference on
Technologies & Business Models for Circular Economy

Conference Proceedings

Sanja POTRČ Miloš BOGATAJ Zdravko KRAVANJA Zorka NOVAK PINTARIČ
EDITORS

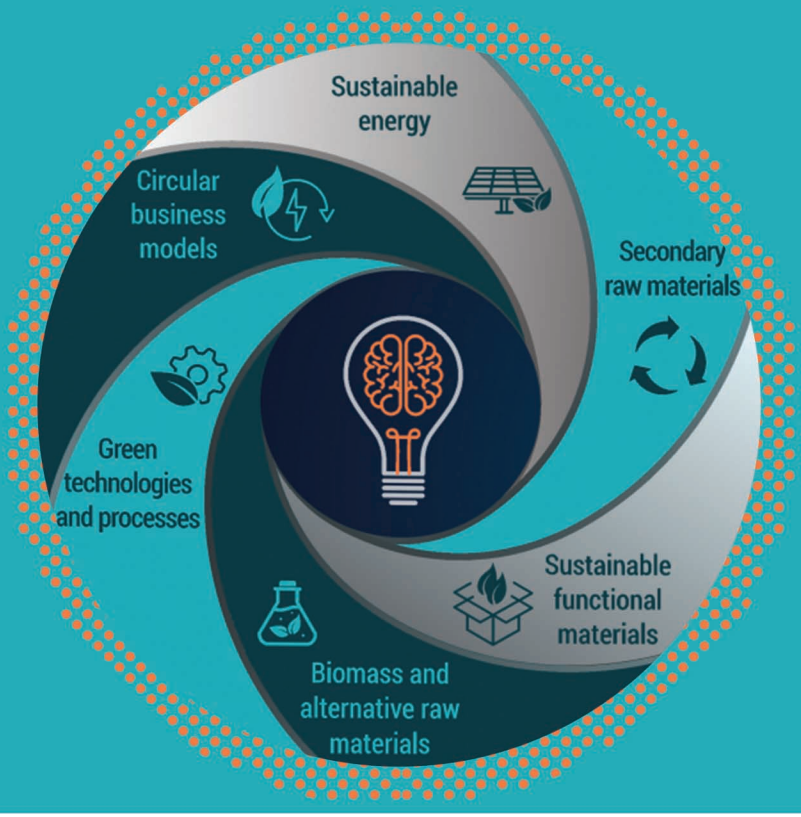

University of Maribor Press

University of Maribor

Faculty of Chemistry and Chemical Engineering

6th International Conference on Technologies & Business Models for Circular Economy

Conference Proceedings

Editors

Sanja Potrč

Miloš Bogataj

Zdravko Kravanja

Zorka Novak Pintarič

February 2024

Title
Naslov
6th International Conference on Technologies & Business Models for Circular Economy

Subtitle
Podnaslov
Conference Proceedings

Editors
Uredniki
Sanja Potrč
(University of Maribor, Faculty of Chemistry and Chemical Engineering)

Miloš Bogataj
(University of Maribor, Faculty of Chemistry and Chemical Engineering)

Zdravko Kravanja
(University of Maribor, Faculty of Chemistry and Chemical Engineering)

Zorka Novak Pintarič
(University of Maribor, Faculty of Chemistry and Chemical Engineering)

Technical editor
Tehnični urednik
Jan Perša
(University of Maribor, University Press)

Cover designer
Oblikovanje ovitka
Jan Perša
(University of Maribor, University Press)

Graphic material
Grafične priloge
Authors of proceedings & editors

Conference
Konferenca
TBMCE, International Conference on Technologies & Business Models for Circular Economy

Date and location
Datum in kraj
September 6th to September 8th 2023, Portorož, Slovenia

Likozar (National Institute of Chemistry, Slovenia), Primož Oven (University of Ljubljana, Slovenia), Dragica Marinič (Slovenian national building and civil engineering institute, Slovenia), Vilma Ducman (Slovenian national building and civil engineering institute, Slovenia).

Published by / *Založnik*
University of Maribor
University Press
Slomškov trg 15, 2000 Maribor, Slovenija
https://press.um.si, zalozba@um.si

Issued by / *Izdajatelj*
University of Maribor
Faculty of Chemistry and Chemical Engineering
Smetanova ulica 17, 2000 Maribor, Slovenija
https://www.fkkt.um.si/, fkkt@um.si

Publication type / *Vrsta publikacije*
E-book

Edition / *Izdaja*
1st

Available at / *Dostopno na*
http://press.um.si/index.php/ump/catalog/book/853

Published at / *Izdano*
Maribor, February 2024

REPUBLIC OF SLOVENIA
MINISTRY OF THE ECONOMY, TOURISM AND SPORT

REPUBLIC OF SLOVENIA
MINISTRY OF COHESION AND REGIONAL DEVELOPMENT

The event was held under the patronage of the Ministry of the Economy, Tourism and Sport and Ministry of Cohesion and Regional Development of the Republic of Slovenia.

Partner country: Netherlands

Netherlands

AVL

CINKARNA

dem
Dravske elektrarne Maribor

Skupina hse

MEREL

KEMOMED
PRINAŠAMO REŠITVE

HELIOS

bia
TRUSTED LAB PARTNER

Gospodarska zbornica Slovenije
Združenje kemijske industrije

Saubermacher Slovenija

CIP - Kataložni zapis o publikaciji
Univerzitetna knjižnica Maribor

331:502.131.1(082)(0.034.2)

INTERNATIONAL Conference on Technologies & Business Models for Circular Economy (6 ; 2023 ; Portorož)
6th International Conference on Technologies & Business Models for Circular Economy [Elektronski vir] : conference proceedings / editors Sanja Potrč ... [et al.]. - 1st ed. - E-publikacija. - Maribor : University of Maribor, University Press, 2024

Način dostopa (URL): https://press.um.si/index.php/ump/catalog/book/853
ISBN 978-961-286-829-1
doi: 10.18690/um.fkkt.1.2024
COBISS.SI-ID 186707203

ISBN 978-961-286-829-1 (pdf)

DOI https://doi.org/10.18690/um.fkkt.1.2024

Price
Cena Free copie

For publisher
Odgovorna oseba založnika Prof. Dr. Zdravko Kačič,
Rector of University of Maribor

Attribution
Citiranje Potrč, S., Bogataj, M., Kravanja, Z., Novak Pintarič, Z., (eds.). (2024). 6th *International Conference on Technologies & Business Models for Circular Economy: Conference Proceedings* Maribor: University Press. doi: 10.18690/um.fkkt.1.2024

Table of Contents

Waste Analysis and Determination of the Average Composition of Municipal Waste With a Focus on the Circular Economy

DOI
https://doi.org/10.18690/um.fkkt.1.2024.1

ISBN
978-961-286-829-1

Jiří Gregor,[1] Jiří Kropáč,[2] Martin Pavlas,[1]
Yee Van Fan[1]

[1] Brno University of Technology, Faculty of Mechanical Engineering, Brno, Czech Republic
Jiri.Gregor@vutbr.cz, pavlas@fme.vutbr.cz, fan@fme.vutbr.cz
[2] Palacký University Olomouc, Faculty of Education, Institute of Education and Social Studies, Olomouc, Czech Republic
jiri.kropac@upol.cz

Waste treatment represents a significant challenge for society and the environment, and its effective management is essential to achieve a sustainable future. This paper focuses on the sorting, analysis and composition of waste in the context of the circular economy, emphasising the established legislative aspects and separation goals in the European Union. The European Union recognises the urgent need to change the linear model of production and consumption to a circular economy in which waste production is minimised, resources are used sparingly, and product lifetime is prolonged with the environmental impact being minimised. To achieve these objectives, the EU has adopted ambitious legislation to improve waste management systems. In our paper, we will focus on key legislative aspects. We analysed how this legislation sets new targets and requirements for waste separation, introduces extended producer responsibility schemes and promotes recycling and resource recovery. As a result, we will present the implementation of the determination of the average waste composition from the perspective of the Czech Republic and selected sub-regions. This paper will contribute to the discussion on practical aspects of the circular economy and will strengthen the awareness of the necessity of efficient waste management for a sustainable future.

Keywords:
sampling,
stratification,
legislation,
certified methodology,
separation targets,
secondary raw material,
sorting,
waste potential,
material recovery,
recycling

University of Maribor Press

1 Introduction

Waste is a key issue in the context of global environmental challenges, be it climate change, biodiversity protection or sustainable development. Effective solutions to this issue require a comprehensive approach that includes proper waste disposal, active and especially effective recycling, systematic reduction of waste generation and promotion of innovative product and packaging design. These steps lead to the effective implementation of the circular economy approach.

The circular economy is an economic model that aims to maximise the use of resources and minimise the generation of waste by designing, manufacturing, using and recycling products, materials and resources so that they remain in circulation for as long as possible. This approach stands in contrast to the traditional linear economy where the standard model is to produce, consume and ultimately dispose of waste.

The circular economy follows the so-called "closed cycle." Products should be designed to be durable, repairable and, above all, easily recyclable. At the end of their useful life, the materials from these products are reintegrated back into the production process, which minimises the need for new raw materials and reduces environmental impacts. Circular economy promotes ideas such as product sharing, repair and reuse, to extend the life of products. This model is a key tool in the fight against over-consumption, environmental degradation and waste accumulation. In practice, it means transforming economic systems from linear waste to sustainable and efficient use of resources.

The above parameters are precisely a key aspect of why it makes sense to address waste composition and monitor potential usability of waste as a raw material.

2 Legislative approach

Legislation is a very important part because, in the case of waste, legislation establishes targets and requirements that must be respected. For this paper, the following documents will be analysed:

- Directive (EU) 2018/851 of the European Parliament and of the Council.

- Act No. 541/2020 (Czech law).

Directive (EU) 2018/851 of the European Parliament and of the Council of 30 May 2018 amending Directive 2008/98/EC on waste. This directive is fundamental in terms of the management of waste management. The Directive sets targets for the material recovery of municipal waste, which are defined as follows:

- A common EU target to recycle 65% of municipal waste by 2035 (55% by 2025, 60% by 2030 and 65% by 2035).

The Directive, for example, gives in Annex IV A as an example of an economic instrument to implement the waste hierarchy the introduction of a volume-based payment system, whereby generators pay for waste based on the actual amount of waste generated and which encourages the sorting of recyclables at source and the reduction of mixed waste.

Furthermore, the following key elements emerge from Directives (EU) 2018/849, (EU) 2018/850, (EU) 2018/851 and (EU) 2018/852) adopted in May 2018 following inter-institutional negotiations between Parliament and Council:

- Common EU target to recycle 70% of packaging waste by 2030.
- Binding target to reduce landfilling to a maximum of 10% of municipal waste by 2035.
- Ban on landfilling of separated waste, requiring separate collection of bio-waste by 2023 and of textiles and household hazardous waste by 2025.
- Promoting economic instruments to discourage landfilling.
- Simplified and improved definitions and harmonised methods for calculating recycling rates across the EU.
- Specific measures to promote reuse and stimulate industrial symbiosis - a by-product of one sector is used as a raw material for another.
- Mandatory extended producer responsibility schemes for producers to market greener products and promote recovery and recycling schemes (e.g. for packaging, batteries, electrical and electronic equipment).
- Reducing the amount of biodegradable waste going to landfill to 75% of the total weight in 1995 by 2010, 50% by 2013 and 35% by 2020.

Act No. 541/2020 Coll. Waste Act

The EU requirements and objectives are subsequently implemented in the Czech legislation within the framework of the Waste Act 541/2020 Coll. From 1 January 2030, it is prohibited to landfill waste with a dry calorific value higher than 6.5 MJ/kg. These wastes, which can be classified as energy recoverable, also include MSW. The calorific value of MSW can be around 9 MJ/kg in the raw state (up to 15 MJ/kg on dry basis), which is well above the above limit. At the same time, as of the same date, waste that can be effectively recycled in the current state of scientific and technical progress cannot be landfilled.

The national requirements and targets for the management of MSW defined in Act No 541/2020 Coll. on Waste also include the following requirements and targets applicable to MSW:

- To increase the level of preparation for re-use and the level of recycling of municipal waste to at least 55% of the total weight of municipal waste generated in the Czech Republic by 2025.
- To increase the level of preparation for re-use and the level of recycling of municipal waste to at least 60% of the total weight of municipal waste produced in the Czech Republic by 2030.
- By 2035, increase the level of preparation for re-use and the level of recycling of municipal waste to at least 65 % of the total weight of municipal waste produced in the Czech Republic.
- To dispose of no more than 10 % of the total weight of municipal waste generated in the Czech Republic by landfilling in 2035 and subsequent years.
- Energy recovery in 2035 and in the years thereafter shall not exceed 25 % of the total weight of municipal waste produced in the Czech Republic.

3 Certified methodology

This part is devoted to the analysis of the potential for material recovery from mixed municipal waste. The potential will be evaluated based on the analyses and fieldwork carried out, which led to the determination of the average composition. The overall approach has been described in great detail within a certified methodology for the

analysis and composition of municipal waste. This methodology was developed within the framework of the TIRMSZP719 project (Kropač 2020), where the Ministry of the Environment of the Czech Republic (MoE) was the main supervisor, and the fieldwork should be carried out according to this proposed guideline. A relatively large number of entities in the Czech Republic are engaged in fieldwork, among the most important are EKO-KOM a.s., Institute of Circular Economy z.ú. and others.

These subjects historically carried out fieldwork without the use of certified methodology (it was not available) and used the procedures used in the research project SP/2f1/132/08 "Research on the properties of municipal waste and optimization of its use". These procedures were always adapted to the needs of the subjects and the objectives set. This resulted in different structures from different subjects, i.e. comparability and especially repeatability of results was eliminated in case more than one subject was sampled.

Comparability and repeatability of results was the main requirement for the design of the certified methodology.

The certified methodology further defines the following parameters:

- Sampling (multi-level stratification, Šomplak 2022).
- Minimisation of economic costs.
- Recommendations for the sampling and transport method.
- Method of sorting, necessary documentation and overall administration.
- The tool for evaluating the data obtained and establishing clear results with the accuracy considered.
- Recommendations for laboratory analysis.

An integral part of the method is the so-called sorting module, which is divided into three main categories of sorting. The MoE sets the requirement that the first two levels are mandatory, and the third is recommended. The sorting module, e.g. at the third level, can be modified according to the needs of the sampling objectives. Specifically, this may be a more detailed specification of e.g. plastics or papers in terms of fractional level, i.e. what is actually in the plastics in terms of e.g. PET

bottles, hollow packaging, films, etc. This approach may be of particular interest from the point of view of different processing facilities, where the potential that may be present in e.g. separate collection can be estimated. An example of a sorting module for all three levels is shown in Figure 1.

I. level	*II. level*	*III. level*	*Weight (g)*
Paper	Packaging	**Cardboard**	
		Other - packaging paper	
	Non Packaging	**Magazines and leaflets**	
		Newspaper and office paper	
	Other		
Plastic	Packaging	**Plastic foils**	
		3D plastic	
		Transparent PET	
		Coloured PET	
		PS	
		Other packaging plastic	
	Non Packaging		
Bio	Kitchen waste	**Fruit and vegetable**	
		Residues from the preparation of fruit and vegetable	
		other food	
	Garden Bio		
Wood			
Glass	Packaging		
	Non Packaging		
Metal	Packaging	**Ferromagnetic**	
		Aluminium	
		Other packaging metals	
	Non Packaging	**Ferromagnetic**	
		Other non packaging metals	
Textil	Clothes		
	other textile materials		
Composite and TetraPak	Tetra Pak		
	Others		
Electrical equipment			
Batteries and accumulators			
Other waste	Diapers and sanitary waste		
	Minerals waste		
	Hazardous waste		
	Complex products		
	Others - without category		
Fine fraction (below 40 mm)			
Fine fraction (below 20 mm)		**Ash**	
		Other organic waste	
Fine fraction (below 10 mm)		**Ash**	
		Other organic waste	

Figure 1: Sorting module

Source: own.

3.1. Practical application of the methodology

The results presented in this paper are part of the results of the TIRSMZP719 and CEVOOH projects. The results were obtained by implementing a sampling programme by a certified methodology also developed within the TIRSMZP719 project. The main motivation for developing the methodology was mainly the comparability and repeatability of the results.

The analyses aimed to establish the average composition of mixed municipal waste in the Czech Republic in the detail given by the certified methodology and to obtain a national tool comparable to similar tools for monitoring the composition of

MMW[1] in other EU countries. Given the limited resources for carrying out the analyses (fieldwork), a multi-stage stratification was adopted. The stratification is voluntary within the certified methodology. First, all municipalities in the Czech Republic (6 258 municipalities in total) were considered and then divided into individual similarity groups (clusters or clusters). Small municipalities, and military areas were excluded from the clustering (2 443 municipalities). Ten clusters were created with the following characterization:

- C1 Cities - local "district" centres.
- C2 Regional towns and regional centres.
- C3 Towns with rural character.
- C4 District towns - tens of thousands of inhabitants.
- C5 District towns - up to ten thousand inhabitants.
- C6 Rural municipalities A.
- C7 Rural municipalities B.
- C8 Rural municipalities C.
- C9 Rural municipalities D.
- C10 Capital city of Prague.

From the above distribution, 10 representatives and 10 alternates were selected to represent the characteristics (freely available information from the CSO[2]) of each cluster. The selected representatives were contacted and cooperation on sampling possibilities was agreed. Each representative was provided with the necessary technical equipment (pedestals, 40-20-10 sieves, samplers, etc.) and space was secured to carry out the fieldwork. Towards the end of the project, sampling also took place in other locations (beyond the 10 selected representatives).

Sampling was based on the technical capabilities of each site, always involving the collection of specific containers or the provision of specific collections. For these purposes, the BinGen tool was used to randomly select containers in a given village. Of course, the key was to have a complete list of bins so that random selection could

[1] Mixed municiapl waste
[2] Czech Statistical Office - www.czso.cz/csu/czso/home

take place. In localities where this information was unavailable, a street draw was made from which samples (containers) were randomly taken.

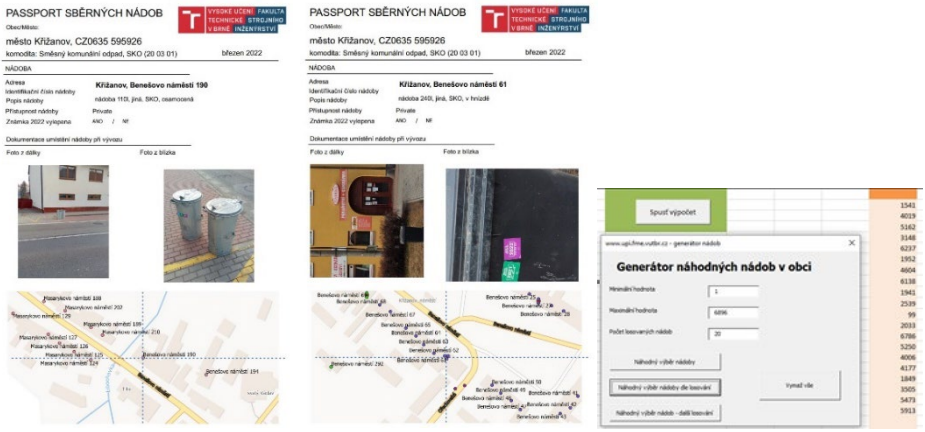

Figure 2: BinGen and export of selected bins

Source: own.

3.2 Waste composition for the Czech Republic

It is not recommended to carry out the analyses according to the proposed methodology from compactor collection vehicles. If a mixed sample is to be generated and a collection vehicle is used, it is strongly recommended not to separate the waste. Compaction, significantly affects the results, i.e. moisture transfer, contamination, ability to sort the individual components being monitored properly, etc.

Based on the certified methodology, a sample of 1 100 l has been determined as a representative sample. At the same time, a sample from the so-called bag sample may be used, again in an appropriate proportion to the representative sample.

The total number of investigated (sub) samples was 635 with a total tonnage of 19.6 t. In the framework of the fieldwork, the sorting was carried out to level III (the mandatory level according to the certified methodology is level I and II; level III is recommended):

- Level I (first) sorting - 635 sub-samples, approx. 19.6 t.
- Level II (second) sorting level - 631 sub-samples, approx. 19 t.
- III (third) sorting level - 609 sub-samples, approx. 15 t.

The sampling was carried out in Brno, Louka, Valašské Klobouky, Třebíč, Křečkov, Velké Popovice, Červené Řečice, Křižanov, Kralupy nad Vltavou, Hradec Králové, Polná and Prague. The length of fieldwork was about a year and covered all seasons (taking into account seasonality), in the period 3/2020-8/2021 - fieldwork was interrupted due to the COVID-19 pandemic.

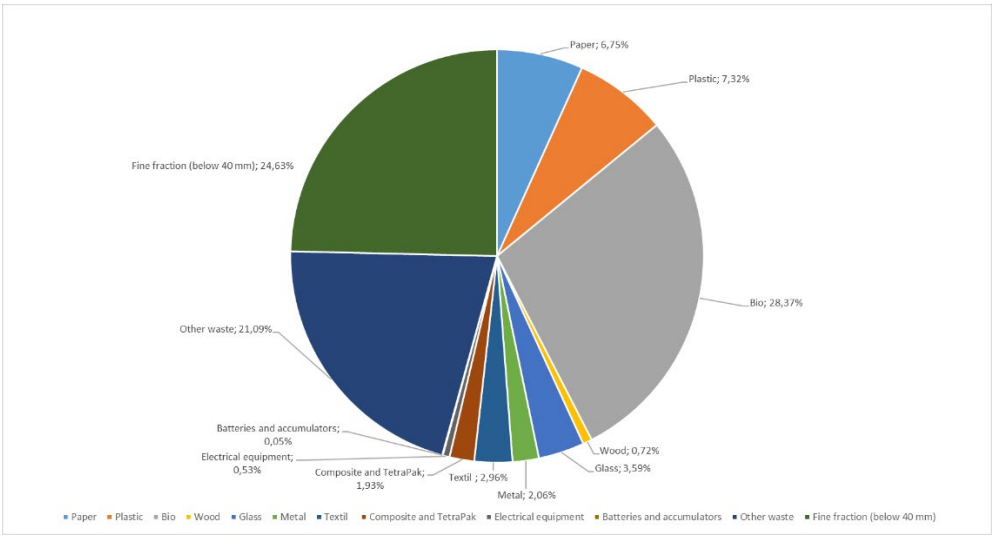

Figure 3: Average composition of municipal waste
Source: own.

4 Analysis of material recovery potential

The average composition shows that the largest parts belong to the following fractions:

- Bio waste - approximately 29%.
- Other waste - approximately 21% (significant dominance of sanitary waste)
- Fine fractions (aggregated) - approximately 25%.

- Paper - approximately 7%.
- Plastic - approximately 7%.
- Other commodities (categories) below 5%

Where specific components that are potentially material recoverable are concerned, these are prioritised (synergies with separate collection):

- Plastic
- Paper
- Glass
- Metal
- Textile
- Bio
- Batteries
- Electrical equipment
- Wood

From the above categories, a theoretical estimation of the potential from MMW that can be redirected to separate collection or to other locations relevant to separate waste collection will be made.

4.1 Plastic waste

Plastic waste is as standard collected separately in the form of a yellow bin. What goes in the bin can vary in place and time, so it is necessary to see at each location what can be put in the bin. The following items can be diverted in whole or in part from the MMW:

- Films - approx. 3.5% - the assumption for diversion is 1 - 1.5% (these are films or bags in which waste is disposed of, it is assumed that waste bags and sacks will always be present in the MSW as this is the primary packaging for waste, therefore a conservative approach is set that approximately one-third of films can be diverted)

- 3D plastics - approx. 2% - the assumption for diversion is a total of - 2% (3D packaging plastics, these are preferably hollow packaging or primarily HDPE packaging, which can be easily diverted to the yellow bin)
- PET clear and coloured - approx. 1% - the assumption for diversion is an overall amount of - 1% (PET beverage bottles can be completely diverted to the yellow bin or the backup stream)
- PS – 0.1 % - the assumption for diversion is a total amount of approx. 0.1 % (polystyrene packaging can be completely diverted)
- Other Packaging - 0.1% (no assumption of direct diversion for other packaging components, so the total is retained)
- Other non-packaging - 0.4% - assumption for redirection is approximately half - approximately 0.2% (here the assumption is that approximately one half of the component can be redirected to the yellow bin, although it will not be consistent with the packaging component share and EKO-KOM's rewards)

The total diversion potential for plastics is about 3.5%.

Figure 4: Example of plastic waste after sorting
Source: own.

4.2 Paper waste

Paper waste is as standard collected separately in the form of a blue bin. The blue bin is locally very similar in terms of packaging materials. An exception is municipalities that also collect e.g. tetra-pack in the blue bin. The following components can be fully or partially diverted from the MMW:

- cardboard and cardboard (packaging part) - 2.5% - the assumption for diversion is a total amount of - 2.5%.
- magazines and leaflets - 1% - the assumption for diversion is a total of 1%.
- Newspaper and office paper - 1% - the assumption for redirection is a total amount of - 1%.

The total potential for redirection for paper is approximately 4.5%.

Figure 5: Example of paper waste after sorting
Source: own.

4.3 Glass waste

Glass waste is as standard collected separately in green (coloured) or white (transparent) containers. The glass containers can be, for example, connected with two inlets and an internal partition or they can be two separate containers. The following components can be fully or partially diverted from the MMW:

- Glass - packaging - 3.3% - the assumption for diversion is a total amount of - 3.3%.
- Glass - non-packaging – 0.2 % - the assumption for diversion is a total amount of 0.2 %.

The total potential for diversion for glass is about 3.5 %.

Figure 6: Example of glass waste after sorting
Source: own.

4.4 Metal waste

Metal waste is as standard collected in a grey bin. The following components can be fully or partially diverted from the MMW:

- Ferromagnetic - 1% - the prerequisite for diversion is the total amount of - 1%.
- Aluminium - 1% - the assumption for diversion is a total amount of - 1%

The total potential for redirection for metals is approximately 2%.

Figure 7: Example of metal waste after sorting
Source: own.

4.5 Textiles waste

Textile impacts are collected in separate containers or textiles can be taken to collection centres or directly to the Salvation Army. There can be a small complication with textiles in that some may fall outside the waste inventory. Given

that it is a relatively heavy (by weight) component, it can be concluded that this particular stream may have an impact on meeting recycling targets. At the same time, it should be noted that from 1 January 2025 there is an obligation to ensure a separate collection of textiles in all municipalities. In this respect, textiles can be considered to be diverted entirely out of the MMW, approximately 3%.

Figure 8: Example of textile waste after sorting
Source: own.

4.6 Biowaste

Collection of bio-waste is highly variable. Some municipalities use bio-waste collection in the form of home composting (waste enters the off-register waste management system), or separate collection in the form of brown bins or a centralised collection point for bio-waste or ad-hoc collections in case of seasonality. Of course, there are also municipalities where no collection of bio-waste is yet in place. Alternatively, it may be a combination of the above. The results of the fieldwork carried out show that bio-waste represents almost a third of the total black bin. A significant added value in diverting bio-waste from the black bin to the brown bin is the introduction of a door to door system, which was also confirmed in the fieldwork. It is indeed the introduction of a door to door system, the situation will not be improved by providing e.g. home composters.

- Fruit and vegetables - approx. 5% - these are whole pieces of fruit and vegetables that can easily be diverted to material recovery, from a conservative perspective it will be chosen that 80% will go outside the MMW, i.e. 4%.

- Vegetable residues from fruit and vegetable preparation - approx. 8% - this is one of the residues from the preparation of fruit and vegetables, this part is suitable for composting or use within the biogas station. It is assumed that half of this component can be redirected, i.e. 4%.
- other food products - approx. 11% - this is the component mainly related to food residues, which are preferably of animal origin. In this respect, a pessimistic scenario will be set and no redirection will take place.
- from gardens and parks - about 6% - this is material that comes from gardens and parks, i.e. primarily green maintenance. Here the assumption is that the total stream can be diverted away from the MSW and in the form of composting. Thus, the total flow will be redirected in the full 6%.

The total potential for diversion for BIO waste is about 14%.

Figure 9: Example of Bio waste after sorting
Source: own.

4.7 Batteries

Batteries are not collected separately in the Czech Republic in the form of container collections. They are end-of-life products and can be disposed of in collection centres or other designated places, e.g. shops and shopping centres (e.g. together with fluorescent lamps). The whole category can be completely diverted from the MMW, which reaches a value of about 0.1% in terms of average composition.

4.8 Electrical equipment

Similar to the battery category, electrical equipment is not collected separately in the Czech Republic in the form of containerised collections. They are end-of-life products and can be disposed of in collection yards or other designated places. The

entire category can be completely diverted from the MMW, which is about 0.5% in terms of average composition.

Figure 10: Example of electrical waste after sorting
Source: own.

4.9 Wood (furniture and similar material)

Wood, or it may be bulky waste, is collected in the Czech Republic under the collection yard regime. These collection yards operate on the principle of either re-use centres or energy recovery. The total stream of wood (treated only) can be diverted out of the MMW stream, in full. This will be approximately 0.7%.

5 Conclusion

This paper summarises an approach to waste composition analysis, where a large number of samplings were carried out throughout the Czech Republic (2020 - 2022). A detailed analysis of the separation targets set and other important steps that are key in waste management was analysed in the framework of legislation. It was necessary to analyse the potentially recoverable materials contained in the mixed municipal waste container. The research team carried out more than 600 samples with a total weight of 20 t during two years of field research.

Based on practical experience, e.g. from sorting lines (Gregor 2018, CET), an estimate was made to evaluate the potential amount of waste that can realistically be diverted from mixed municipal waste. The potential was assessed rather conservatively, especially focusing on the possibility of introducing a door-to-door system or e.g. collection of dry recyclables (Gregor 2018). From the expert

assessment, it was evaluated that approximately 32% (by weight percentage) of mixed municipal waste (black bin) can be effectively diverted into separated components.

This relatively large potential can effectively contribute to high separation targets and appropriate waste handling/recycling.

Acknowledgments

The authors gratefully acknowledge the financial support provided by the Technology Agency of the Czech Republic (TACR) as part of the Program Environment for Life, specifically through the project CEVOOH (SS02030008).

References

Gregor, J.; Kropáč, J.; Pavlas, M. Sorting Line Modelling as an Integral Part of Complex Tools for Decision-making in Waste Management. *Chemical Engineering Transactions,* 2018, 70, n. 1, p. 1561-1566. ISSN: 2283-9216.

Gregor, J.; Kropáč, J.; Pavlas, M. Collection Of Dry Recyclables As An Effective Step In Waste Management?. In *1ST INTERNATIONAL CONFERENCE ON TECHNOLOGIES & BUSINESS MODELS FOR CIRCULAR ECONOMY*. Portorož, Slovinsko: University of Maribor Press, 2018. s. 1-10. ISBN: 978-961-286-211-4.

Kropáč, J.; Gregor, J.; Pavlas, M. Residual Municipal Waste Composition Analysing – New Methodic for Czech Waste Management. In *Recycling & Abfallverwertung Abfallwirtschaft & Ressourcenmanagement Deponietechnik & Altlasten Internationale Abfallwirtschaft*. Leoben, Austria: Montanuniversität Leoben, 2020. s. 791-794. ISBN: 978-3-200-07190-2.

Kropáč, J.; Gregor, J.; Pavlas, M. Municipal Waste Composition Analysis – Approaches to and Solutions for Czech Waste Management. In *2nd International Conference on Technologies & Business Models for Circular Economy: Conference Proceedings*. Portorož, Slovinsko: University of Maribor Press, 2020. s. 1-10. ISBN: 978-961-286-353-1.

Šomplák, R.; Kopa, M.; Omelka, M.; Nevrlý, V.; Pavlas, M. Multi-level stratification of territories for waste composition analysis. *JOURNAL OF ENVIRONMENTAL MANAGEMENT,* 2022, roč. 318, č. 1, s. 1-12. ISSN: 0301-4797.

Waste Rubber Incorporated in the Alkali-Activated Metakaolin's Aluminosilicate Network Enhanced by Microwave Irradiation

Barbara Horvat, Branka Mušič

Slovenian National Building and Civil Engineering Institute, Ljubljana, Slovenia
barbara.horvat@zag.si, branka.music@zag.si

Building materials represent the possibility of prolonging the life of waste materials. The key is to ensure that the products are suitable for their function. So we activated metakaolin with the alkaline Na-silicate solution in the ratio that ensures the prevention of efflorescence and high mechanical strength (Horvat and Ducman, 2019). As the waste material (to be incorporated in the aluminosilicate network (ASN) of the alkali-activated metakaolin) ground waste rubber from electric cables was used in the preselected mass ratios. Its inclusion in products, like paving stones, can reduce stiffness, improve durability, dampen vibrations, and reduce road noise. The mechanical strengths of test samples with rubber present on the active surface or slightly below were higher compared to samples where rubber was encapsulated throughout the volume. Compressive strength was higher when samples were irradiated with low powers of microwaves while irradiation with higher powers led to the foaming of alkali-activated slurry. The encapsulation quality of the ground rubber was evaluated by SEM while the chemical influence on ASN was determined by EDS, FTIR, and XRD. Slipperiness change on the active surface of pavement stones proved that the addition of the ground rubber enhanced the walking safety of the product.

DOI
https://doi.org/10.18690/um.fkkt.1.2024.2

ISBN
978-961-286-829-1

Keywords:
waste rubber, alkali-activated metakaolin, encapsulation of organic in inorganic material, microwave irradiation, mechanical properties

University of Maribor Press

1 Introduction

Rubber represents a major challenge at the end of its life cycle due to its enormous quantities and recycling issues (Leong et al., 2023). Synthetic polymer (rubber) is used for tires, electrical cables, etc., and is made by the cross-linking process (vulcanization) (Coran, 2013). This crosslinking makes rubber more elastic (Flory, n.d.), which makes waste rubber interesting for recycling in construction materials as fillers (Nuzaimah et al., 2018). Its inclusion in various civil engineering products could provide many benefits, such as reducing stiffness and brittleness, improving the durability and longevity of the new composite material, dampening vibrations, and reducing road noise (Mutalib et al., 2021) while extending the life of the rubber and increasing the benefits to the users of the civil engineering product.

At the same time, the civil engineering and building industry consumes almost 70 $m_{\%}$ of the mass of Mount Everest in raw materials yearly and creates more than 30 $m_{\%}$ of global waste (Miller, n.d.). One of the solutions in this industry is to replace conventional materials, prepared from raw materials at high temperatures, like cement, with alkali-activated material (AAM) which is synthesized at temperatures lower than 100 °C and from materials that contain enough Si and Al in amorphous content, either as raw or waste material (Češnovar et al., 2019; Horvat et al., 2019a, 2019b, 2022a; Horvat and Ducman, 2019, 2020; Pavlin et al., 2021). Si and Al bind with O into tetrahedrons which are connected through O-bridges. This formation is called an aluminosilicate network (ASN) where the additional chemical bond of Al and O is compensated by the presence of elements from the 1st and the 2nd group of the periodic system (Škvára, 2007) which are introduced through alkalis.

Besides AAMs already having a lower impact on the environment when compared to conventional materials, the use of energy for their synthesis can be additionally lowered by replacing conventional (surface) heating with microwave irradiation (volumetric heating) (Horvat et al., 2023, 2022b). With volumetric heating, final mechanical strengths are reached in shorter times (Horvat et al., 2023), which decreases the time of the product from synthesis to the market leading to lower costs for the industry.

Combining both materials for driving/walking surfaces, i.e. coarsely ground waste rubber and AAM, would not just lower the impact on the environment but also result in the product with a less slippery surface, a quieter ride, and longer service life of the driving/walking surface, decrease the incidence of human falls and dampen the impact on the vehicle shock absorbers and human/animal joints, leading to higher quality life and better health.

In the paper, coarsely ground rubber was combined with alkali-activated metakaolin slurry as part of the active surface or spread throughout the volume, which has not yet been seen in the literature. The focus of the work was, besides testing improvement of samples being less slippery, on the quality of the encapsulation of the rubber in the ASN to avoid potential pollution through the back-spread of the ground rubber into the environment, not to cause additional "micro-plastic" issues.

2 Methods – evaluation of the material

Chemical evaluation of precursor metakaolin (MK) was performed by X-ray fluorescence (XRF; Thermo Scientific ARL Perform'X Sequential XRF) along with the determination of the amount of organic compound and carbonates through loss on ignition (LOI) for 2 hours at 550 °C and 950 °C, respectively.

Mineralogical analysis of MK, along with Rietveld refinement using external standard (corundum, Al_2O_3), was performed by X-ray powder diffraction (XRD; Empyrean PANalytical X-ray Diffractometer, Cu X-Ray source).

The precursor was dried, milled, and sieved below 125 μm for LOI, XRF, and XRD. Results were reported in our previous work (Horvat et al., 2023, 2022c) and also the optimal mixture of MK and used alkali (Na-silicate solution, Geosil, 344/7, Woelner, Ludwigshafen, Germany, 16.9% Na_2O, 27.5% SiO_2). The theoretically determined mass ratio (using software in MS Excel platform developed in project No. C3330-17-529032 "Raziskovalci-2.0-ZAG-529032" and upgraded in the ARRS project under Grant No. J2-3035) between MK and liquid alkali was 1:0.66, respectively. However, for the synthesis, MK was used as received (particle size distribution was evaluated by sieving through test sieves with mesh 5 mm, 4 mm, 2 mm, 1 mm, 0.4 mm, 0.125 mm, 0.09 mm, 0.063 mm).

On rubber waste from old electrical cables, received coarsely ground below 2 mm (particle size distribution was evaluated by sieving through test sieves with mesh 5 mm, 4 mm, 2 mm, 1 mm, 0.4 mm), thermogravimetric analysis and differential thermal analysis (TG/DTA; STA 409 PC Luxx, Netzsch, Germany) were performed in airflow from the room temperature to 1000 °C with a rate of 10 K/min to evaluate the temperature of ignition where the majority of the material would have already combusted. The rubber was ignited for 2 hours (LOI) at 550 °C (and at 950 °C) to determine the amount of ignition residual loss coming from the inside of the cables (conductive material, the metals, etc.), potential construction and demolition waste (Si, Al, and alkali (earth) metals), and inorganic content present in the rubber material. Rubber was evaluated by Fourier-transform infrared spectroscopy (FTIR; PerkinElmer Spectrum Two, ATR mode) where larger particles of different colour pigments were evaluated independently.

Besides FTIR performed on the rubber, it was performed also on MK powder, and on the ASN (along with the non-reacted MK) gently scratched with the spatula from the inside of the AAM (to exclude the rubber). For the XRD analysis of the ASN (and non-reacted MK), AAM was gently crushed in the mortar with the pastel and sieved below 0.4 mm to remove as much of the rubber as possible (XRD of the rubber sieved below 0.4 mm was performed, too).

On not polished and not coated MK powder, rubber (ignited for LOI determination and as received) and AAMs, scanning electron microscopy (SEM; Jeol JSM-IT500, low vacuum conditions) with energy-dispersive X-ray spectroscopy (EDXS; Oxford Instruments, Link Pentafet) was performed.

At 14 days of AAMs, geometrical densities along with mechanical strengths (bending and compressive) were measured. For the evaluation of mechanical strengths compressive and bending strength testing machine (ToniTechnik ToniNORM) was used.

3 Methods – synthesis of the material

Rubber was used as an active-surface partial cover (S) or volumetrically (V) spread in the alkali-activated metakaolin mixture (MK_b) in mass ratios presented in Table 1. For the one-surface partial cover, two different mass percentages of rubber were

used, i.e. 1.7 $m_{\%}$ (S_{min}) and 5.3 $m_{\%}$ (S_{max}) calculated on the mass of the metakaolin slurry while for volumetrically spread rubber, 9.0 $m_{\%}$ of rubber was used (also calculated on the mass of the slurry).

Table 1: Masses of the used ingredients.

Mixture	MK [g]	Alkali [g]	Rubber [g]
MK_b	50	33	/
S_{min}	50	33	0.7
S_{max}	50	33	2.2
V	50	33	7.5

For the volumetrical distribution of the rubber, rubber particles were homogenized with dry MK before being mixed with Na-alkali silicate solution until complete wetting and moulded into silicone-urethane rubber moulds of prisms measuring (2×2×8) cm^3.

For the one-surface rubber cover of the prism (measuring (2×2×8) cm^3), the bottom of the mould (measuring (2×8) cm^2) was partially (S_{min}) to almost fully (S_{max}) covered with coarsely ground rubber before fresh alkali-activated MK slurry was cast onto it. Casted slurries were manually pressed to help rubber particles penetrate them.

Three different curing procedures of all mixtures presented in Table 1 were evaluated: curing solely at room conditions (55% moisture, 22 °C) for 14 days, irradiating fresh slurry with microwaves (frequency 2.45 GHz, inverter microwave, i.e. microwaves are constantly on if chosen; Panasonic, NN-CD575M) for 1 min at 100 W (positively influencing the dissolution of reagents while dehydration is not severely affected (Horvat et al., 2023, 2022b)) or for 1 min at 1000 W (physical foaming of the slurry (Horvat et al., 2023, 2022b)), and additionally further curing all volumetrically heated specimens at room conditions for 14 days.

Each prism was irradiated separately in the 1st observed dosimetry maxima (approximately 6 cm away from the centre) without any cover on the moulds.

4 Methods – upscaling into pavement stones

Mixtures MK_b, S_{min}, and S_{max} (800 g of MK was used per pavement stone) were cast into moulds with a bottom surface measuring (20×20) cm². Rubber was uniformly spread either on the bottom of the mould or all over the top of the slurry. Rubber in mixture S_{max} was uniformly spread over the mesh (cut into the PVC foil placed directly onto the slurry) of 2 cm wide stripes that were 2 cm apart.

On the top of all casted mixtures with/without the rubber, PVC foil was placed onto which stone measuring (20×20) cm² with a smooth surface and weighting 3 kg was laid (the whole procedure up to placing the smooth stone is shown in the Supplement in Figure S1). Besides the stone offering uniformly distributed pressure onto the slurry, additional force, 2.5 kN, was introduced with a compressive and bending strength testing machine pressing onto the stone (HPM 25/5, Zavod za raziskave materiala in konstrukcij Ljubljana). Pressure onto the layer of the rubber is presented in Table 2 and depends on the placement of the rubber and the masses/forces above it (forces presented onto the rubber sum up).

Table 2: Pressure onto the rubber.

Source of the pressure onto the surface (20×20) cm²	Slurry 1.3 kg [kPa]	Stone 3 kg [kPa]	Additional force 2.5 kN [kPa]
Rubber on the bottom	0.32	0.76	62.50
Rubber on the top	/	0.76	62.50

Pavement stones were cured solely at room conditions and de-moulded 1 hour, 2 hours, 24 hours, and 48 hours after casting alkali-activated slurries. The stone on top of the PVC foil was removed just before de-moulding.

Change in the slipperiness of the active surface of the pavement stone was tested according to the SIST-TS CEN/TS 16165 Annex C to test the influence of the addition of the ground rubber regarding the accident safety of the product.

The contact surface area at the test measures 95.76 cm² while for striped pavement stone, the contact area splits into the contact area with AAM and the contact area with rubber. If the pendulum slides over striped pavement stone perpendicular to the stripes, the contact area with rubber is 45.60 cm² (50.16 cm² with AAM) but if

the pendulum slides over striped pavement stone along the stripes, the contact area with rubber is 50.40 cm² (45.36 cm² with AAM).

5 Results – materials used

Particle size distributions of MK and coarsely ground rubber along with their photographs are presented in Figure 1. While MK has more than 90 m% of particles below 0.09 mm, coarsely ground rubber has 80 m% of particles bigger than 0.4 mm.

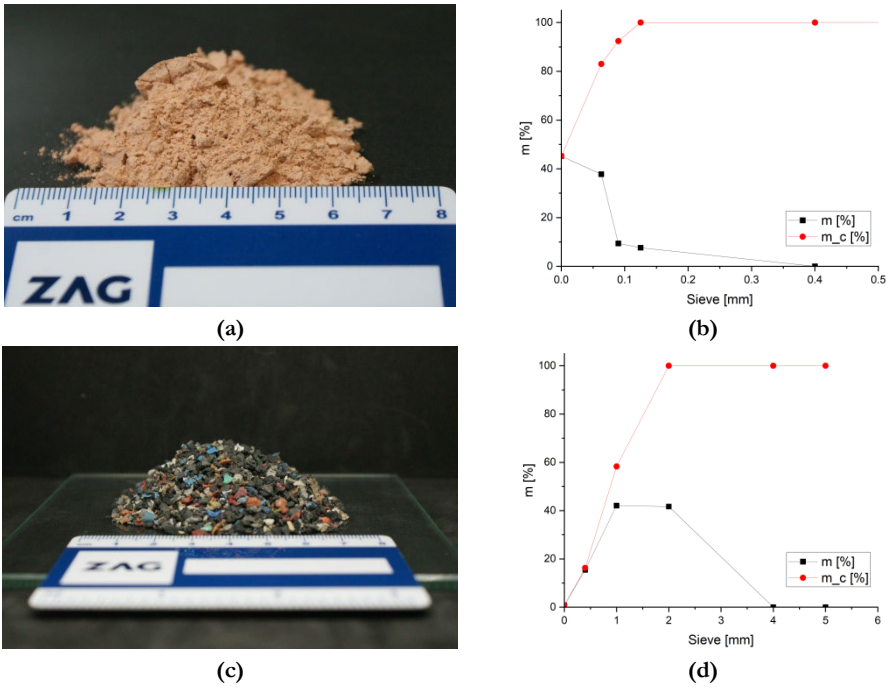

Figure 1: (a) MK and (c) coarsely ground rubber, with their particle size distribution (b) and (c), respectively.
Source: own.

Thermal analysis performed on the rubber and used to determine the temperature where the majority of the organic material is removed is shown in Figure 2. The majority combusts up to 550 °C where rubber leftover becomes black. However, the mass loss continues further on, leaving the material light grey (white) at 950 °C.

SEM micrographs of MK and rubber are presented in Figure 3 and their EDXS analysis is in Table 3 (areas of the acquisition on the rubber are in the Supplement in Figure S2). From SEM micrographs of MK, it is clear that the precursor used in the synthesis is a fine powder of uniform chemistry (the greyscale of the particles is narrow). However, rubber is the complete opposite, i.e. besides the majority of the rubber particles being tremendous for observation under SEM even at lower magnifications (Figure 3 (b_i/b_{ii})). Its smaller fraction (Figure 3 (c)) shows severe non-uniformity in size, shape, and chemistry, which is presented in Table 3 according to the greyscale level of the waste rubber/"rubber" particles and their shape. After ignition at 550 °C, rubber showed severe deterioration (Figure 3 (d_i)) with few less damaged areas (Figure 3 (d_{ii})). Nonetheless, it was easy to crush all larger rubber particles into powder with just a gentle pressing with a spatula (Figure 3 (e)). Ignition of rubber at 950 °C left no undamaged parts of the rubber (Figure 3 (f)), and the remaining rubber was easily crushed with a spatula to powder (Figure 3 (g)).

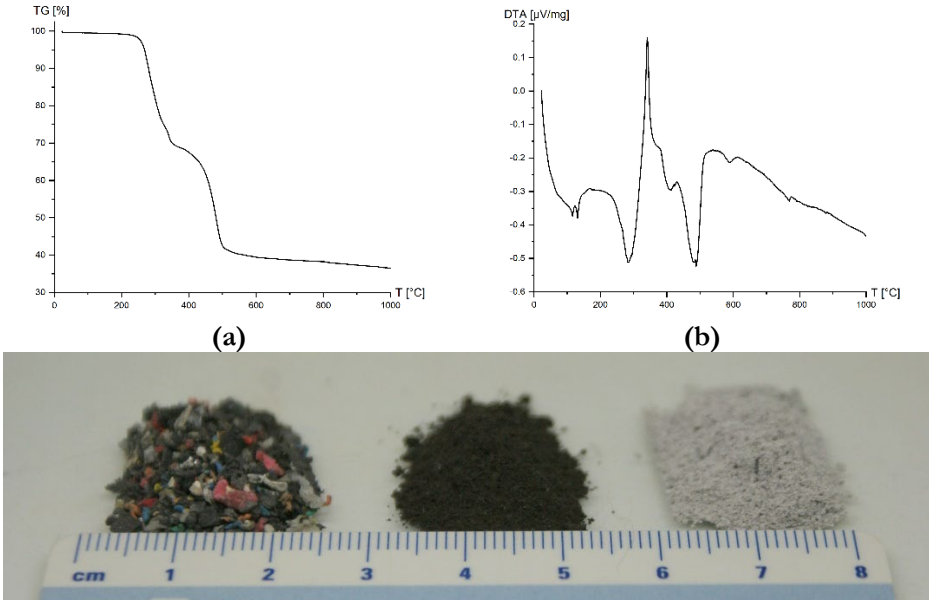

Figure 2: (a) TG and (b) DTA of coarsely ground rubber. (c, from left to right) Rubber before ignition, rubber after ignition at 550 °C (crushed with a spatula), and after 950 °C (crushed with a spatula).

Source: own.

While MK consists mostly of Si and Al (and Fe, hence the orange-red colour of the MK powder), coarsely ground rubber from electric cables is much more than just organic polymer, i.e., it contains also conductive elements present in the metallic wires of electric cables and also elements that are present in construction materials surrounding electric cables in the walls. However, non-rubber materials (plates, fibres), even metallic, are hard to find under SEM (Figure 3 (e-1)), which means that their $m_{\%}$ is low, but are all present and not affected by thermal treatment.

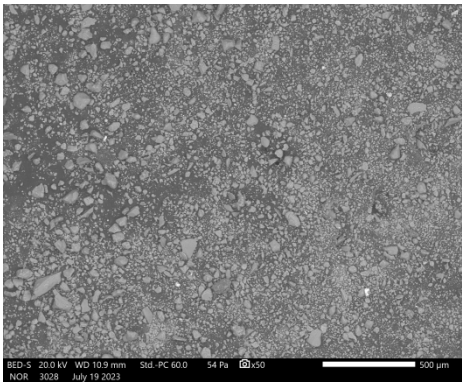

(a-1)

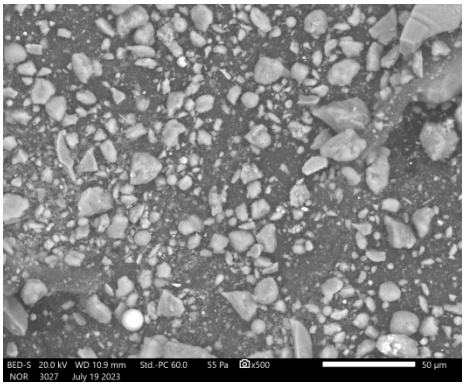

(a-2)

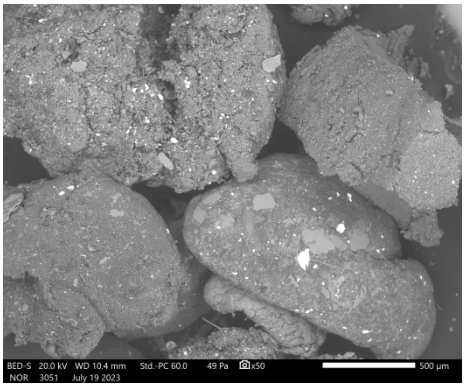

(b_i-1)

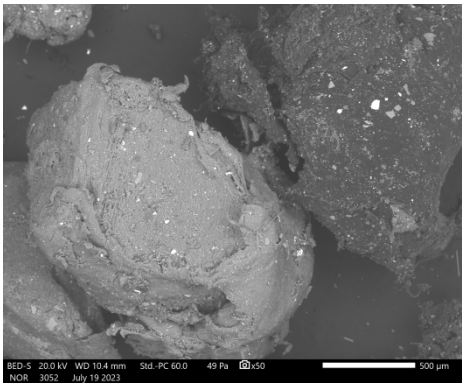

(b_{ii}-1)

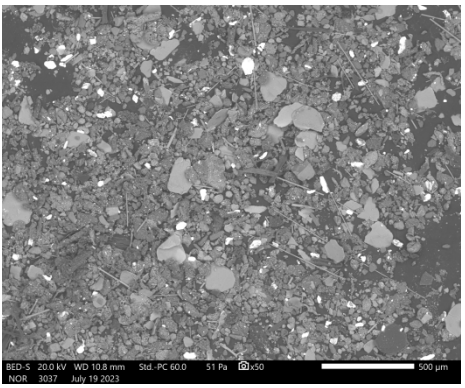

(c-1)

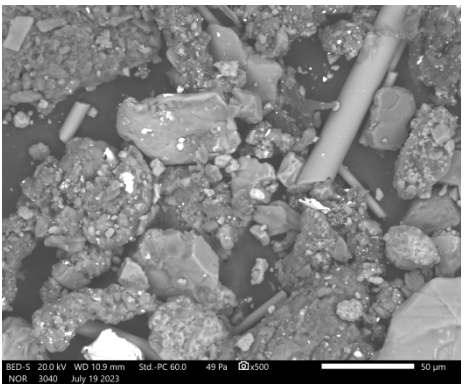

(c-2)

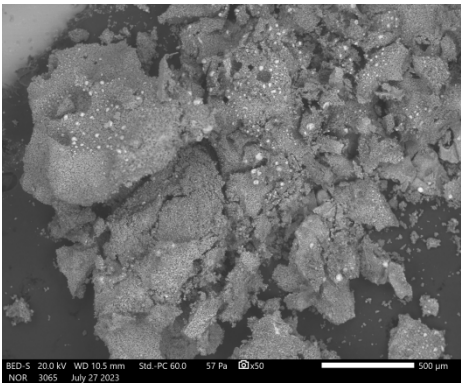

(d_i-1)

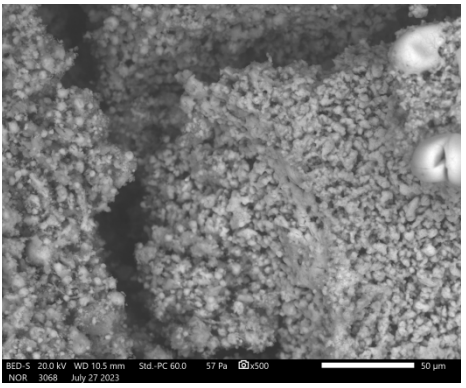

(d_i-2)

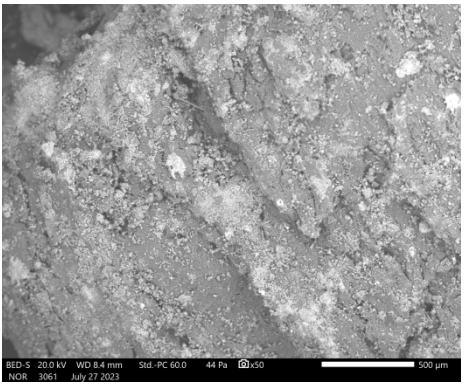

(d_{ii}-1)

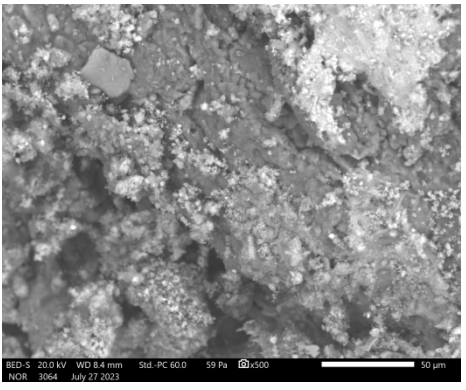

(d_{ii}-2)

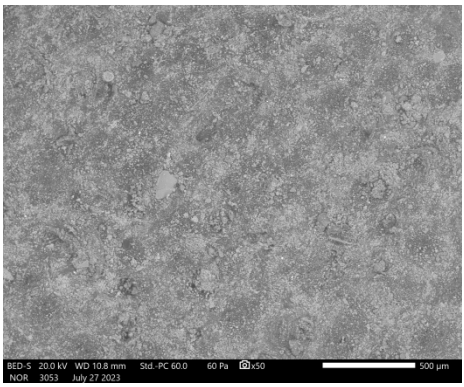

(e_i-1)

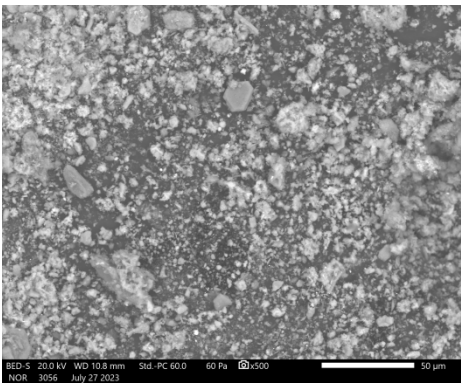

(e_i-2)

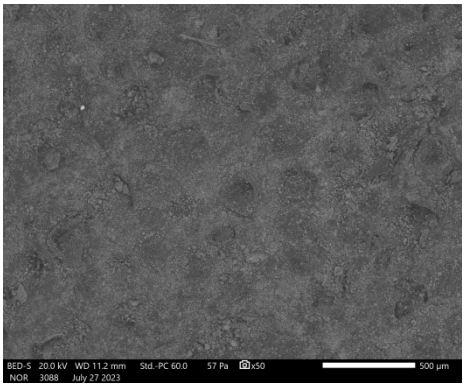

(e_{ii}-1)

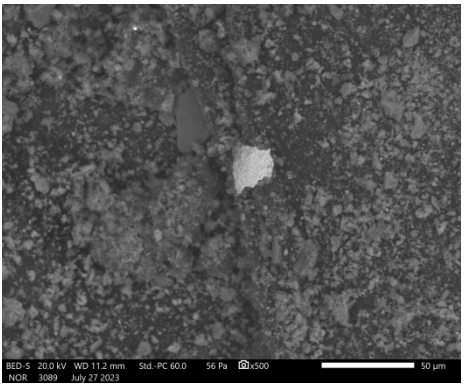

(e_{ii}-2)

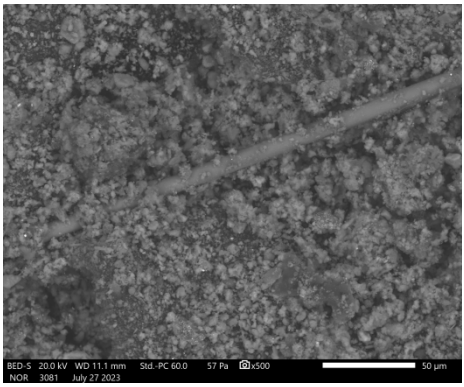

(e_{iii}-2)

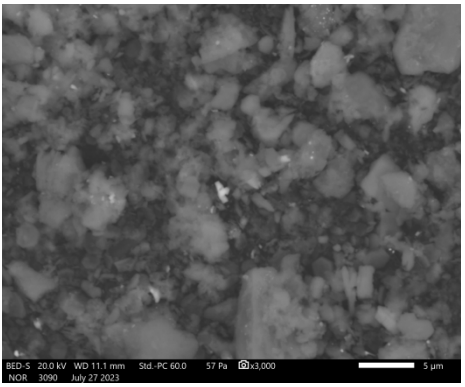

(e-3)

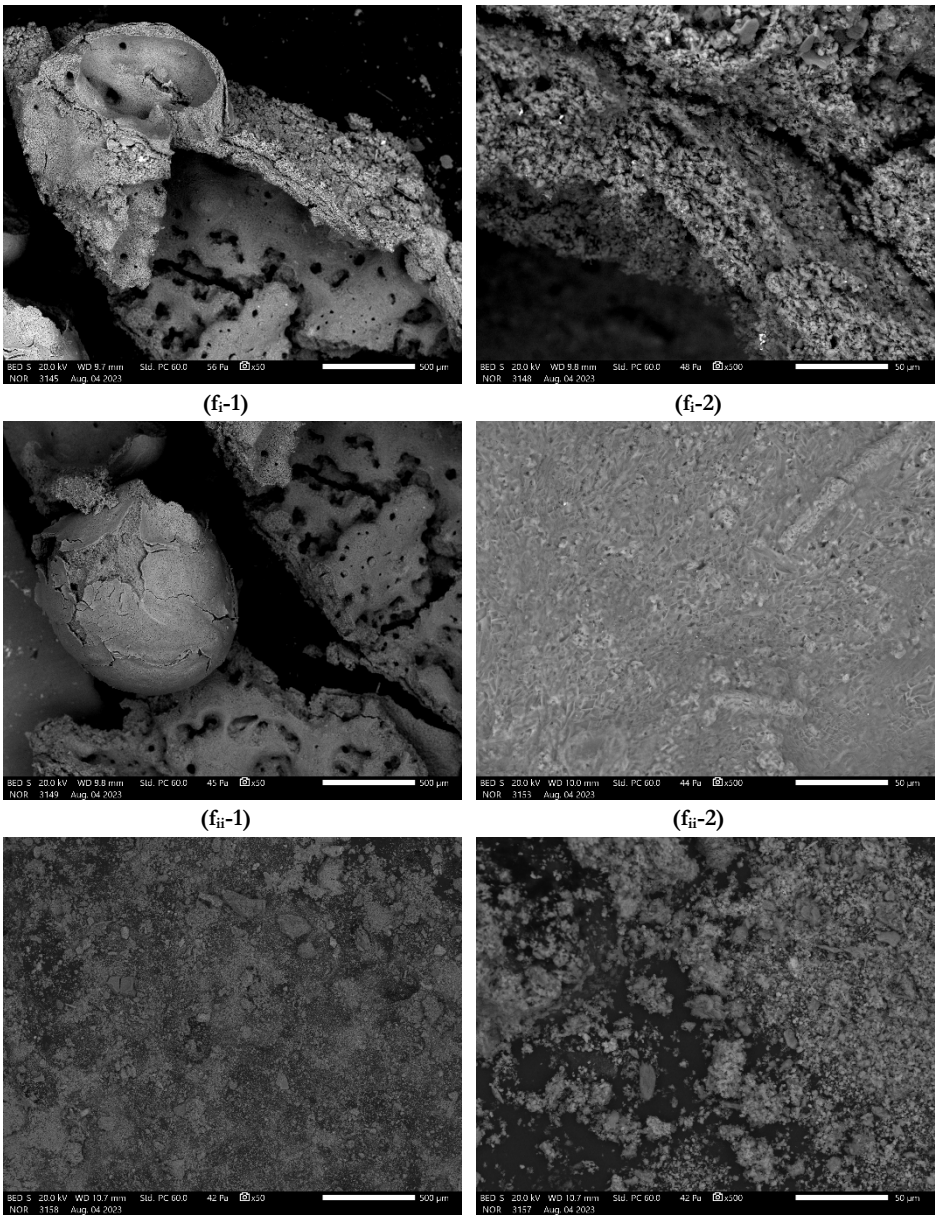

(f_i-1) **(f_i-2)**

(f_{ii}-1) **(f_{ii}-2)**

(g-1) **(g-2)**

Figure 3: SEM micrographs of (1) 50-times, (2) 500-times and (3) 3000-ground magnified (a) MK, (b) coarsely ground rubber, (c) finer fraction of coarsely ground rubber, (d) rubber ignited at 550 °C which was (e) gently crushed with a spatula, (f) rubber ignited at 950 °C which was (g) gently crushed with a spatula. (i, ii, iii) indicate additional micrographs on the same sample with the same magnification.

Source: own.

Thermal treatment of rubber at 550 °C removed 41.45 m% of organic material (LOI at 550 °C for MK is just 1.29 m%) while increasing the m% of Cl (Table 3). However, Si and Al present in ignited material, not encapsulated anymore by organic material that does not react with alkali (Afshinnia and Poursaee, 2015), could now be at least partially reactive in alkali and contribute to ASN formation. Thermal treatment of coarsely ground rubber at 950 °C decreased mass by an additional 25.21 m% (0.77 m% for MK), i.e., the whole mass loss at 950 °C was 66.31 m% (2.06 m% for MK). Higher ignition temperature increased the amount of Cl, i.e., Cl could not be removed with thermal treatment up to 950 °C (it must be chemically bound in the system).

FTIR measurements of MK, Geosil, and distilled water, all crucial in alkali-activated synthesis, along with the larger rubber particles of different colours and rubber ignited at 550 °C and gently crushed with a spatula, are presented in Figure 4. From all materials present in the final product, alkali and MK contributed to the formation of ASN, according to XRF and XRD analysis of MK (Horvat et al., 2023, 2022b), to EDXS evaluation, and according to FTIR results, where not just for MK but also for the alkali (Geosil), peak (pink circle in Figure 4) indicating the presence of Si-O-Al and/or Si-O-Si bonds is present. FTIR of rubber ignited at 550 °C shows no resemblance to rubber before ignition, leading to the conclusion that bonds in the rubber degraded under temperature (as can be seen in SEM micrographs in Figure 3). As from EDXS results (Table 3), also from FTIR results of ignited waste coarsely ground rubber, ignited rubber might have the potential to be used in alkali-activation synthesis as a precursor or at least as a reactive filler because of the wide peak marked in a pink square in Figure 4. If the peak is narrow and sharp, the peak would indicate the presence of crystalline material. Because it is wide, however, it has the potential to contain amorphous content consisting of a material having Si-O-Al and Si-O-Si bonds which are crucial for ASN formation.

Worth mentioning is also that rubber ignited at 550 °C and 950 °C becomes severely hydroscopic, i.e., droplets cover the surface of the powder pressed in the XRD sample holder after being left at room conditions for a few days. The hydrophilic nature of the ignited rubber can be seen also in Figure 4 where this effect was additionally followed by FTIR on pulverized rubber ignited at 950 °C (Figure 4 (b)) while the material was exposed to room conditions during the FTIR measurement.

Table 3: Average EDXS of MK and rubber in mass percentage ($m_{\%}$) and atomic percentage ($a_{\%}$) without C, O, and elements below 0.1 $m_{\%}$.

Elements [$m_{\%}$]	Shade	Si	Al	Na	K	Ca	Mg	Ti	Fe	Cu	Zn	Sn	Ba	Pb	S	Cl	F
MK	Uniform	14.8	13.3		0.1	0.2		0.5	4.4								
Rubber fine	White	0.4	0.9			0.5	0.9	0.1	3.6	21.5	3.4	12.8	0.9		0.2	0.2	
	Light grey plates	11.0	4.8	0.5	3.8	1.1	8.6	0.2	1.0	0.3			0.1			0.2	2.9
	Middle grey random	1.7	2.8		0.2	6.0	8.2		0.3	1.3	0.5	0.1				1.7	
	Dark grey plates	1.3	0.7		0.1	1.9	1.9		0.2	0.5	1.0	0.6	0.1		0.2	0.4	
	Middle grey fibres	10.6	4.0	0.2	0.2	8.8	1.8	0.1	0.2	0.4						0.2	0.2
Rubber coarse	Light grey	0.4	1.1			3.8	1.1			0.2	0.1					7.3	
	Middle grey	2.6	3.8		0.4	3.7	4.0		0.3	0.3	0.5			0.1		0.5	0.1
	Dark grey		0.6			0.3	0.1										
Rubber fine 550 °C	White	0.3	0.7			0.3			0.3	19.1	0.5				3.7	0.4	
	Light grey	3.3	5.4	0.1	0.4	3.5	10.5		0.3	0.1	0.6		0.5		0.1	5.0	0.1
	Middle grey	2.4	3.7	0.1		3.9	2.1		0.1	0.2	0.5				0.1	5.5	
	Dark grey plates	0.7	21.2	0.2		1.0	1.0			0.2	0.6					1.1	
Rubber coarse 550 °C	Light grey	1.3	2.9			7.2	0.8		0.2	0.2	1.2			0.5		10.6	
	Grey	2.3	4.1		0.1	3.8	1.3		0.3	0.3	1.6				0.3	3.1	
Rubber coarse 950 °C	Light grey	1.0	1.1		0.2	14.7	9.6		0.2	0.3	0.5				0.2	21.6	
	Grey	7.4	7.4	0.2	0.8	17.8	0.9		0.4	0.6	3.0				0.2	5.8	
Elements [$a_{\%}$]	Shade	Si	Al	Na	K	Ca	Mg	Ti	Fe	Cu	Zn	Sn	Ba	Pb	S	Cl	F
MK	Uniform	9.5	8.9		0.1	0.1		0.2	1.6								
Rubber fine	White	0.4	0.8			0.3	0.9	0.05	1.6	7.8	1.2	2.9	0.1		0.1	0.2	
	Light grey plates	7.0	3.2	0.4	1.8	0.5	6.4	0.06	0.3	0.08			0.02			0.1	2.8
	Middle grey random	1.1	1.7		0.1	2.7	5.7		0.1	0.3	0.1	0.02				0.8	
	Dark grey leafs	0.7	0.4		0.04	0.7	1.3		0.04	0.1	0.2	0.08	0.01		0.09	0.2	
	Middle grey fibres	6.7	2.6	0.2	0.1	3.9	1.3	0.04	0.08	0.1						0.1	0.2
Rubber coarse	Light grey	0.2	0.7			1.6	0.7			0.06	0.04					3.3	
	Middle grey	1.5	2.2		0.2	1.5	2.7		0.1	0.07	0.1			0.01		0.3	0.1
	Dark grey		0.3			0.1	0.08										
Rubber fine 550 °C	White	0.2	0.5			0.2			0.1	5.5	0.1				2.1	0.2	
	Light grey	2.0	3.5	0.06	0.2	1.6	7.5		0.1	0.03	0.2		0.07		0.07	2.5	0.08
	Middle grey	1.4	2.2	0.06		1.6	1.4		0.03	0.05	0.1				0.04	2.5	
	Dark grey plates	0.4	13.5	0.2		0.4	0.7			0.05	0.2					0.5	
Rubber coarse 550 °C	Light grey	0.8	1.8			3.1	0.5		0.07	0.07	0.3			0.04		5.18	
	Grey	1.3	2.5		0.05	1.6	0.9		0.08	0.08	0.4				0.2	1.5	
Rubber coarse 950 °C	Light grey	0.7	0.8		0.1	7.6	8.2		0.07	0.1	0.2				0.1	12.6	
	Grey	5.3	5.6	0.1	0.4	9.0	0.8		0.1	0.2	0.9				0.1	3.3	

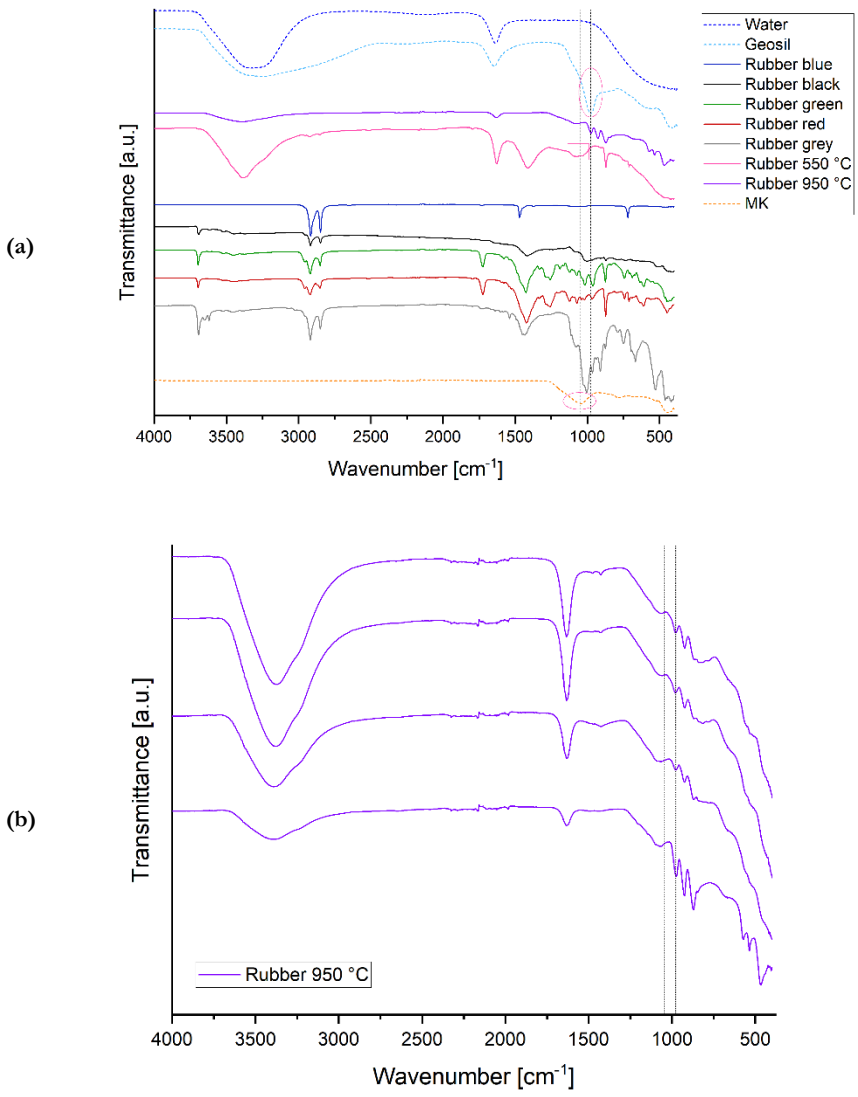

Figure 4: FTIR of (a) MK, alkali (Geosil), distilled water, larger particles of rubber of different colours, and rubber ignited at 550 °C and 950 °C. Circles denote peaks relevant to ASN formation while square denotes a potentially relevant peak for ASN formation. (b) FTIR of rubber ignited at 950 °C measured with shorter-longer exposure to room conditions (bottom to upper curve respectively).

Source: own.

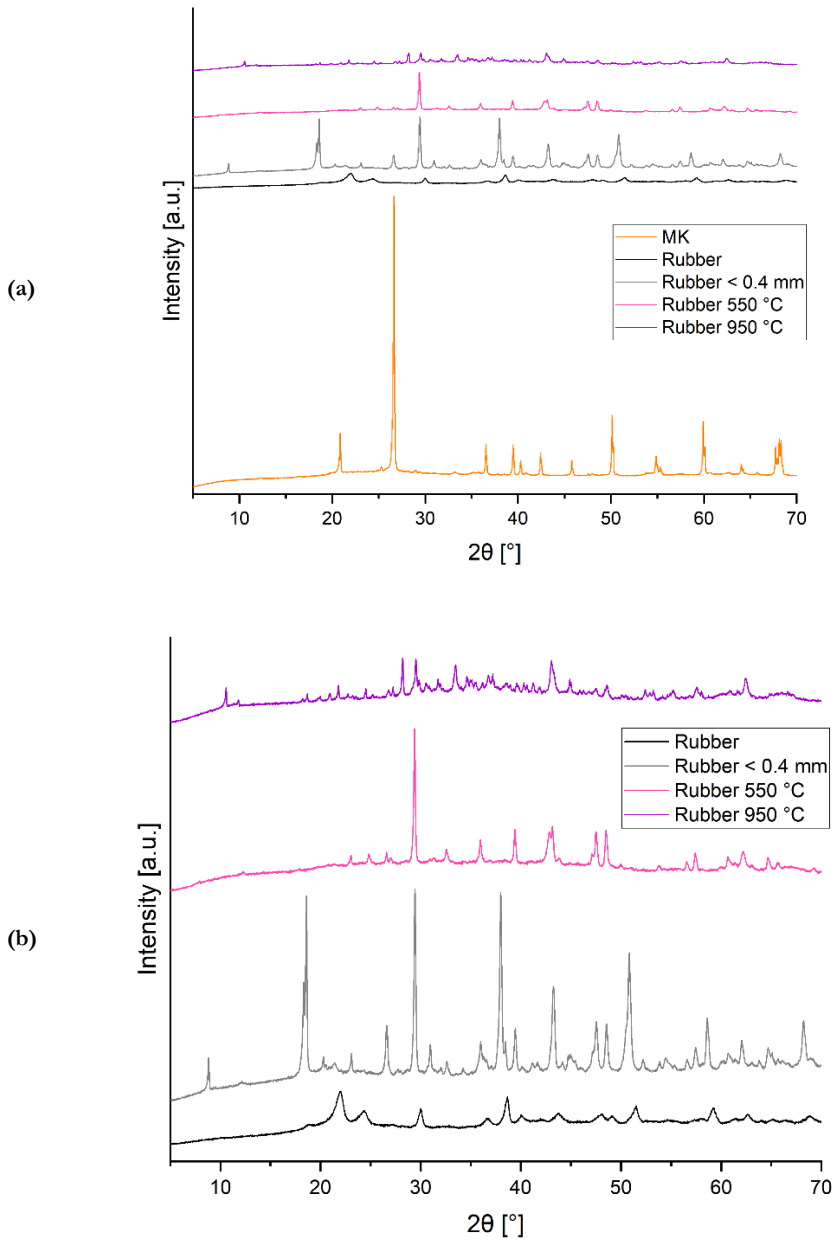

Figure 5: XRD of (a) MK, rubber as received, rubber sieved below 0.4 mm and rubber ignited at 550 °C and 950 °C crushed with a spatula, and XRD of (b) rubber solely.

Source: own.

The longer the exposure, the more prominent the water peaks (between 3000 cm^{-1} and 3500 cm^{-1}, and 1550 cm^{-1} and 1700 cm^{-1}), i.e., the bottommost curve was performed first (this curve is also shown in Figure 4 (a) while FTIR of rubber ignited at 550 °C was measured after longer exposure to room conditions).

XRD of MK and rubber (as received, fraction smaller from 0.4 mm, ignited at 500 °C and 950 °C) is shown in Figure 5. While waste coarsely ground rubber was not optimally prepared for XRD measurement (milled and sieved below at least 125 μm), it still showed crystal structure. However, its fraction, smaller from 0.4 mm, had more and more prominent peaks. While some peaks are in common with rubber ignited at 550 °C and 950 °C, the difference between all rubber patterns is noticeable.

6 Results – laboratory scale AAM

The curing procedure (treatment solely at room conditions, or also with microwaves with lower/higher power)) did not affect the adhesion of the rubber to alkali-activated metakaolin slurry but the amount of the rubber did (Figure 6). While the amount of rubber used for S_{max} was too big (excess rubber is easily removed before using the product), the amount of rubber in S_{min} could still be increased.

(a) **(b)**

Figure 6: 14-day-old samples with the surface distribution of the rubber before and after mechanical tests. Left to right: S_{min}/S_{max} cured solely at room conditions, S_{min}/S_{max} cured with microwaves for 1 min at 100 W, S_{min}/S_{max} cured with microwaves for 1 min at 1000 W.
Source: own.

In the case of the use of a bigger amount of rubber particles (S_{max}), slurry did not come in contact with all the rubber particles while in the case of a smaller amount of rubber particles (S_{min}), rubber particles got at least partially encapsulated into the

alkali-activated metakaolin slurry leaving no option for the rubber particles to be redistributed back to the environment (if the alkali-activated material does not get affected by aging and weather). However, this means not only that the amount of uniformly distributed rubber particles is important but also the force with which slurry (with certain rheological parameters) is pressed onto the rubber particles.

While curing with microwaves at 1000 W, slurry pulled the rubber even deeper inside into the prism, but at the lower energy of microwaves, the depth of the rubber particles was influenced solely by the pressure while moulding. This means that adhesion forces between the alkali-activated metakaolin slurry and rubber particles were strong enough for the rubber to move with the slurry while it was physically foamed (microwave irradiation at 1000 W) (Horvat et al., 2023, 2022b) and in this way, rubber did not negatively influence the newly formed bonds in the alkali-activated material.

As in the case of the surface distribution of the rubber particles, it is also in the case of their volumetric distribution (Figure 7), i.e., the adhesion of the rubber particles with metakaolin slurry, regardless of the curing, was satisfactory. It is almost impossible for the rubber particles to be distributed back into the environment, even more, cutting alkali-activated metakaolin foam on its sides (slurry cured with microwaves at 1000 W, 3rd prism from the left in Figure 7) did not pull rubber particles out from the alkali-activated foam but cut them just as the alkali-activated foam's skeleton was cut (most right prism in Figure 7 (a)).

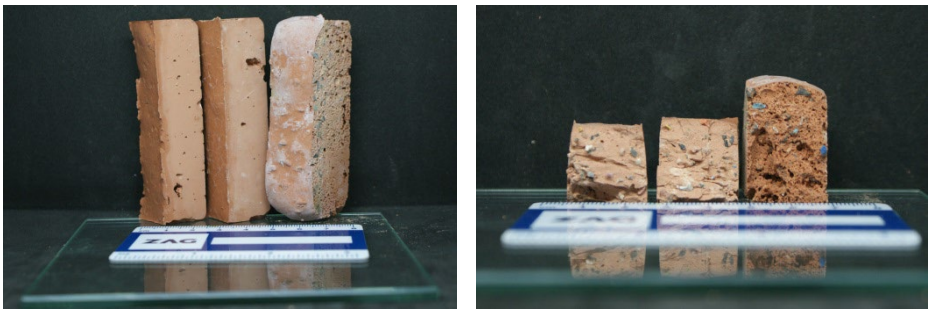

(a) **(b)**

Figure 7: 14-day-old samples with the volumetric distribution of the rubber before and after mechanical tests. Left to right: V cured solely at room conditions, V cured with microwaves for 1 min at 100 W, and V cured with microwaves for 1 min at 1000 W.

Source: own.

Mechanical strengths (compressive and bending) and the geometrical densities of 14-day-old samples are shown in Figure 8. Densities are affected by the addition of the rubber particles but this effect is lesser when compared to non-foamed (curing at room conditions and with microwaves at 100 W) and foamed (microwave irradiation at 1000 W) alkali-activated metakaolin. Compressive strength is higher if samples were cured with microwaves at 100 W due to enhancement in the dissolution of ingredients, and the smallest if samples were cured with microwaves at 1000 W due to the foaming effect (Horvat et al., 2023, 2022b). A logical decrease in compressive strength occurs when rubber is volumetrically spread while the not-expected higher compressive strength happens in the surface addition of a higher amount of rubber particles.

SEM micrographs of AAMs with a focus on the encapsulation of the rubber in the AAM with volumetrically spread rubber are shown in Figure 9. In samples cured at room conditions and at 100 W for 1 min, all rubber particles were at least partially covered with random-shaped, sharp-edged particles of a similar grey shade as the ASN and also as the non-reacted parts of MK. Those particles are found also in the holes where rubber particles were located (Figure 9 (b-1)).

The sample that was treated at 1000 W for 1 min (Figure 9 (c)), which was enough for the sample to foam and completely harden, was enough also for the encapsulation of the rubber by completely trapping it in the AAM but had just a few rubber particles that had a new layer on their surface, i.e., under SEM, they were very hard to find (Figure 9 (c_i)). On the other hand, for samples treated solely at room conditions or at 100 W for 1 min, rubber without a significant amount of less organic particles on its surface was hard or impossible to find.

Semi-quantitative chemical analysis, EDXS, of the ASN and rubber is presented in Table 4 (areas of the acquisition of the signal are shown in the Supplement Figure S3). As elemental composition in the ASN can be compared among samples cured with different procedures, so can be elemental composition acquired on the rubber with the greyish surface, which is just a bit darker grey than ASN itself. However, particles present on the surface of the rubber are chemically comparable to ASN and not to the rubber with the greyish layer.

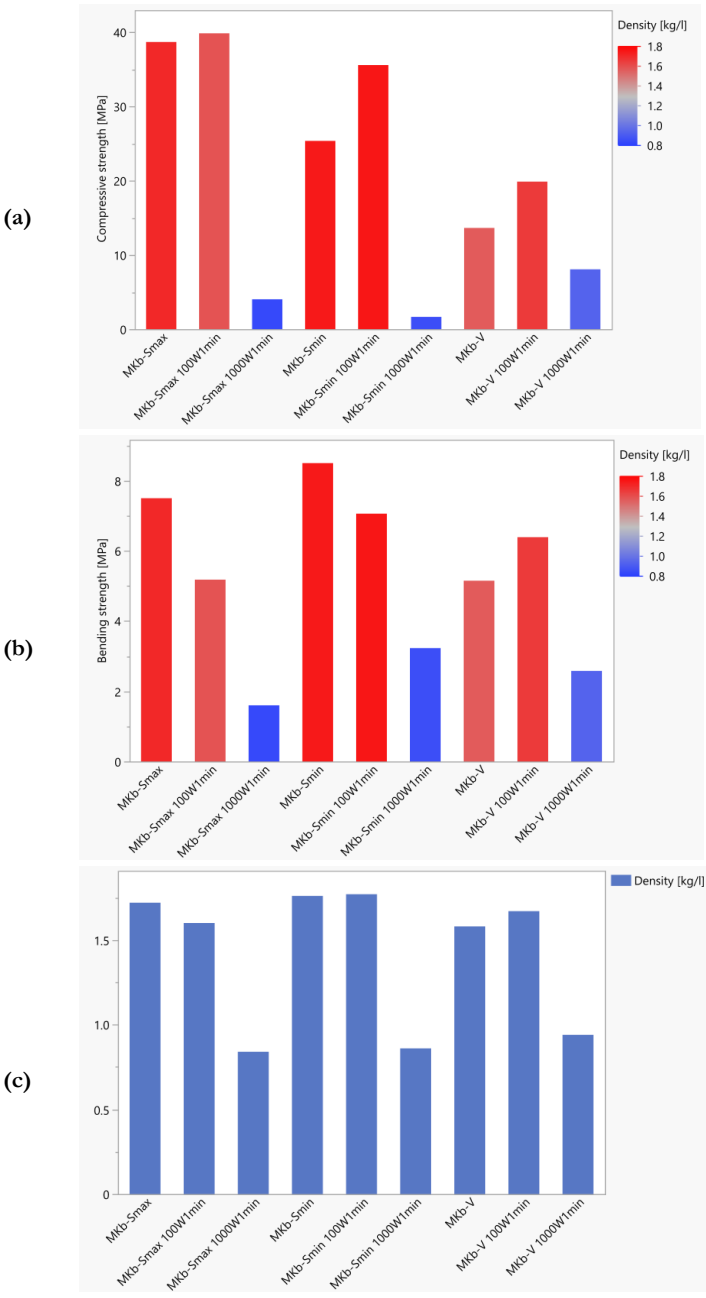

Figure 8: Mechanical strengths and geometrical density of 14-day-old samples.

Source: own.

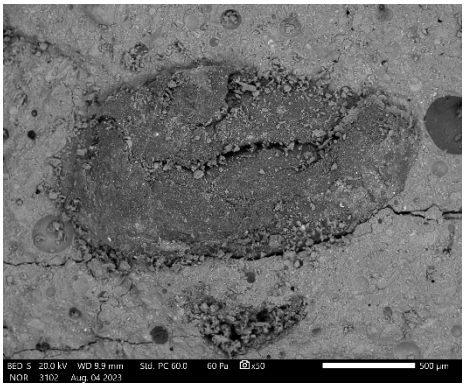

(a-1)

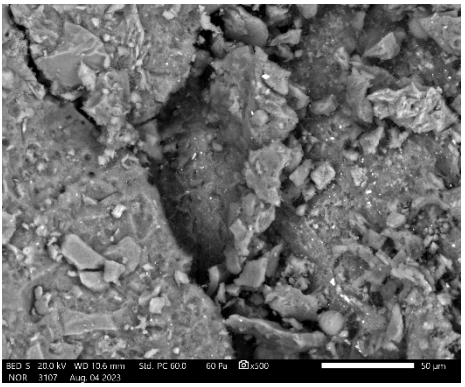

(a-2)

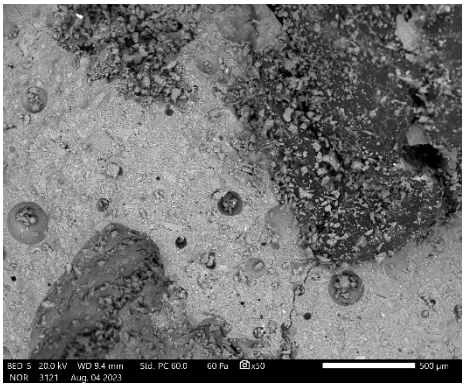

(b-1)

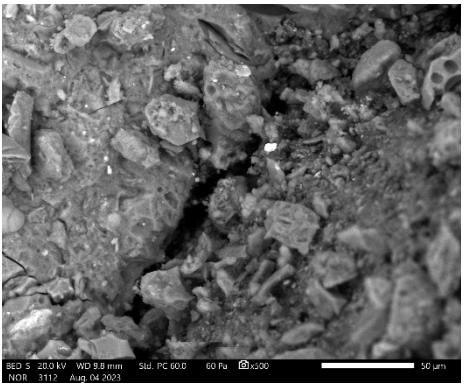

(b-2)

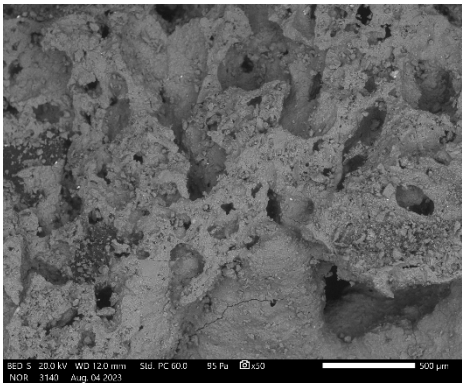

(c-1)

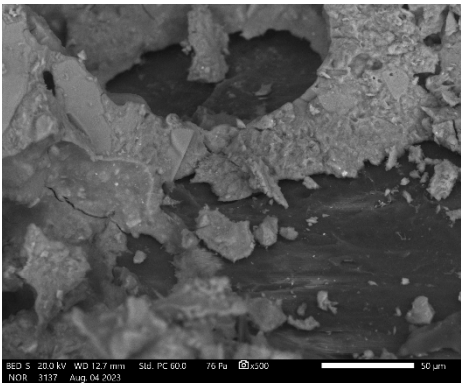

(c-2)

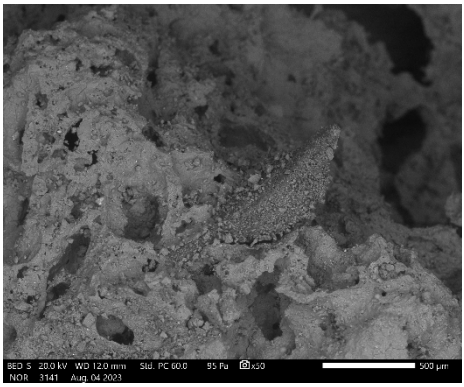

(c_i-1)

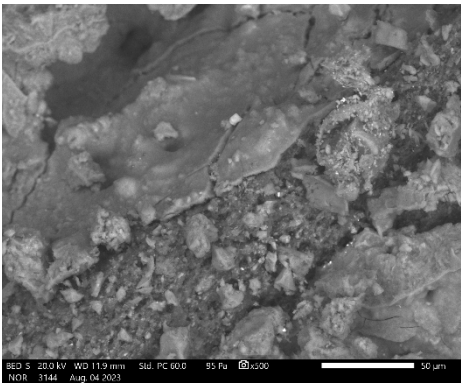

(c_i-2)

Figure 9: SEM micrographs of AAMs with volumetrically spread rubber (V) cured at (a) room conditions, (b) at 100 W for 1 min, and (c, c_i) 1000 W for 1 min where micrographs are (1) 50-times and (2) 500-times magnified.

Source: own.

Table 4: Average EDXS of AAM in mass percentage ($m_{\%}$) and atomic percentage ($a_{\%}$) without C, O, and elements below 0.1 $m_{\%}$.

Elements [$m_{\%}$]	Si	Al	Na	K	Ca	Mg	Ti	Fe	Cu	Zn	W	Cl
ASN V T_0	20.3	10.6	7.0	0.1	0.4		0.5	1.0				0.1
Rubber layer V T_0	2.6	7.1	1.0	0.1	2.0	1.3	0.1	0.3	0.3	0.1		0.6
ASN V 100W	20.0	7.5	5.4	0.1	0.3		0.3	2.2			0.3	
Rubber layer V 100W	4.2	3.0	1.3	0.1	0.5	0.2		0.3		0.3		
Particle on rubber V 100W	16.1	9.1	6.1	0.1	0.8		0.4	1.0			0.1	
ASN V 1000W	16.3	7.4	8.8		0.5		0.4	1.0				
Rubber layer V 1000W	7.8	4.9	5.5	0.2	1.9		0.3	0.5		0.3		0.1
Rubber dark V 1000W	0.3	0.1	0.3									
Elements [$a_{\%}$]	Si	Al	Na	K	Ca	Mg	Ti	Fe	Cu	Zn	W	Cl
ASN V T_0	13.5	7.3	5.7	0.05	0.2		0.2	0.3				0.06
Rubber layer V T_0	1.5	4.2	0.7	0.05	0.8	0.9	0.04	0.09	0.08	0.03		0.3
ASN V 100W	13.1	5.1	4.3	0.05	0.1		0.1	0.7			0.03	
Rubber layer V 100W	2.4	1.7	0.9	0.05	0.2	0.2		0.08		0.07		
Particle on rubber V 100W	10.3	6.1	4.7	0.06	0.3		0.1	0.3				
ASN V 1000W	10.4	4.9	6.8		0.2		0.1	0.3				
Rubber layer V 1000W	4.7	3.1	4.1	0.09	0.8		0.1	0.1		0.07		0.06
Rubber dark V 1000W	0.2	0.08	0.2									

FTIR of all AAMs (while trying to exclude the rubber at the sample preparation), presented in Figure 10, shows similar behaviour for AAMs cured in the same manner no matter the addition of the rubber. The higher the energy input into the curing, the lower the presence of the water (peak between approximately 3000 cm^{-1} and 3600 cm^{-1}, and peak with minima around 1640 cm^{-1}) and the shift of the minima of the "ASN" more towards the MK (to the left), i.e., away from the "ASN" peak of the alkali.

For XRD measurement AAMs were crushed in mortar with pastel and sieved below 0.4 mm to remove at least larger rubber particles. All patterns are similar (Figure 11), showing impact from MK, which means that at least the majority of the rubber particles were successfully removed, i.e., they were removed beyond detection. As reported before, curing at room temperature solely or also with microwaves does not affect alkali activation on a crystalline level (Horvat et al., 2022c). The same does not addition of rubber.

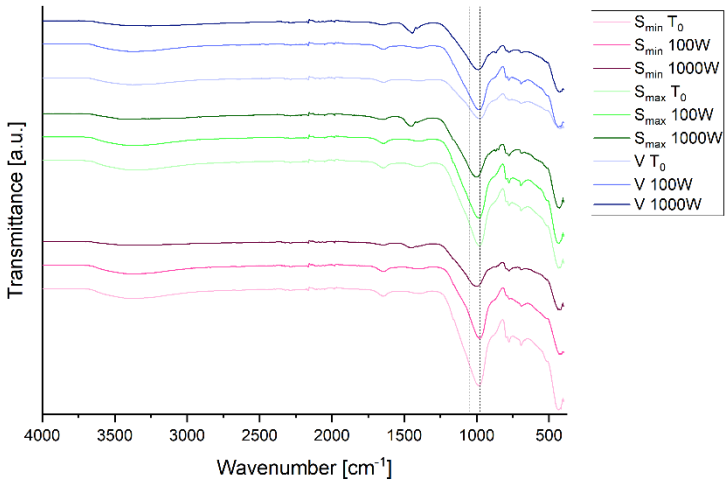

Figure 10: FTIR of AAMs (S_{min}, S_{max}, V) cured at room conditions (T_0), and for 1 min at 100 W or 1000 W. Vertical dotted lines represent "ASN" peak minima for MK (left) and alkali (right).

Source: own.

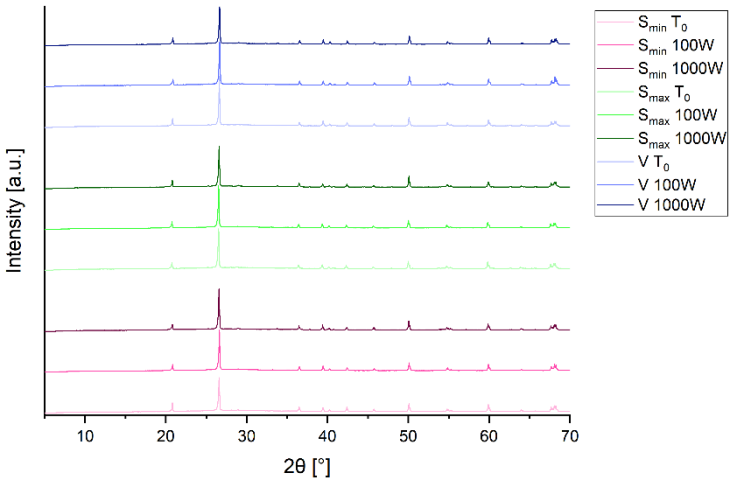

Figure 11: XRD of AAMs (S_{min}, S_{max}, V) cured at room conditions (T_0), and for 1 min at 100 W or 1000 W.

Source: own.

7 Results – pilot products

Upscaling of material presents additional challenges that can not be spotted on a laboratory scale, i.e., the path to perfect pavement stones is presented in Figure 12, and the Supplement in Figure S1. If de-moulding was too early (Figure 12 (a)), the bottom surface of the AAM was rough, with bubbles and the pavement stone was curved. If samples were de-moulded at least 2 hours after moulding (Figure 12 (c)), "slurry" was already hardened enough and could not be inflicted by the gentle de-moulding. However, samples that were de-moulded 24 hours after casting the slurry into the moulds were completely hardened and could not be inflicted by de-moulding at all.

Besides pavement stones having no curvature, if de-moulding was done later, the constantly present load on top of the slurry resulted in pavement stone having a smooth shiny surface where there were no (or hardly any) bubbles seen (Figure 12 (b)).

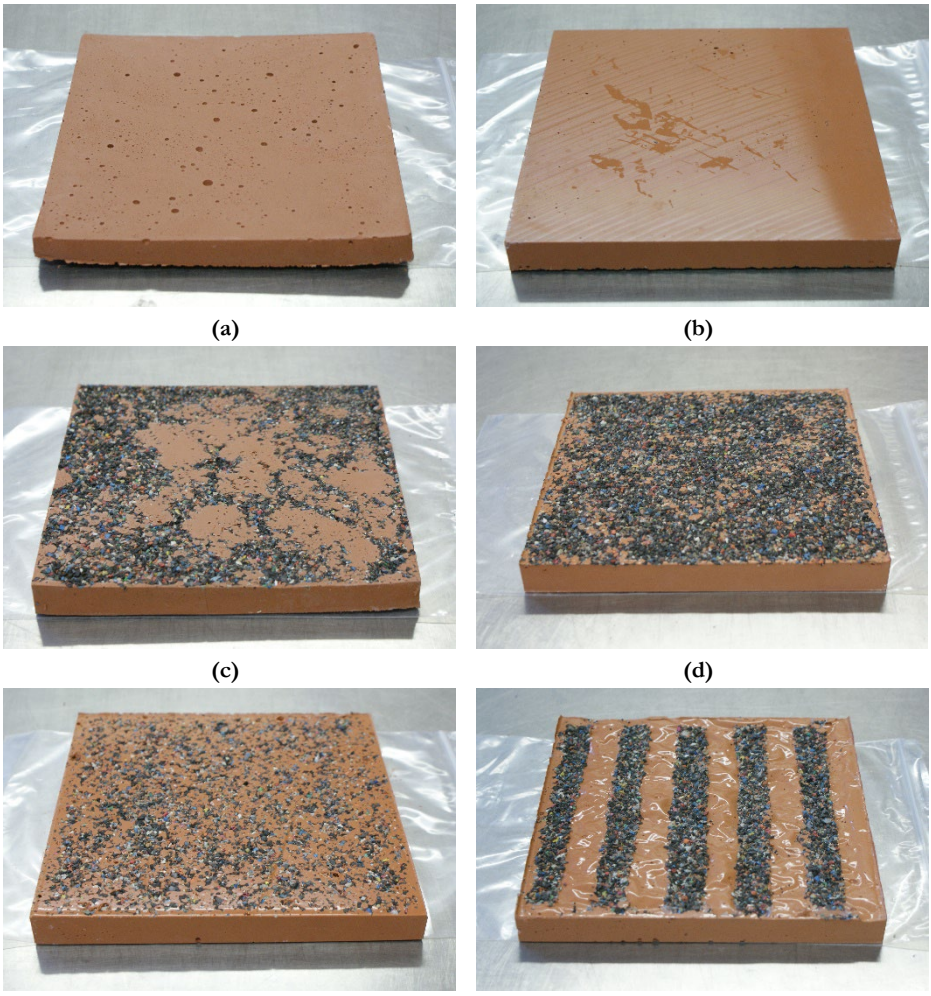

Figure 12: (a) MK_b de-moulded after 1 hour, and (b) after 24 hours, both pressed with "stone". (c) S_{max} with rubber particles on the bottom and pressed with the highest used force, de-moulded after 2 hours. De-moulded after 24 hours (d) S_{max} with rubber particles on the top and pressed with "stone", (e) S_{min} with rubber particles on the top and pressed with "stone", (f) S_{max} with PVC stripes on the top covered with rubber particles and pressed with the smooth stone.

Source: own.

If the coarsely ground rubber was uniformly sprinkled on the bottom of the mould, putting the highly viscous slurry over rubber particles changed their distribution into random, i.e., highly dependent on the moulding procedure (Figure 12 (c)). If the

pressure inflicted onto the casted slurry was too high, the slurry started escaping the mould next to the smooth stones placed on top of the slurry (placement of the stone is shown in Figure S1). Nonetheless, in this stage, it was still possible to correct the future pavement stone, i.e., the slurry was just put back into the mould, covered with PVC again, and with smooth stone that offered constant pressure onto the slurry.

To maintain a uniform distribution of the rubber particles over the entire surface, it was necessary to sprinkle coarsely ground rubber on top of the formed and already moulded slurry precisely and evenly (the procedure is shown in the Supplement in Figure S1). While the amount of rubber used in the S_{min} sample was fully integrated into the pavement stone (Figure 12 (e)), the amount of rubber used in S_{max} was exceeded. From the difference between used and fallen-off rubber, the amount of the integrated rubber into the slurry while being pressed by 0.76 kPa is approximately 0.11 g/cm^2.

To evaluate the hypothesis behind this work that the *addition of the coarsely ground rubber onto the surfaces of alkali-activated pavement stones enhances walking safety*, slipperiness was evaluated on not curved pavement stones in dry and wet conditions and is presented in Table 5. The lower the angle of the measurement, the lower the friction and the higher the slipperiness. Taking into account, that the wet walking surface defined as slippery for areas with a higher frequency of users (hospitals, shopping centres) is 35°or lower, and for all other areas 25°, the alkali-activated MK without rubber (mixture MK_b) is highly slippery for all areas. However, the minimal addition of the coarsely ground rubber used in this work (S_{min}) is enough to consider the pavement stones to be non-slippery for areas with lower frequencies, but it is still not good enough for high-frequency areas. For those areas, the maximal addition of the rubber used (S_{max}) was satisfactory, especially if the rubber was placed with a pattern (stripes) and not uniformly all over the surface. The result in the wet conditions was similar for striped pavement stone when tested parallel or perpendicular to the stripes, i.e., 5 $S_{\%}$ (surface percentage) bigger rubber contact surface (more rough area) for pendulum sliding over pavement stone parallel to the stripes was an insignificant difference for the overall coefficient of the friction.

Worth taking into consideration is also that all the pavement stones prepared with the maximal amount of the coarsely ground rubber did not have perfectly smooth surfaces (hills and valleys), i.e., movement of the pendulum could have been additionally hindered by it and not solely by the addition of the rubber.

Table 5: Angle reached by a pendulum which slid over the surface of the pavement stone.

Sample	Angle [°]	
	Dry	**Wet**
MK_b	63.8	14.6
S_{min} rubber up	64.0	27.4
S_{max} rubber up	57.2	36.4
S_{max} rubber down and bigger force	67.8	57.8
S_{max} rubber up and striped – parallel	54.4	45.4
S_{max} rubber up and striped – perpendicular	68.6	45.6

8 Conclusions

The hypothesis that the coarsely ground waste rubber spread onto the surface of alkali-activated slurry can give to the alkali-activated material's surface enhancement in being non-slippery was proven in this preliminary work. However, the optimal amount of addition of the rubber particles should be evaluated in further work, as well as the most optimal pattern of the rubber on the pavement stone's surface, and forces that offer good encapsulation of the rubber and the highest possible friction in the wet conditions.

Besides that, coarsely ground waste rubber has a high potential to be used on the surface of alkali-activated materials if ignited at 550 °C or 950 °C. While showing a high hydroscopic effect, it could be used as a precursor in alkali activation and not just as a filler.

Acknowledgment

This work is part of the ARRS project of Barbara Horvat, Ph.D., and was financially supported by the Slovenian Research Agency under Grant No. J2-3035 and also by Slovenian Research Agency program group no. P2-0273.

References

Afshinnia, K., Poursaee, A., 2015. The influence of waste crumb rubber in reducing the alkali–silica reaction in mortar bars. Journal of Building Engineering 4, 231–236. https://doi.org/10.1016/j.jobe.2015.10.002

Češnovar, Traven, Horvat, Ducman, 2019. The Potential of Ladle Slag and Electric Arc Furnace Slag Use in Synthesizing Alkali Activated Materials; the Influence of Curing on Mechanical Properties. Materials 12, 1173. https://doi.org/10.3390/ma12071173

Coran, A.Y., 2013. Vulcanization, in: The Science and Technology of Rubber. Elsevier, pp. 337–381. https://doi.org/10.1016/B978-0-12-394584-6.00007-8

Flory, P.J., n.d. Molecular Theory of Rubber Elasticity. Polymer Journal 17, 1–12.

Horvat, B., Češnovar, M., Traven, K., Pavlin, M., König, K., Ducman, V., 2022a. Influence of Homogenization of Alkali-Activated Slurry on Mechanical Strength, in: 3rd International Conference on Technologies & Business Models for Circular Economy: Conference Proceedings. Presented at the International Conference on Technologies & Business Models for Circular Economy, University of Maribor Press, pp. 11–50. https://doi.org/10.18690/um.fkkt.2.2022.2

Horvat, B., Ducman, V., 2020. Influence of Particle Size on Compressive Strength of Alkali Activated Refractory Materials. Materials 13, 2227. https://doi.org/10.3390/ma13102227

Horvat, B., Ducman, V., 2019. Potential of Green Ceramics Waste for Alkali Activated Foams. Materials 30. https://doi.org/doi:10.3390/ma12213563

Horvat, B., Ducman, V., Pavlin, A.S., 2019a. Waste Foundry Sand as Precursor in Alkali Activation Process. Livarski vestnik 66, 13.

Horvat, B., Mušič, B., Pavlin, M., Ducman, V., 2023. Microwave Irradiation of Alkali-activated Metakaolin Slurry, in: 5th International Conference on Technologies & Business Models for Circular Economy: Conference Proceedings. Presented at the International Conference on Technologies & Business Models for Circular Economy, University of Maribor Press, pp. 9–24. https://doi.org/10.18690/um.fkkt.1.2023.2

Horvat, B., Mušič, B., Pavlin, M., Ducman, V., 2022b. Microwave irradiation of alkali-activated metakaolin slurry. Presented at the 5th International Conference on Technologies & Business Models for Circular Economy. https://doi.org/10.18690/um.fkkt.6.2022

Horvat, B., Pavlin, A.S., Ducman, V., 2019b. Foundry wastes as potential precursor in alkali activation technology, in: Technologies & Business Models for Circular Economy. Presented at the 2nd International Conference on Technologies & Business Models for Circular Economy, Univerzitetna založba Univerze v Mariboru/University of Maribor Press.

Horvat, B., Pavlin, M., Ducman, V., 2022c. Influence of microwaves in the early stage of alkali activation on the mechanical strength of alkali-activated materials. Ceramics International. https://doi.org/10.1016/j.ceramint.2022.12.133

Leong, S.-Y., Lee, S.-Y., Koh, T.-Y., Ang, D.T.-C., 2023. 4R of rubber waste management: current and outlook. J Mater Cycles Waste Manag 25, 37–51. https://doi.org/10.1007/s10163-022-01554-y

Miller, N., n.d. The industry creating a third of the world's waste [WWW Document]. URL https://www.bbc.com/future/article/20211215-the-buildings-made-from-rubbish (accessed 7.18.23).

Mutalib, N.A.N.A., Mokhatar, S.N., Budiea, A.M.A., Jaini, Z.M., Kamarudin, A.F., Noh, M.S.M., 2021. A review: Study on waste rubber as construction material. IOP Conf. Ser.: Mater. Sci. Eng. 1144, 012003. https://doi.org/10.1088/1757-899X/1144/1/012003

Nuzaimah, M., Sapuan, S.M., Nadlene, R., Jawaid, M., 2018. Recycling of waste rubber as fillers: A review. IOP Conf. Ser.: Mater. Sci. Eng. 368, 012016. https://doi.org/10.1088/1757-899X/368/1/012016

Pavlin, M., Horvat, B., Frankovič, A., Ducman, V., 2021. Mechanical, microstructural and mineralogical evaluation of alkali-activated waste glass and stone wool. Ceramics International S0272884221004168. https://doi.org/10.1016/j.ceramint.2021.02.068

Škvára, F., 2007. Alkali Activated Material - Geopolymer 16.

Supplement

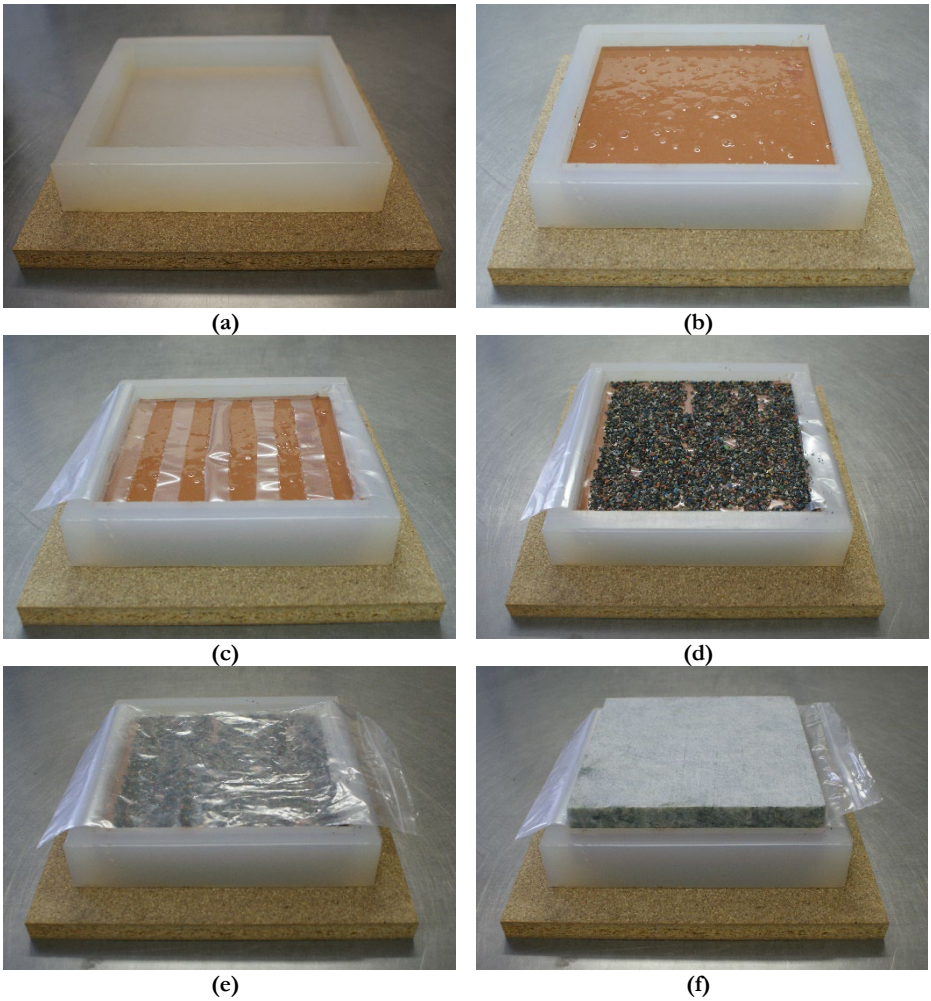

Figure S1: Pavement stone-making procedure.
Source: own.

EDXS areas of the acquisition of the signal from rubber are shown in Figure S2 and are labeled according to Table 3.

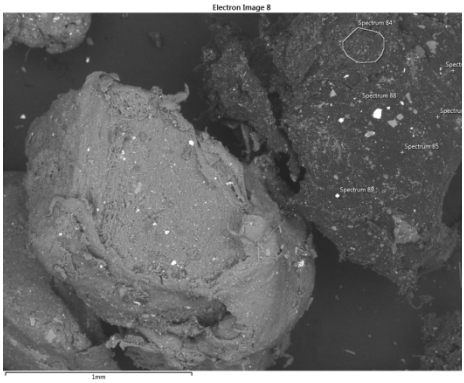

(b-dark grey)

(b-light grey)

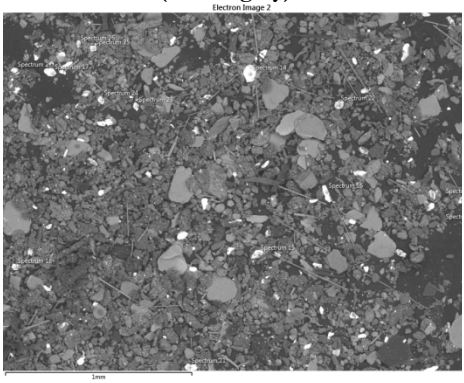

(c-white)

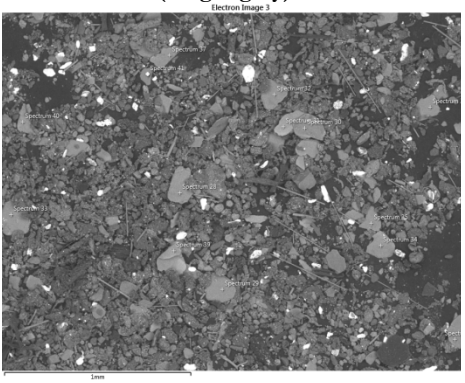

(c-light grey)

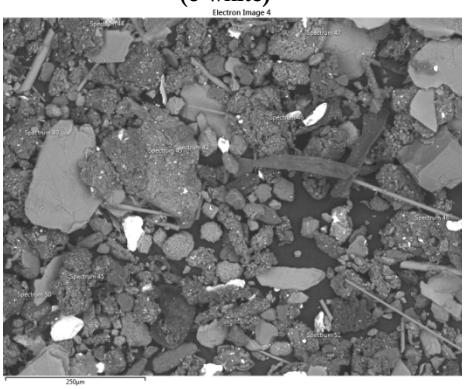

(c-middle grey random)

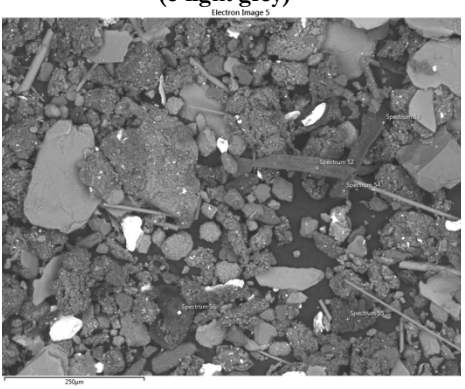

(c-dark grey leaves)

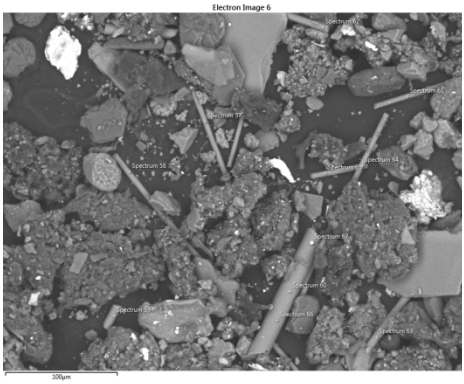

(c-middle grey fibres)

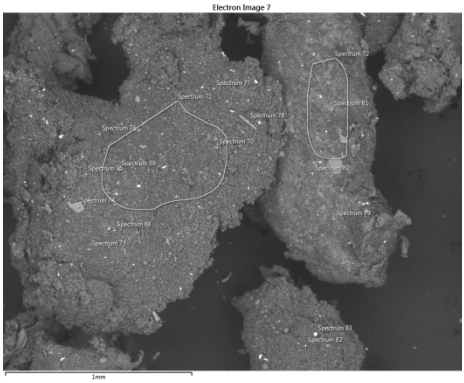

(c-middle grey)

(d-light grey/grey)

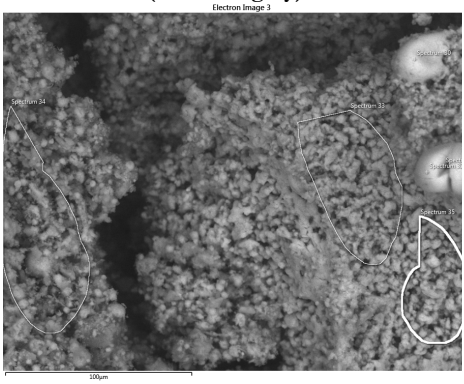

(d-light grey)

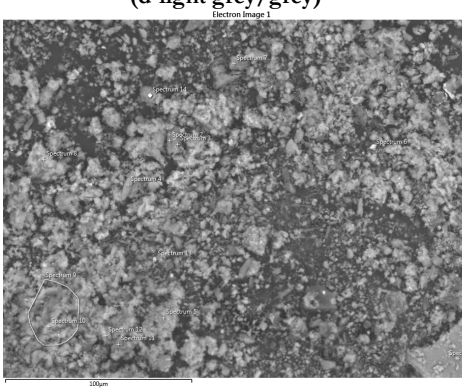

(e-light grey)

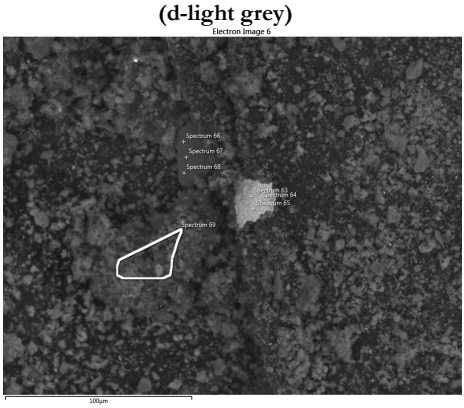

(e-white/middle grey/plates)

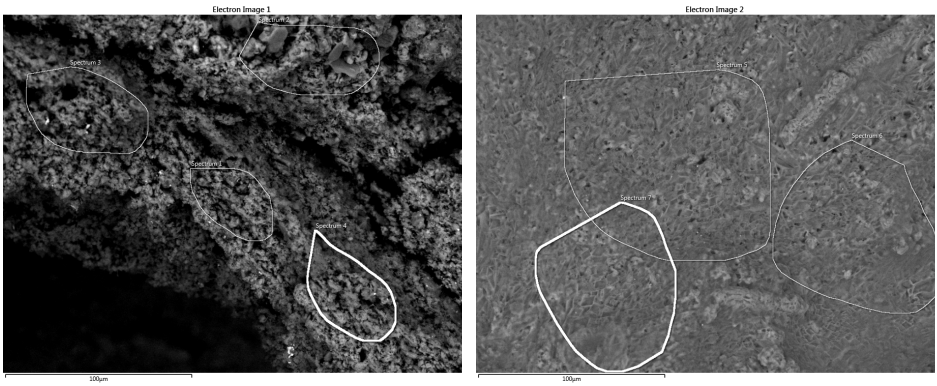

(f-grey) **(f-light grey)**

Figure S2. Locations of EDXS analysis performed on (b) coarse rubber and (a) fine rubber, and on rubber ignited at 550 °C (d) without and (e) with the gentle crushing of ignited rubber, and (f) ignited at 950 °C. Areas of the acquisition are labeled according to their greyscale and shape.

Source: own.

EDXS areas of the acquisition of the signal from ASN and rubber incorporated in the AAM are shown in Figure S3.

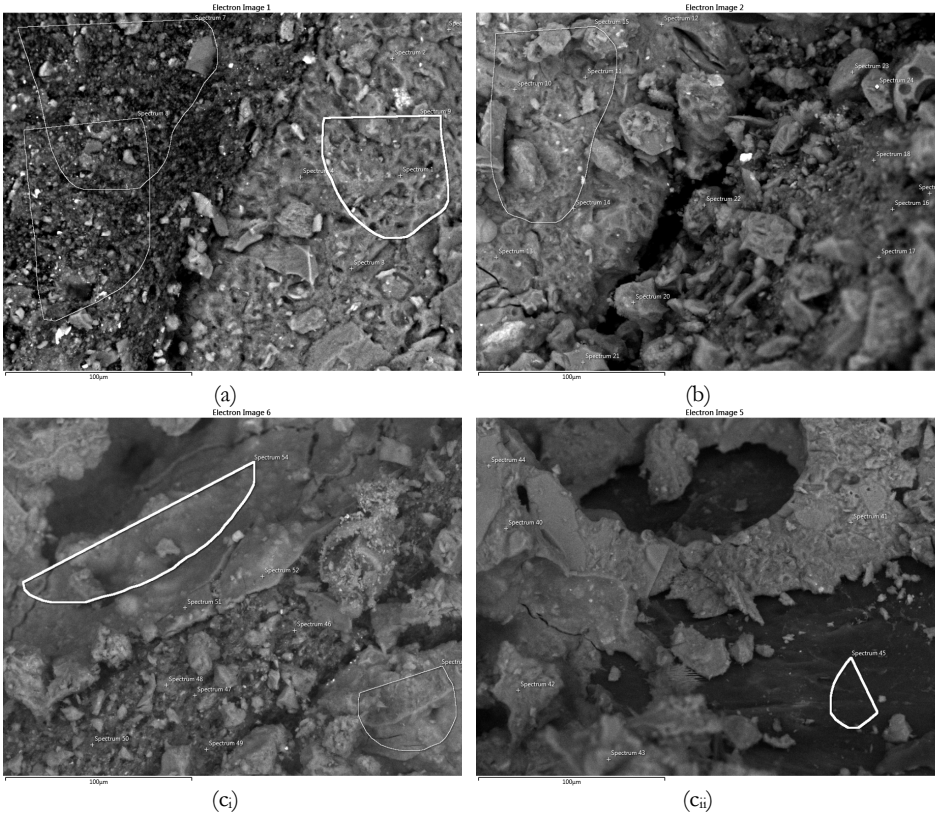

Figure S3: Locations of EDXS analysis performed on AAM cured (a) solely at room conditions, (b) at 100 W for 1 min, and (c_i, c_{ii}) at 1000 W for 1 min.
Source: own.

Production of Micellar Structures From Medicinal Mushrooms

Nika Kučuk, Mateja Primožič, Željko Knez, Maja Leitgeb

University of Maribor, Faculty of Chemistry and Chemical Engineering, Laboratory of Separation Processes and Product Design, Maribor, Slovenia
nika.kucuk@um.si, mateja.primozic@um.si, zeljko.knez@um.si, maja.leitgeb@um.si

DOI
https://doi.org/10.18690/um.fkkt.1.2024.3

ISBN
978-961-286-829-1

Fungal micellar membranes, which consist of cellulose, chitin, and proteins, are one of the important and largest groups of microorganisms. Micellar structures are promising biological materials with great advantages, because they can be adapted very well to different cultivation parameters, are biodegradable and their production is relatively inexpensive. Their fibrous structure makes them very promising for biotechnological and cosmetic applications, but also for various industries such as packaging and construction. The therapeutic mushrooms Ganoderma lucidum and Pleurotus ostreatus were used for the production of micellar membranes. In addition, the morphological, chemical, and hydrodynamic properties were also investigated. Micellar membranes were successfully obtained from both therapeutic mushrooms. By optimizing the growth parameters, it was possible to achieve the highest yield and the highest water absorption capacity of the micellar membranes with advantageous characteristics.

Keywords:
micellar structures, medicinal mushrooms, *Ganoderma lucidum*, *Pleurotus ostreatus*, characterization

University of Maribor Press

1 Introduction

In recent years, the preparation of smart biological materials, sustainable and environmentally friendly products for biomedical applications has become increasingly important (Silva et al. 2021). Various natural, sustainable resources, such as lignin, cellulose, pectin, protein products, etc., are the most important resources for the production of biopolymeric materials. These are environmentally friendly, biodegradable and renewable materials, with many other important characteristics (Baranwal et al. 2022). However, the main problems in obtaining these biopolymer-based materials are the high costs of the development process and purification. Furthermore, production must be accompanied by a high yield of products (Perera et al. 2023).

Therefore, the synthesis of polymeric vital substances (carbohydrates) from biological resources such as fungi (mushrooms) represents an innovative approach, as it is simple, economical, high-yielding and less time-consuming (Martinez-Medina et al. 2021; Sivaprasad et al. 2021).

The micellar structures originating from fungi, which consist mainly of cellulose, chitin and proteins, represent one of the largest groups of microorganisms (Manan et al. 2021). The mycelium is the vegetative part of the fungus and consists of a large group of interwoven hyphae. Micellar structures are important biological materials with many advantages. They can adapt to different growth conditions, are biodegradable and their production is associated with low costs (Majib et al. 2023). Their fibrous structure makes them unique and promising for use in various biological fields. A major advantage of using micellar films over bacterial cellulose membranes is the final purification process, as this step only requires heat treatment of the film (Antinori et al. 2021; Haneef et al. 2017).

Micellar membranes based on medicinal mushrooms are fibrous and self-growing polymeric biocomposites with acceptable properties. They have the ability to strongly mimic the extracellular matrix of human tissue. Micellar structures are potential bioscaffolds, which is why their use in tissue engineering is particularly promising (Alaneme et al. 2023; Khamrai et al. 2018). The desired properties of coatings or wound healing patches include protection of the wound by limiting the loss of body fluid, reduction of water loss from the patches, compatibility with tissue,

and high mechanical strength, which can be achieved by a film of micellar structures (Verma et al. 2023).

The aim of the study was to obtain micellar structures from *Ganoderma lucidum* and *Pleurotus ostreatus*, which are important representatives of medicinal mushrooms. In order to achieve the highest yield of micellar structures and the maximum water absorption capacity, various growth parameters were optimized. A scanning electron microscopy (SEM) analysis was performed to determine the morphological characteristics of the micellar structures and to measure the diameter of the pores and hyphae. Fourier transform infrared spectroscopy (FT-IR) was used to investigate the presence of chemical functional groups on the surface of micellar membranes. In addition, the hydrophilicity/hydrophobicity of the surface of the membranes was evaluated by determining the contact angle. The kinetics of swelling were also investigated. Figure 1 presents the experimental design of the study.

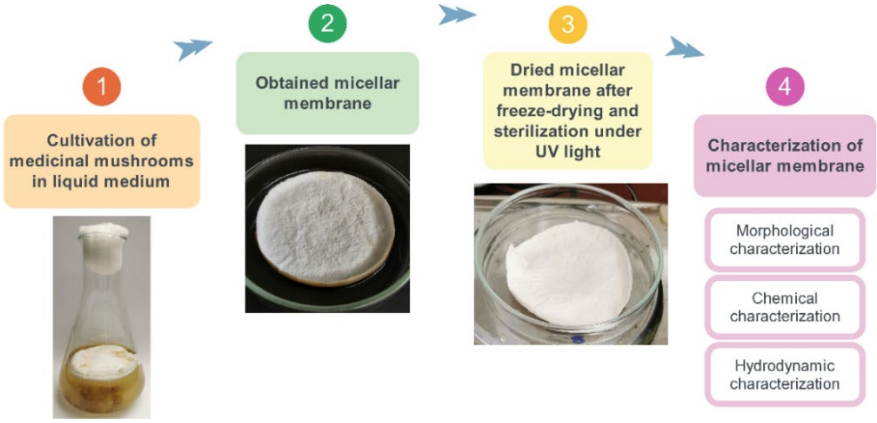

Figure 1: Experimental design
Source: own.

2 Materials and methods

2.1 Preparation of mycelium membranes

The freshly prepared fungal culture of *P. ostreatus* and *G. lucidum* was transferred to the liquid growth medium in the Erlenmeyer flasks and incubated at 27 °C under static conditions. After complete growth, the resulting micellar membranes were

removed from the culture medium and purified by subsequent washing with deionized water. The micellar membranes were subjected to a freeze-drying process. They were then sterilized under UV light.

2.2 Water uptake capacity

To determine the water uptake capacity, the micellar membranes were cut into pieces of 10 mm diameter. The dry membranes were first weighed and then immersed in deionized water at room temperature. The membrane pieces were removed from the water and placed on blotting filter paper to remove the excess, unabsorbed water molecules on the membrane surface. The percentage of swelling was calculated using Equation 1:

$$\%\ of\ swelling = \frac{w_{wet} - w_{dry}}{w_{dry}} \cdot 100 \quad (1)$$

where w_{wet} represents the weight of wet micellar membranes, and w_{dry} represents the weight of dry micellar membranes.

2.3 Scanning Electron Microscopy Analysis

SEM analysis was performed using a scanning electron microscope (FE, SEM SIRION, 400 NC, and FEI) to examine the morphology of the dried mycelial membranes. The diameter of the hyphae and the diameter of the pores in the membranes were determined. Before analysis, the membranes were coated with a layer of gold.

2.4 Fourier Transform Infrared Spectroscopy (FT-IR)

FT-IR analysis was performed to determine the presence of chemical functionalities on the surface of the obtained micellar membranes. The spectra were detected over a 4000–500 cm−1 range and recorded by the FT-IR spectrophotometer (Perkin Elmer 1600 Fourier transform infrared spectroscopy).

2.5 Determination of hydrophobicity/hydrophilicity of membranes

The hydrophobicity or hydrophilicity of the surface of the micellar membranes was determined by measuring the contact angle with a digital camera Basler Aca1300-200um connected to a computer with a CCTV lens (Tamron, Japan) using the Open Drop algorithm. The membrane samples were illuminated, then the water absorption in the membrane was recorded with a camera. The contact angle was measured using the ImageJ program.

3 Results and discussion

Micellar membranes were successfully prepared from the two selected therapeutic mushrooms *P. ostreatus* and *G. lucidum*. After harvesting, the mycelium was completely inactivated to stop its growth, one of the most important properties for possible use as a potential bio-scaffold. Freeze-dried mycelial membranes were sterilized under UV light. The mycelial membranes were spread on potato dextrose agar (PDA) plates and did not regrow. Both fungal strains appeared inactive after UV light treatment.

The maximum yield of micellar membranes with favorable properties and the highest water uptake capacity was achieved by the combination of selected cultivation parameters. The best characteristics for micellar membranes of *G. lucidum* were obtained with malt extract medium and of *P. ostreatus* with glucose medium. The composition of the optimal media (malt extract medium and the glucose medium) is shown in Table 1. Complete growth of the mycelial membranes of *G. lucidum* and *P. ostreatus* was achieved after 14 days and 21 days at a constant temperature of 27 °C under static conditions.

Table 1: The composition of the optimal medium.

Growth medium	Chemical	Concentration (g/L)
Malt extract medium	Malt extract	10.00
	Yeast extract	4.00
Glucose medium	Glucose	49.20
	Yeast extract	4.90
	KH_2PO_4	0.88
	$MgSO_4 \cdot 7\ H_2O$	0.50

The average diameter of the mycelial membranes obtained was measured with a beak scale. In general, the membranes of *G. lucidum* were slightly heavier and thicker than those of *P. ostreatus*.

SEM examinations determined the average diameters of hyphae and pores. The micellar structures of *P. ostreatus* resulted in a larger average diameter of the hyphae. However, the membranes of *G. lucidum* were found to have a larger average pore diameter.

Using FT-IR analysis, no significant differences in the chemical functionalities of the micellar structures were detected when different liquid growth media were used.

Table 2 presents characteristics of the obtained micellar membranes grown in the optimal medium for both medicinal mushrooms used.

Table 2: The characteristics of the obtained micellar membranes grown in the optimal medium for the individual medicinal mushroom.

Characteristics	*G. lucidum*	*P. ostreatus*
Average diameter of the membrane (mm)	0.94	0.77
Average diameter of the hyphae (μm)	0.43	1.31
Average diameter of the pores in the membrane (μm)	40.30	25.10
Hydrophilicity/ hydrophobicity	Hydrophobic surface	Hydrophilic surface
Present functional groups	O-H stretching, CH_2 asymmetric stretching, CH_2 symmetric stretching, amide I (β-sheet), amide II, C-H bending, PO_2^- asymmetric stretching, C-C stretching + C-O stretching + C-H deformation, C-OH stretching, C-O stretching, C-C stretching, glucan β-anomer C-H bending	

The water absorption capacity of the membranes of the two medicinal mushrooms was also investigated. The results of the time-dependent swelling profile are shown in Figure 2.

The time-dependent swelling profile for the micellar membranes from both selected therapeutic mushrooms was comparable. However, the micellar membranes of P. ostreatus were found to have a higher water uptake capacity (> 600 %) than the membranes of G. lucidum (500 %) after 24 hours.

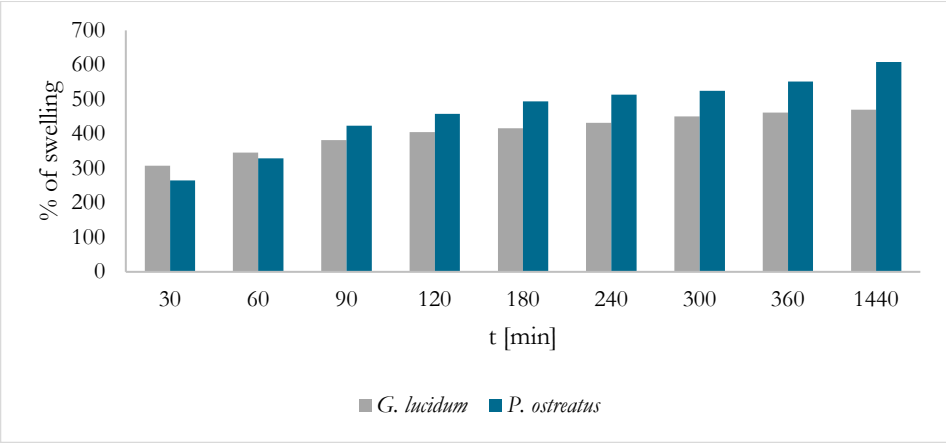

Figure 2: Percentage of swelling of micellar membranes.
Source: own.

4 Conclusion

Micellar membranes from therapeutic fungi are self-growing biocomposites with suitable characteristics. The micellar structures obtained from therapeutic mushrooms are promising fibrous, self-growing polymeric biocomposites. They have favorable properties for potential use in various industries such as packaging and construction. In addition, micellar structures can also be functionalized with different bioactive compounds, which can be successfully used for various cosmetic and biomedical applications, as they mimic the extracellular matrix of human body tissue.

They are a particularly promising platform for tissue engineering applications, especially for wound healing and innovative skin materials. To the best of our knowledge, only mycelium extracts and their derivatives have been used and tested for various applications, e.g. in cosmetics and biomedicine, but not the membranes themselves as functional materials.

Acknowledgments

The authors acknowledge the financial support from the Slovenian Research Agency (ARIS) within the frame of program P2-0046 (Separation Processes and Production Design), project No. J2-3037 (Bionanotechnology as a tool for stabilization and applications of bioactive substances from natural sources), project No. L2-4430 (Production, Isolation and Formulation of Health Beneficial Substances from *Helichrysum italicum* for Applications in Cosmetic Industry), and young researcher ARIS fellowship contract number No. 1514/FKKT-2023.

References

Alaneme, K.K., Anaele, J.U., Oke, T.M., Kareem, S.A., Adediran, M., Ajibuwa, O.A., and Anabaranze, Y.O. (2023). Mycelium based composites: A review of their bio-fabrication procedures, material properties and potential for green building and construction applications. *Alexandria Engineering Journal* 83:234–250. doi:10.1016/j.aej.2023.10.012.

Antinori, M.E., Contardi, M., Suarato, G., Armirotti, A., Bertorelli, R., Mancini, G., Debellis, D., and Athanassiou, A. (2021). Advanced mycelium materials as potential self-growing biomedical scaffolds. *Scientific Reports* 11 (1):12630. doi:10.1038/s41598-021-91572-x.

Baranwal, J., Barse, B., Fais, A., Delogu, G.L., and Kumar, A. (2022). Biopolymer: A Sustainable Material for Food and Medical Applications. *Polymers (Basel)* 14 (5):983. doi:10.3390/polym14050983.

Haneef, M., Ceseracciu, L., Canale, C., Bayer, I.S., Heredia-Guerrero, J.A., and Athanassiou, A. (2017). Advanced Materials From Fungal Mycelium: Fabrication and Tuning of Physical Properties. *Scientific Reports* 7 (1):41292. doi:10.1038/srep41292.

Khamrai, M., Banerjee, S.L., and Kundu, P.P. (2018). A sustainable production method of mycelium biomass using an isolated fungal strain Phanerochaete chrysosporium (accession no: KY593186): Its exploitation in wound healing patch formation. *Biocatalysis and Agricultural Biotechnology* 16:548–557. doi:10.1016/j.bcab.2018.09.013.

Majib, N.M., Sam, S.T., Yaacob, N.D., Rohaizad, N.M., and Tan, W.K. (2023). Characterization of Fungal Foams from Edible Mushrooms Using Different Agricultural Wastes as Substrates for Packaging Material. *Polymers* 15 (4):873. doi:10.3390/polym15040873.

Manan, S., Ullah, M.W., Ul-Islam, M., Atta, O.M., and Yang, G. (2021). Synthesis and applications of fungal mycelium-based advanced functional materials. *Journal of Bioresources and Bioproducts* 6 (1):1–10. doi:10.1016/j.jobab.2021.01.001.

Martinez-Medina, G.A., Chávez-González, M.L., Verma, D.K., Prado-Barragán, L.A., Martínez-Hernández, J.L., Flores-Gallegos, A.C., Thakur, M., Srivastav, P.P., and Aguilar, C.N. (2021). Bio-funcional components in mushrooms, a health opportunity: Ergothionine and huitlacohe as recent trends. *Journal of Functional Foods* 77:104326. doi:10.1016/j.jff.2020.104326.

Perera, K.Y., Jaiswal, A.K., and Jaiswal, S. (2023). Biopolymer-Based Sustainable Food Packaging Materials: Challenges, Solutions, and Applications. *Foods* 12 (12):2422. doi:10.3390/foods12122422.

Silva, A.C.Q., Silvestre, A.J.D., Vilela, C., and Freire, C.S.R. (2021). Natural Polymers-Based Materials: A Contribution to a Greener Future. *Molecules* 27 (1):94. doi:10.3390/molecules27010094.

Sivaprasad, S., Byju, S.K., Prajith, C., Shaju, J., and Rejeesh, C.R. (2021). Development of a novel mycelium bio-composite material to substitute for polystyrene in packaging applications. *Materials Today: Proceedings, International Conference on Sustainable materials, Manufacturing and Renewable Technologies 2021* 47:5038–5044. doi:10.1016/j.matpr.2021.04.622.

Verma, N., Jujjavarapu, S.E., and Mahapatra, C. (2023). Green sustainable biocomposites: Substitute to plastics with innovative fungal mycelium based biomaterial. *Journal of Environmental Chemical Engineering* 11 (5):110396. doi:10.1016/j.jece.2023.110396.

Bacterial Cellulose Membranes Enriched With Bioactive Compounds From Avocado Seeds

Kaja Kupnik, Mateja Primožič, Željko Knez, Maja Leitgeb

University of Maribor, Faculty of Chemistry and Chemical Engineering, Maribor, Slovenia
kaja.kupnik@gmail.com, mateja.primozic@um.si, zeljko.knez@um.si, maja.leitgeb@um.si

Lately, biologically active materials are an extensive topic of research and the employment of bacterial cellulose membranes (BCMs) as carriers has proven to be one of the more interesting applications, especially in the biomedical, cosmetic, food, and pharmaceutical fields. However, bacterial cellulose itself is not antibacterially effective, which is one of the most desired property. To increase its applicability, BCMs can be modified or enriched with biologically active compounds. While humanity is striving for an extensive strategy for the transition to circular economy, the food wastes present a sustainable and renewable source that can be processed into value-added products. The production of BCMs by cultivation of *Komagataeibacter hansenii* was carried out. BCMs were further enriched with bioactive compounds obtained from avocado seeds using ethanol as a solvent. The developed BCMs have shown great potential with their antibacterial activity against *Escherichia coli* and *Staphylococcus aureus* for further applications in biomedicine, cosmetic, food, and pharmaceutical industries.

DOI
https://doi.org/10.18690/um.fkkt.1.2024.4

ISBN
978-961-286-829-1

Keywords:
bacterial cellulose, nanocellulose, avocado seed, antibacterial activity, membrane

University of Maribor Press

1 Introduction

The claim for sustainable biologically active materials has remarkably increased in recent times, due to their characteristics that make them appropriate as an extensive potential for applications in biomedical, cosmetic, food, and pharmaceutical fields.

Komagataeibacter hansenii is one of the acetic acid bacteria which produce bacterial cellulose (BC). Under the static conditions, at the air-liquid interface, BC membranes (BCMs) are formed, exhibiting three dimensional open fibrous network structure (Fatima et al. 2023). By means of its hydrophilic nature, nontoxicity, flexibility, biocompatibility, good barrier and mechanical properties, BC have been extensively researched and used (Bodea et al. 2020). The porosity and high specific surface area ensures high liquid absorption capacity (Zheng et al. 2020). It was already applied as a base for artificial blood vessels, implants, stents, part of the drug delivery systems, and mostly as a wound dressing material (Swingler et al. 2021; Rajwade et al. 2015). Most frequently, BC dressings are based on wet form, as it provides suitable moisture degree, which is advantageous for healing of the wounds (Nuutila and Eriksson 2021).

However, one of the most sought-after characteristics of advanced biologically active materials is antimicrobial activity, which BC itself lacks. Therefore, BC is commonly modified with divergent antimicrobial agents, such as metal/metal oxide nanoparticles, antibiotics, and organic compounds (e.g., amino acids, curcumin, chitosan,…) (Zielińska et al. 2022; Krasowski et al. 2021; Moritz et al. 2014).

As the occurrence of drug-resistant bacteria is increasing rapidly (Xuan et al. 2023), there is a constant search for antimicrobials. Plants produce a wide range of phytochemicals, being a rich source of different active compounds (Bergonzi et al. 2022). On the other hand, huge waste of food commodities and by-products occurred due to improper food handling at every step of post-harvest. Plant extracts, obtained from different food wastes are hence a promising alternative, as they prove to be a renewable resource that can be processed into products with added value.

Avocado seeds (AS) are one of the underutilized inedible parts of fruit, which are discarded and present enormous quantity of waste biomass. AS are rich in biologically active substances such as polyphenols, acetogenins, triterpenoids, and

others (Jimenez et al. 2021). In our recent study (Kupnik et al. 2023), AS extracts exhibited significant antimicrobial activity against 13 out of 15 tested microorganisms, which often pose a problem in antimicrobial resistance, are transmitted by food or are colonized during food packaging. High concentrations of antimicrobial compounds, i.e., hesperidin, 2,3-dihydroxybenzoic acid, and vanillin, were found in AS extracts, which can synergistically contribute to high antimicrobial properties of AS extracts.

Therefore, the objective of presented study was to produce BCMs enriched with AS extract in order to prepare effective biocomposites for potential antibacterial applications in divergent fields and industries.

2 Methods

2.1 Production of BCMs

First, for the growth and production of BCMs, Hestrin and Schramm medium was used. The HS medium was prepared as followed: 2.0% (w/v) glucose, 0.5% (w/v) peptone, 0.5% (w/v) yeast extract, 0.27% (w/v) Na_2HPO_4, and 0.15% (w/v) citric acid with the pH of 6.0. The inoculum was prepared by transferring *K. hansenii* in 50 mL of HS medium. The suspension was then shaken with 150 revolutions per minute at 27 °C for 48 hours. The suspension was used to inoculate prepared flasks with 100 mL of production media, followed by static cultivation at 27 °C until membranes were formed. Obtained BCMs were gathered, washed with dH_20 and submerged in 1.0 M NaOH solution for 2 hours at 80 °C in order to remove impurities and microbial cells from membrane. BCMs were then repeatedly washed with distilled water to obtain neutral pH in washed liquid.

2.2 Preparation of ethanolic AS extracts

AS were detached from the ripe avocado fruits and washed with water. AS were cut into little pieces and dried at room temperature. Dried AS were then ground and subjected to Soxhlet extraction method. Approximately 25 g of dried AS were extracted using 150 mL of ethanol as a solvent in Soxhlet extractor. Extractions were carried out for approximately 6 hours or until four recycles were completed. Rotary

evaporator at reduced pressure and 40 °C was used in order to evaporate the solvent. Obtained AS extracts were stored at -20 °C until their further usage.

2.3 Enrichment of BCMs with AS extract

The Soxhlet AS extract solutions were prepared in concentrations of 10 and 100 mg/mL, respectively. The BCMs were immersed in prepared AS extract solutions for 48 hours. In order to facilitate the diffusion of the extract into the BCMs, the magnetic stirrer with 150 rpm was used. After adsorption process, enriched BCMs with AS extract were soaked over a filter paper for removal of excess extract solution.

2.4 Antibacterial activity

Antibacterial effectiveness of prepared BCMs was evaluated against Gram-negative bacterium *E. coli* and Gram-positive bacterium *S. aureus*. The agar diffusion method was used, following the protocol detailed in our previous study (Kupnik et al. 2021) with some adjustments. Briefly, 100 µL of prepared bacterial suspension was spread evenly on suitable agar plates, according to selected bacteria. Next, 1×1 cm pieces of BCMs were laid on the inoculated agar plates. Prepared agar plates with samples were incubated at optimal growth conditions for *E. coli* and *S. aureus* (37 °C, 24 hours). Pure BCM was used as a negative control. The indicator of the antibacterial effectiveness was the inhibition zone (measured in mm) formed around sample.

3 Results

BCMs were produced in HS medium and harvested after 21 days of fermentation. Procedure and final BCMs enriched with AS extract are presented in Figure 1.

A result of immersing pure BCMs in prepared AS extract solutions were orange-colored BCMs. This is due to perseorangin, a pigment present in AS, which is a result of a polyphenol oxidase-dependent reaction (Hatzakis et al. 2019).

Furthermore, BCMs enriched with AS extract were assessed for their antibacterial activity using agar diffusion method. The collected results are presented in Table 1.

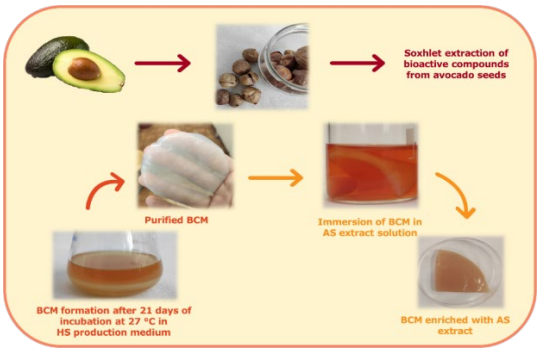

Figure 1: Procedure of production and enrichment of BCMs with AS extract
Source: own.

Table 1: Zone inhibition of enriched BCMs against *E. coli* and *S. aureus*

	1. BCM + 10 mg/mL AS extract	2. BCM + 100 mg/mL AS extract
E. coli	17 ± 3 mm	22 ± 2 mm
S. aureus	17 ± 1 mm	21 ± 1 mm

As expected, BCMs immersed in AS extract solution with a higher concentration (100 mg/mL) showed better antibacterial effect than BCMs immersed in AS extract solution with a concentration of 10 mg/mL. Enriched BCMs inhibited the growth of *E. coli* by an average of 17-22 mm, and *S. aureus* by 17-21 mm.

Figure 2 shows inhibition zones of BCMs against *E. coli*.

The result of the research showed prosperous development of antibacterially effective BCMs enriched with AS extracts.

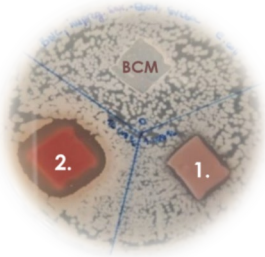

Figure 2: Inhibition zones against *E. coli*
Source: own.

4 Conclusions

Based on obtained results, the BCMs enriched with AS extracts, with exceptional antibacterial activity, showed a great possibility for their further use in biomedicine, and in the field of food packaging, cosmetic, and pharmacy.

Noteworthy, the utilization of waste avocado seeds enables and encompasses a broader strategy towards a circular economy as the volume of waste could be greatly reduced. Additionally, a renewable resource could be exploited for conversion into the presented sustainable value-added antibacterial biocomposites.

Acknowledgments

This research was funded by the Slovenian Research and Innovation Agency (ARIS) within the frame of program P2-0046 (Separation Processes and Production Design), P2-0424 (Design of novel nano/material properties & applications), project No. J2-3037 (Bionanotechnology as a tool for stabilization and applications of bioactive substances from natural sources), L2-4430 (Production, Isolation and Formulation of Health Beneficial Substances from *Helichrysum italicum* for Applications in Cosmetic Industry), and young researcher ARRS fellowship Contract No. 2187/FS-2019. The authors acknowledge the use of research equipment for the production of biological substances and their detection, procured within the project "Upgrading national research infrastructures - RIUM", which was co-financed by the Republic of Slovenia, the Ministry of Higher Education, Science and Innovation, and the European Union from the European Regional Development Fund, and the system of downstream processes for performance of obtaining biological substances (Package 21, ARIS).

References

Bergonzi, M.C., Heard, C.M., and Garcia-Pardo, J. (2022). Bioactive Molecules from Plants: Discovery and Pharmaceutical Applications. *Pharmaceutics* 14 (10):2116. doi:10.3390/pharmaceutics14102116.

Bodea, I.M., Cătunescu, G.M., Stroe, T.F., Dîrlea, S.A., and Beteg, F.I. (2020). Applications of bacterial-synthesized cellulose in veterinary medicine – a review. *Acta Veterinaria Brno* 88 (4):451–471. doi:10.2754/avb201988040451.

Fatima, A., Ortiz-Albo, P., Neves, L.A., Nascimento, F.X., and Crespo, J.G. (2023). Biosynthesis and characterization of bacterial cellulose membranes presenting relevant characteristics for air/gas filtration. *Journal of Membrane Science* 674:121509. doi:10.1016/j.memsci.2023.121509.

Hatzakis, E., Mazzola, E.P., Shegog, R.M., Ziegler, G.R., and Lambert, J.D. (2019). Perseorangin: A natural pigment from avocado (Persea americana) seed. *Food Chemistry* 293:15–22. doi:10.1016/j.foodchem.2019.04.064.

Jimenez, P., Garcia, P., Quitral, V., Vasquez, K., Parra-Ruiz, C., Reyes-Farias, M., Garcia-Diaz, D.F., Robert, P., Encina, C., and Soto-Covasich, J. (2021). Pulp, Leaf, Peel and Seed of Avocado Fruit: A Review of Bioactive Compounds and Healthy Benefits. *Food Reviews International* 37 (6):619–655. doi:10.1080/87559129.2020.1717520.

Krasowski, G., Junka, A., Paleczny, J., Czajkowska, J., Makomaska-Szaroszyk, E., Chodaczek, G., Majkowski, M., Migdał, P., Fijałkowski, K., Kowalska-Krochmal, B., and Bartoszewicz, M. (2021). In Vitro Evaluation of Polihexanide, Octenidine and NaClO/HClO-Based

Antiseptics against Biofilm Formed by Wound Pathogens. *Membranes* 11 (1):62. doi:10.3390/membranes11010062.

Kupnik, K., Primožič, M., Knez, Ž., and Leitgeb, M. (2021). Antimicrobial Efficiency of Aloe arborescens and Aloe barbadensis Natural and Commercial Products. *Plants* 10 (1):92. doi:10.3390/plants10010092.

Kupnik, K., Primožič, M., Kokol, V., Knez, Ž., and Leitgeb, M. (2023). Enzymatic, Antioxidant, and Antimicrobial Activities of Bioactive Compounds from Avocado (Persea americana L.) Seeds. *Plants* 12 (5):1201. doi:10.3390/plants12051201.

Moritz, S., Wiegand, C., Wesarg, F., Hessler, N., Müller, F.A., Kralisch, D., Hipler, U.-C., and Fischer, D. (2014). Active wound dressings based on bacterial nanocellulose as drug delivery system for octenidine. *International Journal of Pharmaceutics* 471 (1):45–55. doi:10.1016/j.ijpharm.2014.04.062.

Nuutila, K. and Eriksson, E. (2021). Moist Wound Healing with Commonly Available Dressings. *Advances in Wound Care* 10 (12):685–698. doi:10.1089/wound.2020.1232.

Rajwade, J.M., Paknikar, K.M., and Kumbhar, J.V. (2015). Applications of bacterial cellulose and its composites in biomedicine. *Applied Microbiology and Biotechnology* 99 (6):2491–2511. doi:10.1007/s00253-015-6426-3.

Swingler, S., Gupta, A., Gibson, H., Kowalczuk, M., Heaselgrave, W., and Radecka, I. (2021). Recent Advances and Applications of Bacterial Cellulose in Biomedicine. *Polymers* 13 (3):412. doi:10.3390/polym13030412.

Xuan, J., Feng, W., Wang, J., Wang, R., Zhang, B., Bo, L., Chen, Z.-S., Yang, H., and Sun, L. (2023). Antimicrobial peptides for combating drug-resistant bacterial infections. *Drug Resistance Updates* 68:100954. doi:10.1016/j.drup.2023.100954.

Zheng, L., Li, S., Luo, J., and Wang, X. (2020). Latest Advances on Bacterial Cellulose-Based Antibacterial Materials as Wound Dressings. *Frontiers in Bioengineering and Biotechnology* 8.

Zielińska, S., Matkowski, A., Dydak, K., Czerwińska, M.E., Dziągwa-Becker, M., Kucharski, M., Wójciak, M., Sowa, I., Plińska, S., Fijałkowski, K., Ciecholewska-Juśko, D., Broda, M., Gorczyca, D., and Junka, A. (2022). Bacterial Nanocellulose Fortified with Antimicrobial and Anti-Inflammatory Natural Products from Chelidonium majus Plant Cell Cultures. *Materials* 15 (1):16. doi:10.3390/ma15010016.

DOI
https://doi.org/10.18690/um.fkkt.1.2024.5

ISBN
978-961-286-829-1

Influence of Ammonium Polyphosphates and 2,4,6-Triamino-1,3,5-Triazine on the Mechanical-Physical Properties of Polyurethane and Alkali-Activated Materials

Branka Mušič, Barbara Horvat

Slovenian National Building and Civil Engineering Institute, Ljubljana, Slovenia
branka.music@zag.si, barbara.horvat@zag.si

In building constructions, the tendency towards an ever-better material directs us to composite materials. In this work, we prepared an organic-organic and organic-inorganic composite material by incorporating fire retardants, ammonium polyphosphates, and 2,4,6-triamino-1,3,5-triazine, into a polyurethane network and an aluminosilicate network (ASN) of alkali-activated material. Polyurethane foams (PUR) are well-known materials that, due to their properties, such as low weight-to-strength ratio, low electrical and thermal conductivity, flexibility, and relatively simple preparation process, are used in various industries, also in the construction industry, e.g., for thermal insulation of windows and doors or fixing and sealing joinery. Opposite, the ASN of alkali-activated metakaolin, successfully paves the way for new applications, such as high-temperature protection. In this paper, these interactive properties of prepared composites are studied using thermal testing and mechanical analysis. It was found that inhibitors significantly increase the fire resistance of PUR systems while they slightly reduce the mechanical properties. Incorporating polymer flame retardant into ASN in building products, such as façade panels, can decrease the mechanical properties but can offer the non-flammable building envelope not get heated from burning surroundings, i.e., not becoming a convection heat source, but rather represent a fire-distinguisher for flammable materials.

Keywords:
flame retardants,
polyurethane,
alkali-activated metakaolin,
microwave irradiation,
mechanical properties

University of Maribor Press

1 Introduction

Presently, organic halogenated compounds are industrially used fire retardants for various materials as they are required in low concentrations, typically 0.5–1 m% (HBCD use in EPS for Building Applications, ICL-IP Europe BV, 06/07/2014). However, halogenated fire retardants are phased out (HBCD banned since 20164b, currently used alternatives are also organic halides) due to their proven or suspected hazardous effects on the environment and health (Covaci et al., 2006). On the other hand, halogen-free fire retardants are more environmentally friendly with very low toxic potential and are not yet industrially viable. The most frequently studied halogen-free fire retardants are inorganic, IHF-FR (nano oxides, layered clays, hydroxides, etc.), phosphorus-containing compounds, and nitrogen-rich compounds. Those are used as synergistic agents to improve fire retardant properties as their dominant fire retardant mechanism is associated with the dilution of flammable gases, cooling the fire zone, the formation of an effective protective layer during combustion, or the presence of adsorption-desorption sites for combustion gases (Laoutid et al., 2009). Their inclusion in various construction products, such as polyurethane foams and alkali-activated materials, could provide many advantages, such as reducing stiffness and brittleness, improving the durability and longevity of the new composite material, while at the same time increasing the benefits for the users of the construction product, and due to environmental soundness, it allows manufacturers to recycle the material after its life more easily. This is especially beneficial in the building and construction industry to lower its negative environmental footprint, i.e., the building and construction industry annually consumes nearly 70 m% of Mount Everest's mass of raw materials and generates more than 30 m% of the world's waste (Miller et al., 2023 and Dyrud et al., 2023).

Polyurethane foams are materials known for a long time in the market. Their use has increased over the years due to their unique properties, such as low weight-to-strength ratio, low electrical and heat conductivity, better environmental and fire safety, flexibility in the method of application, quick and easy use due to the fast hardening reaction, and relatively easy process of preparation. Due to the listed properties, polyurethane foams are used in various industries, including construction, e.g., for thermal insulation of windows and doors or fixing and sealing joinery. They can even be used as an insulating material on walls and roofs. By

decreasing flammability, i.e., by incorporating halogen-free fire retardants ammonium polyphosphates and 2,4,6-Triamino-1,3,5-triazine, the environment and the fire safety of the whole community can become significantly more protected.

On the other hand, flame-retardant polymeric materials can be used as additives in alkali-activated materials which are not as well-known on the market as polyurethane foam. Alkali-activated materials are very thermally stable and non-flammable but to achieve better mechanical properties, such as reducing stiffness, polymer materials can be added to them, thus showing better properties/flexibility. The selected polymers for forming the composite with alkali-activated materials are flame-retardant polymers with the desire to have as little influence as possible on the inflammability of alkali-activated materials when included in the aluminosilicate network (ASN). Nevertheless, both the PUR and AAM composite systems can exhibit poorer compatibility with the selected polymers, which harms their dispersion in the matrix, which is why studies were made in this presented research work.

In the present research, we tested two completely different construction-industrial materials, polyurethane foam (PUR) and a non-combustible potential substitute for types of cement, mortars, and ceramics, i.e., alkali-activated material (AAM) based on metakaolin and Na-silicate solution where alkali-activated slurry was additionally cured in its early stage by microwaves at 100 W for 1 minute to increase the amount of the ASN. We studied the influence of the used halogen-free fire-retardant polymers – ammonium polyphosphates (APP) and 2,4,6-triamino-1,3,5-triazine (TATA) on the composite systems PUR-APP, PUR-TATA and AAM-APP, and AAM-TATA.

2 Methods – evaluation of the input material

To be able to evaluate the effect of the added flame retardants APP and TATA on all four composite systems PUR-APP, PUR-TATA and AAM-APP, and AAM-TATA separately, we had to study both the input raw materials and analyze the final composites in detail. Both flame retardant additives used were commercially available. First was ammonium polyphosphate, Exolite AP 422 (APP) supplied by Clariant (Mutenz, Switzerland). It is a white fine powder, non-hygroscopic, non-flammable, halogen-free, with a bulk density of 700 kg/m^3, and a melting point of

~240 °C. The second used fire retardant material was 2,4,6-Triamino-1,3,5-triazine (TATA) supplied by Sigma Aldrich (St. Louis, MO, USA). It is white powder, with a bulk density of 800 kg/m^3 and a melting point of ~354 °C. As the basic polyurethane foam for the preparation of new composite materials, we have chosen commercially available the two-component polyurethane foam "Tekapur Polefix" (PUR), supplied by TKK d.o.o. (Srpenica, Slovenia). The Tekapur Polefix contains component A, which is a polyol with several hydroxyl groups and triethyl phosphates, and component B, which is polymethylene polyphenyl polyisocyanate. Chemical evaluation of the metakaolin (MK), a precursor used to prepare the AAM material (noted as Mix 5, reference), and also the AAM composites (AAM-APP noted as Mix 6 and AAM-TATA noted as Mix 7) was performed by X-ray fluorescence using XRF (Thermo Scientific ARL Perform'X Sequential XRF) and by determining the amount of organic compound and carbonates, from the loss on ignition (LOI) for 2 hours at 550 °C and 950 °C, respectively. To determine the quantitative mineralogical composition of used MK, mineralogical analysis was carried out by Rietveld refinement, using corundum Al_2O_3 as an external standard, on X-ray powder diffraction (XRD, Empyrean PANalytical X-ray Diffractometer, Cu X-Ray source) patterns. The precursor was first dried, milled, and further sieved below 125 μm for LOI, XRF, and XRD. Results were reported in published scientific research (Horvat et al., 2023 and Horvat et al., 2022c), as well as the optimal mixture of MK and used alkali (Na-silicate solution, Geosil, 344/7, Woelner, Ludwigshafen, Germany, 16.9% Na_2O, 27.5% SiO_2). The theoretically determined mass ratio (using software in MS Excel platform developed in project No. C3330-17-529032 "Raziskovalci-2.0-ZAG-529032" and upgraded in the ARRS project under Grant No. J2-3035) between MK and liquid alkali was 1:0.66, respectively. For the synthesis, however, MK was used as it was received.

We performed some additional analysis on the incoming raw materials, as follows.

For both powder fire retardant input raw materials, scanning electron microscopy (SEM; Jeol JSM-IT500, low vacuum conditions) was performed at 500-x magnification (BED-S, Sta.-PC 60 and 20 kV). The differences in size and shape are shown in Figure 1.

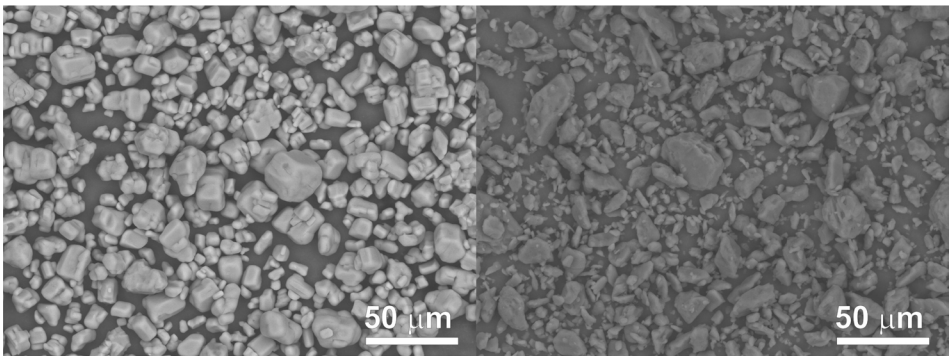

Figure 1: SEM analysis of fire retardants APP (left) and TATA (right).
Source: own.

APP powder is slightly larger than TATA powder, has more rounded edges, and is more regular in shape while TATA has a very wide distribution of irregularly shaped particles.

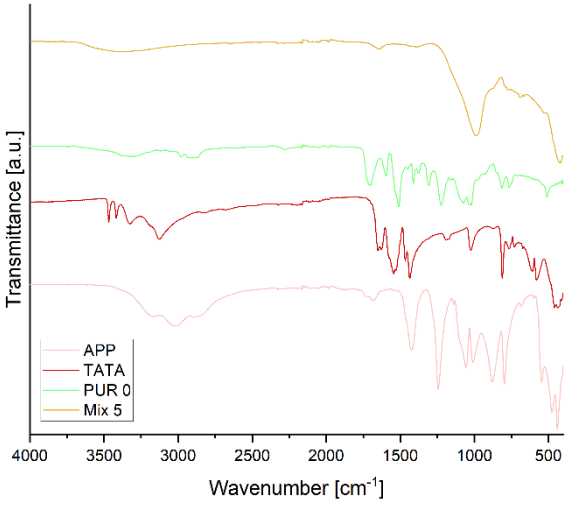

Figure 2: FTIR spectrum of input materials.
Source: own.

Additionally, FTIR and XRD analysis for all input materials that compose the final PUR and AAM composites were evaluated. Those input materials were APP, TATA, Mix 5 (AAM without additives, reference), and pure PUR (noted as PUR 0,

reference). FTIR was performed by Fourier transform infrared spectroscopy (FTIR; PerkinElmer Spectrum Two, ATR mode) – it is represented in Figure 2. XRD was performed by X-ray powder diffraction (XRD; Empyrean PANalytical X-ray Diffractometer, Cu X-Ray source) – it is represented in Figure 3.

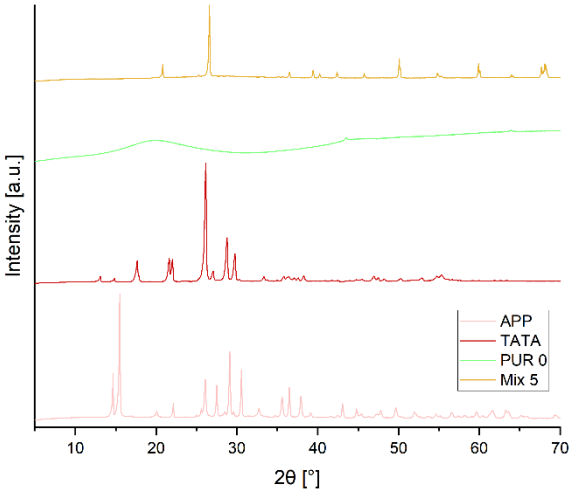

Figure 3: XRD pattern of powder raw materials.
Source: own.

Both analyses were later used to determine the effect of the addition of selected fire retardant additives on the prepared final PUR and AAM composites.

3 Methods – preparation of the composite material

Due to the completely different nature of AAM and PUR materials, which were used as base, support materials for preparing our new composites, we also had to incorporate the fire-resistant polymer materials, APP and TATA, respectively, in a slightly different procedure.

Preparation of PUR samples: The appropriate amount of PUR component B (polyisocyanate) and a flame retardant, APP or TATA, were weighted into a mixing vessel and mixed with a high-speed mechanical stirrer at about 1400 rpm for 10 min to obtain a homogeneous mixture (PUR 0 was without flame retardants and served as reference). After that, the appropriate amount of component A (polyol) was

poured into the mixture which was further homogenized with a stirrer at 1000 rpm and transferred into a mold with enough free space to enable the full expansion of the foam during curing. The foams were stored for 72 hours at room conditions T = 23 °C ± 2 °C (noted as T0) and relative humidity 50% ± 15% in accordance with ISO 291:2008. The structure and resulting performance of polyurethane foams are driven by the stoichiometry of the polymerization reaction which is directly impacted by applied monomers, additives, their chemical composition, and the ratio between the polyols and isocyanates (Hejna et al., 2017, Amran e tal., 2021, Fink e tal., 2018). The ratio used in PUR 0 between polyol and isocyanate was according to the manufacturer's recommendations. Therefore, the mixing weight ratio was 1:1.22. The reference PUR foam (PUR 0) with the addition of APP was designated as PUR 1 and the foam with the addition of TATA was designated as PUR 2. From preliminary research, we found that a maximum of 30% of the fire-retardant additive can be included in the system based on the total weight of the A + B component so that the fire-retardant powder is homogeneously mixed into the B component. In Table 1 the masses of the used ingredients for PUR samples are given.

Table 1: Masses of the used ingredients for PUR samples.

Specimens	Comp. A (g)	Comp. B (g)	APP (g)	TATA (g)
PUR 0	32.7	40.0	0.0	0.0
PUR 1	32.7	40.0	21.8	0.0
PUR 2	32.7	40.0	0.0	21.8

Preparation of AAM samples: MK with added defined amounts of APP and TATA, respectively, was previously homogenized with a laboratory vibrating ball mill (MixMill MM20, Danfoss, Slovenia). The mechanical grinding process (homogenization) took place at room temperature for 3 minutes at a frequency of 30 Hz. 3 hardened stainless steel balls with a diameter of 0.8 mm were used in a 50 mm^3 stainless steel drum. Then, the powdered raw materials (finely homogenized MK with the addition of APP and finely homogenized MK with the addition of TATA) were mixed with a Na-silicate solution and water, as shown in Table 2, until the material was completely wet at 1000 rpm. The amount of added water was determined experimentally to reach sufficient wetting of all solid powders in the mixture.

Table 2: Masses of the used ingredients.

Mixture	MK [g]	Alkali [g]	APP [g]	TATA [g]	H_2O [g]
Mix 5	74.9	33.0	0.0	0.0	7.5
Mix 6	50.0	33.0	24.9	0.0	30.0
Mix 7	50.0	33.0	0.0	24.9	7.5

The mixtures were put into molds made of silicone-urethane rubber. The presented mixtures in Table 2 were evaluated after the curing procedure, which was irradiating fresh slurry with microwaves (frequency 2.45 GHz, inverter microwave, Panasonic, NN-CD575M) for 1 min at 100 W (positively influencing the dissolution of reagents while dehydration is not yet severely affected (Horvat et al., 2022b) and additionally further curing at room conditions for 14 days).

Geometrical densities along with mechanical bending and compressive strengths were measured after 14 days of curing of AAMs in the conditioning room. For the evaluation of mechanical strengths, the compressive and bending strength testing machine (ToniTechnik ToniNORM) was used.

4 Results – composite materials

As mentioned in the "preparation of the composite material" section, AAM and PUR materials are very different. In Figure 4 and Figure 5 below, therefore, we present a visual representation of our test samples. Observing the pictures, we can get a sense of the visual appearance and internal texture of the samples.

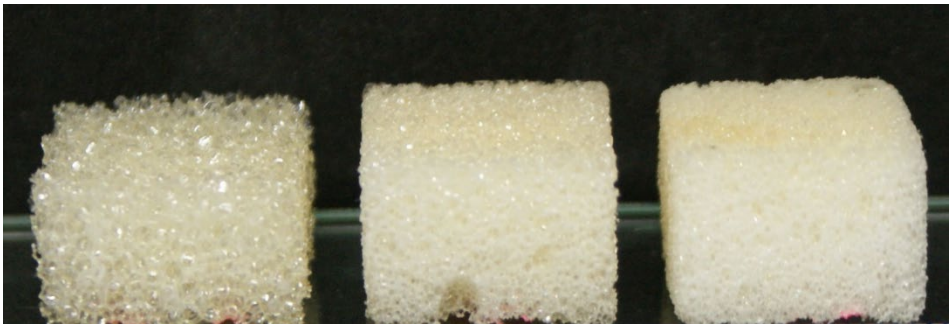

Figure 4: Prepared PUR samples from left to right: PUR 0, PUR 1, and PUR 2.
Source: own.

Figure 5: Images of sample Mix 5, sample Mix 6, and sample Mix 7 (from left to right).
Source: own.

Figure 5 shows how much APP affects the structure formation of the Mix 6 sample.

To show the visual difference between our test samples in even more detail, we also made the SEM analysis of prepared and hardened mixtures of both PUR (Figure 6) and AAM composites (Figure 7). The PUR images were taken at magnification 40x (BED, NOR, Std. PC 60 and 20 kV).

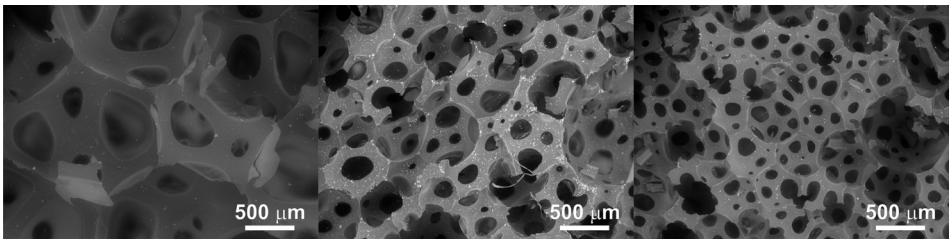

Figure 6:. SEM images of prepared, hardened samples (from left to right) PUR 0, PUR 1, and PUR 2.
Source: own.

It can be seen in the pictures, that both flame retardant additives affect the formation of the skeletal network of polyurethane foam as the pore sizes of PUR 1 and PUR 2 significantly decreased.

In Figure 7, SEM images of AAM composites are presented with a scale of 100 µm, recorded at 150x magnification (BED, NOR, Std. PC 60, and 20 kV). The marked places in Figure 7 show the cracks in the material.

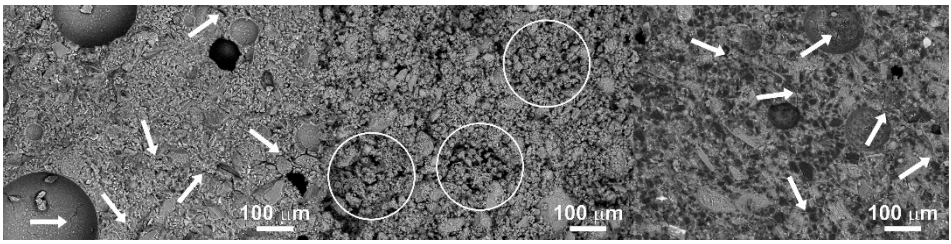

Figure 7: SEM images of prepared, hardened samples (from left to right) Mix 5, Mix 6, and Mix 7.

Source: own.

In all three cases, cracks appeared in the hardened samples Mix 5, Mix 6, and Mix 7, with the largest visible in Mix 6 and the smallest in Mix 7. In Mix 5, cracks are due to dehydration while bubbles are due to the mixing of ingredients (there was no gas formation in the chemical reaction of alkali and MK) where some air bubbles got permanently caught. The highly porous structure in Mix 6 is due to the reaction of APP with alkali, which leads to the release of health-harmful gasses and prolongation of curing. The least porous material, according to SEM, is Mix 7 where TATA was added. TATA did not react with alkali but just filled the empty spaces in the ASN network where it got well encapsulated and stored for the case of fire.

AAM materials are known as very good temperature-resistant materials. Therefore, we tested their response to elevated temperatures. Each sample was cured at room temperature (T0) and then treated at several temperatures at 250 °C, 500 °C, 750 °C, and 1000 °C (laboratory oven Memmert for temperature 250 °C and for higher temperatures furnace Protherm). After the temperature treatment, mechanical strength was evaluated. The remaining broken pieces show the response to temperature. They are shown in Figure 8.

The thermal behaviour of polyurethane foam is also important because the PUR foams are insulators. Therefore, their thermal insulation and flammability are important. In Figure 9, you can see the response to fire of PUR 0, PUR 1, and PUR 2 according to the UL-94 HB standard.

In Figure 9, we can see that in PUR 0, the line is no longer visible after 30 seconds of burning while in the case of PUR 1 with the fire-retardant additive APP and in

the case of PUR 2 with the flame-retardant TATA, the line was still visible after 30 seconds of burning. TATA in PUR 2 works even better because, in the case of PUR 1 with APP additive, we see that the sample started to sag.

Figure 8: From top to bottom, samples of Mix 5, Mix 6, and Mix 7 are shown in temperature treatments from left to right: T0, 250 °C, 500 °C, 750 °C, and 1000 °C.

Source: own.

The thermal conductivity of the PUR specimens was determined in a homemade heat flow setup. The dimensions of the specimens were (100 mm x 60 mm x 10 mm) x 1 mm. Thermal conductivity was determined on the specimens inserted in between cold and hot plates with temperatures of 15 °C and 25 °C, respectively. The thermal conductivity of the specimens are as follows PUR 0 (36.5 mW/mK), PUR 1 (36.4 mW/mK), PUR 2 (35.6 mW/mK). Presented values correspond well to the

apparent densities of the specimens as a higher density (also visible from SEM images of PUR 1 and 2 composites) of the cellular insulation generally contributes to increasing its thermal conductivity. The apparent densities of the PUR specimens were determined according to ISO 845:2006. The densities of the PURs are as follows: PUR 0 (46.70 kg/m^3), PUR 1 (62.61 kg/m^3), and PUR 2 (60.04 kg/m^3). The densities of PUR 1 and PUR 2 are comparable and about 30% higher than PUR 0 (Mušič et al., 2022).

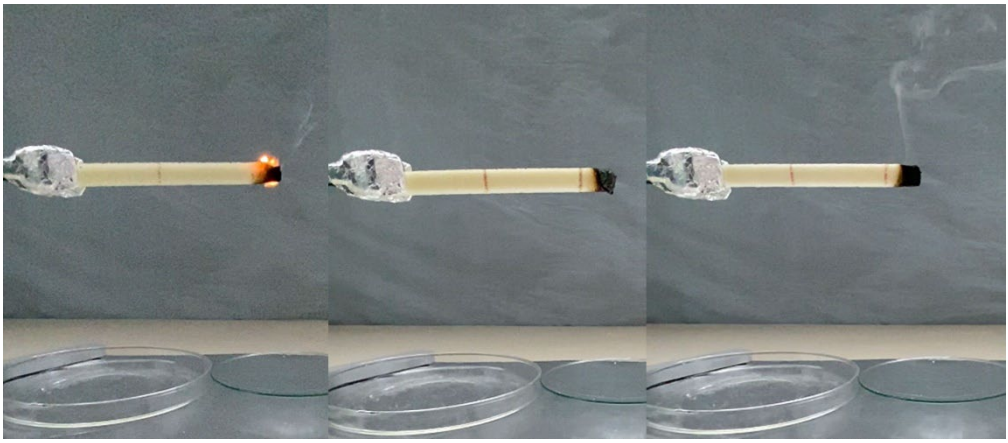

Figure 9: A Horizontal burning test of PUR 0, PUR 1, and PUR 2 samples (from left to right), after 30 s of burning.
Source: own.

The interesting behaviour of AAM composites with increasing temperature was also observed through the distribution of pore sizes and the change in skeletal density.

The pore distribution and skeletal density of the AAM materials were measured by mercury intrusion porosimetry (Micromeritics autopore IV, mercury porosimeter, Series 9500). The pore distribution of heat-treated AAM samples is shown in Figures 10 – 12.

In Figure 10, it can be seen that the size of the distribution of pores moves towards higher values. The changes at about 250 °C are attributed to the dehydration of the material (water leaves the material and on this account the pores increase). As

expected, the bigger differences in the "size of the pores" occurred at 1000 °C which we attribute to the larger cracks that appeared in the material (see Figure 8).

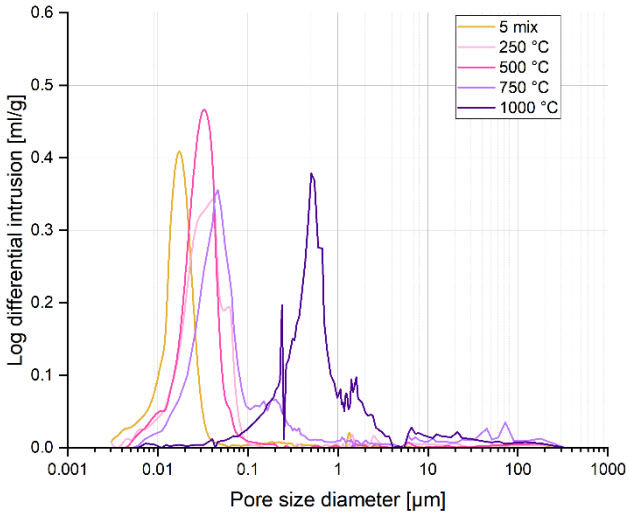

Figure 10: Pore size distribution of Mix 5 samples at different temperature treatments.
Source: own.

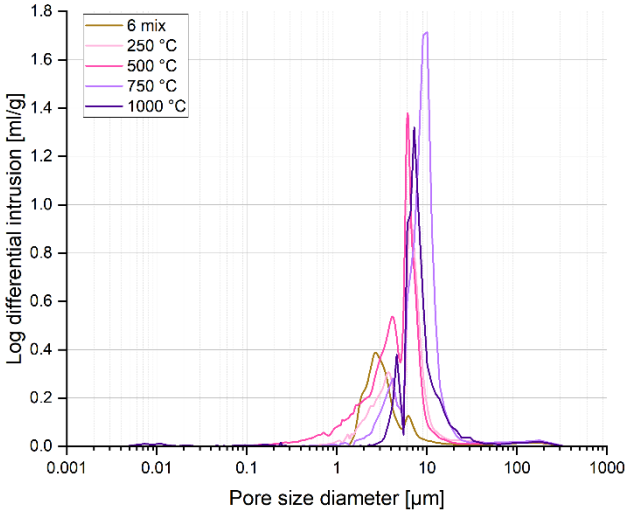

Figure 11: Pore size distribution of Mix 6 sample at different temperature treatments.
Source: own.

In Figure 11, we can see that the original sample Mix 6 at T0 is much more porous than the sample Mix 5. Therefore, it is possible to observe here that with increasing temperature, there is a significantly smaller shift of the peaks to the right towards larger values of the pore size distribution than at sample Mix 5. In Figure 8, we can see that in the case of Mix 6, there were much greater visual differences after temperature treatment, which was also reflected in the mechanical properties presented in the rest of the article.

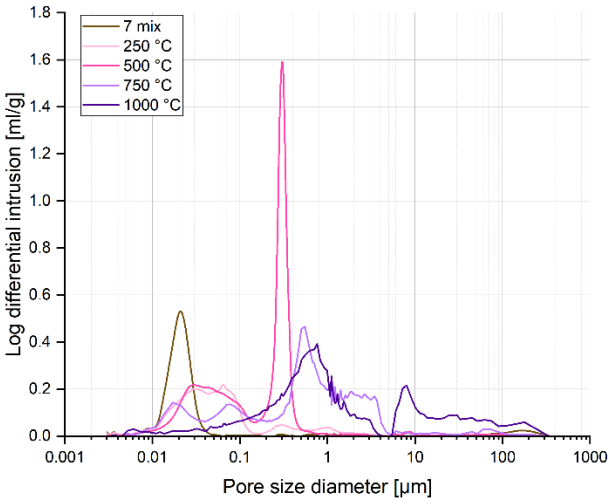

Figure 12: Pore size distribution of Mix 7 sample at different temperature treatments.
Source: own.

Figure 12 shows that at lower temperatures, the pores are smaller and the material is more stable. At around 250 °C, the effect of dehydration of the material is known and the pores partially increase while at ca. 500 °C, the process of thermal decomposition begins and complete decomposition of TATA occurs at slightly more than 700 °C which is also expressed in the increase in the distribution of pores.

It can be seen from Figures 10-12 that the smallest pores in the AAM composite material are formed by Mix 5 while the largest is by Mix 6.

We also observed the behaviour of PUR composites after the addition of fire retardant additives, as we changed the pore size distribution (Figure 13), total porosity (Figure 14), and skeleton density (Figure 15) with it.

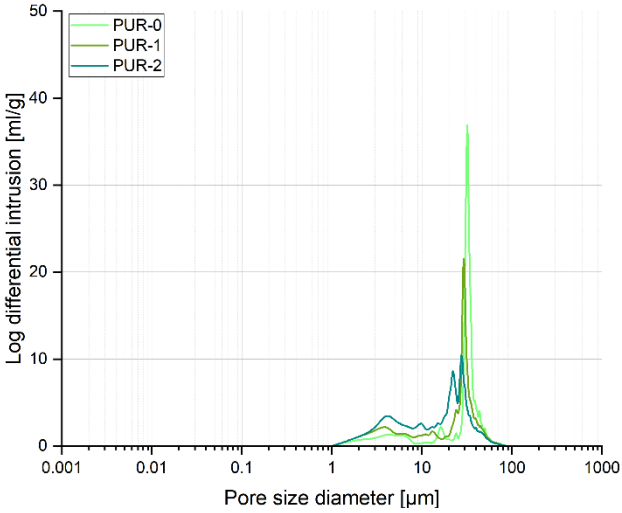

Figure 13: Pore size distribution of PURs at different fire retardant additives.
Source: own.

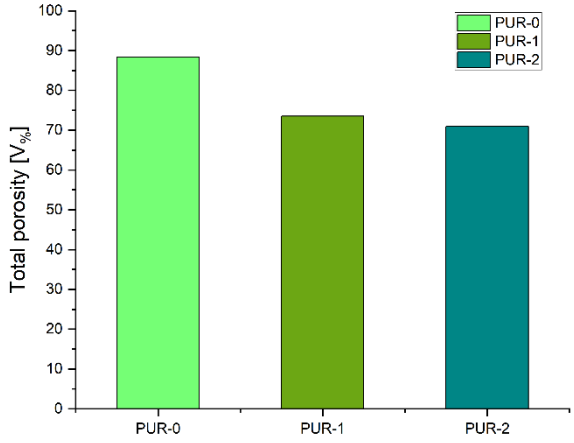

Figure 14: Total porosity of PURs at different fire retardant additives.
Source: own.

It is expected that in PUR 1 and PUR 2 the total porosity decreases, as the fire retardants fill the empty pore spaces, which are the largest in PUR 0.

This also changes the skeletal density, which we measured both for PURs composites (Figure 15) and for AAM composites (Figure 16).

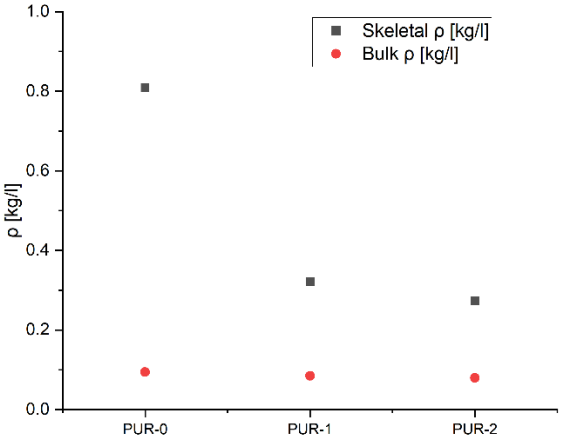

Figure 15: Skeletal and bulk density of PURs at different fire retardant additives.
Source: own.

In Figure 15, we can see that while the bulk density remains the same, the skeletal density changes strongly with fire retardant additives.

It can also be seen that the increasing temperature impacts the densification of the material skeleton. The skeletal density is shown below in Figure 16.

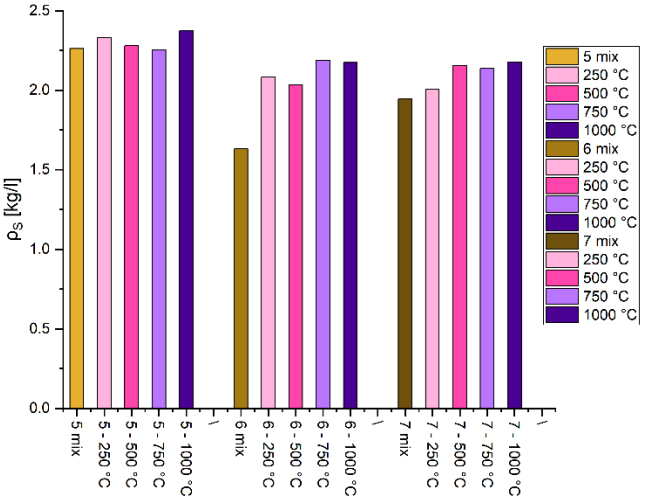

Figure 16: Skeletal density of Mix 5, Mix 6, and Mix 7 at different temperature treatments.
Source: own.

As expected, Mix 5 exhibits the highest skeletal densities (Mix 5 is without organic compounds) while the skeletal densities of Mix 6 and Mix 7 samples are comparable and lower.

However, observing the measurements shown, we have seen that the addition of flame retardant materials affects the physical and mechanical properties of the composites. So, we additionally measured the bending and compressive strength.

The compression and bending behaviour of the PUR specimens were determined on a universal test machine Zwick Z030, Zwick Roell Group, Ulm, Germany. Compression properties were determined according to EN 826:2013. The test specimens were compressed between the two plates of the universal test machine. At a constant rate of 0.5 mm/min, they were applied to the specimen till failure occurred. Bending behaviour was determined according to the requirements of EN12089:2013. The specimens were tested in three-point bending mode in a universal test machine. At a constant rate of 0.5 mm/min, failure occurred. The compressive and bending properties of the specimens are summarized and presented in Table 3. The (σ_M (MPa) represents compressive strength and σ_b (MPa) bending strength.

Table 3: Mechanical properties of PURs.

Specimens	σ_M (MPa)	σ_b (MPa)
PUR 0	335 ± 19	293 ± 6
PUR 1	220 ± 11	260 ± 9
PUR 2	314 ± 16	253 ± 19

The compression and bending strength of the AAM samples were determined on a laboratory test machine (and were measured with ToniPRAX (ToniTechnik, Berlin, Germany) at a force rate of 0.05 kN/s). The compressive and bending properties of the AAM samples are presented in Figures 17 and 18.

Strengths were also measured on PUR samples. We measured using a Durometer device, according to EN ISO 868:2004. Durometer hardness is a dimensionless quantity. It represents a relative comparison of hardness between different but similar classes of materials where hardness is measured at the same durometer scale. A Shore A hardness tester (Zwick, Ulm, Germany) was used.

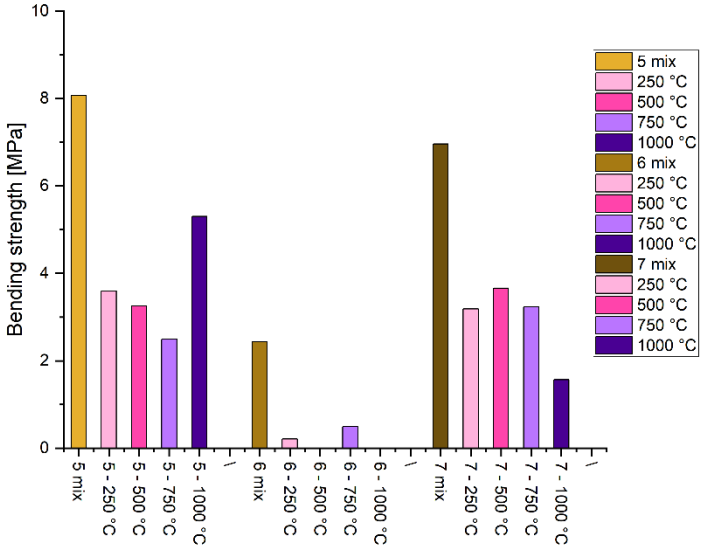

Figure 17. Bending strength of samples Mix 5, Mix 6, and Mix 7 at different temperature treatments.

Source: own.

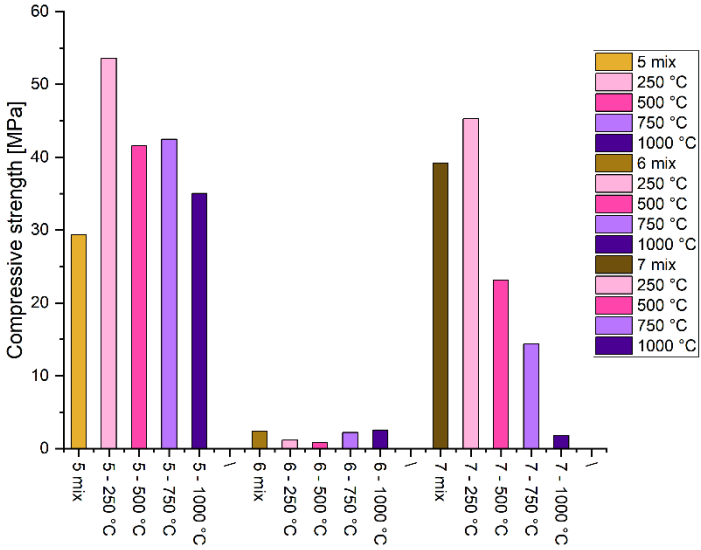

Figure 18. Compressive strength of samples Mix 5, Mix 6, and Mix 7 at different temperature treatments.

Source: own.

Shore hardness measurements also showed differences between the samples with the pristine pure PUR 0 sample once again having higher hardness (Shore A Durometer Hardnesses around 30) than PUR 1 (Shore A Durometer Hardnesses around 16) and PUR 2 (Shore A Durometer Hardnesses around 16 Hardnesses around 14) where an organic flame retardant additive was added.

The changes due to the added APP and TATA which were manifested in the different formation of the network structure in PUR 0, PUR 1, and PUR 2 (which we saw in Figure 1 and the different pore sizes in Figure 2) also impact the hardness of the materials due to polymer additives. Of course, the influence of APP and TATA on the flammability of PUR materials was also expressed in the XRD analysis. Below, Figure 19 shows the XRD pattern of all three PURs, the original PUR 0, PUR 1, and PUR 2.

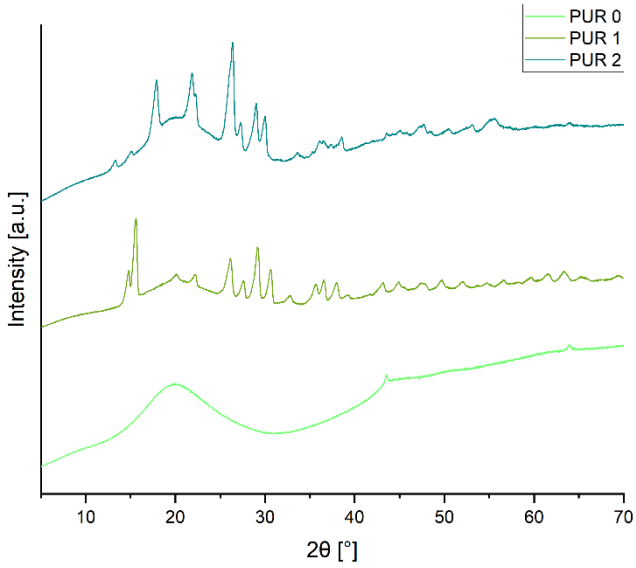

Figure 19: XRD patterns of PUR samples.
Source: own.

Also, the chemical influence of APP and TATA addition on AAM is evident from the FTIR spectrum (Figure 20).

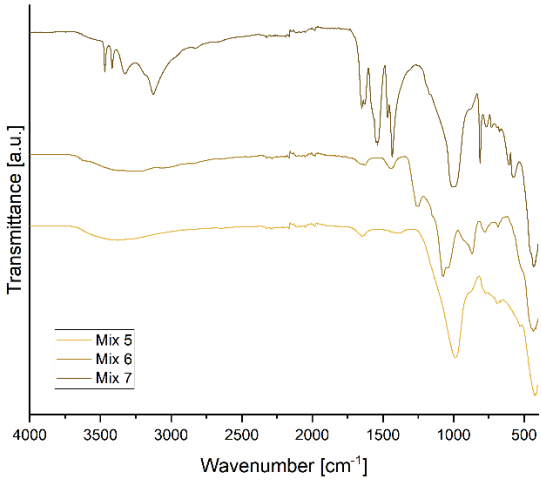

Figure 20: FTIR spectrum of the AAM materials Mix 5, Mix 6, and Mix 7.
Source: own.

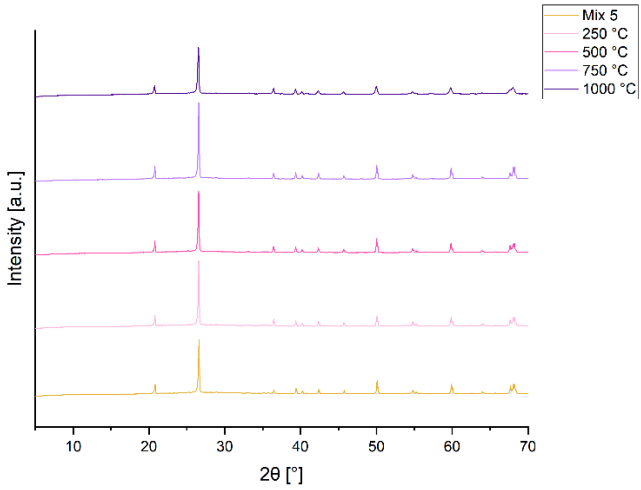

Figure 21: XRD pattern of the sample Mix 5 at different temperature treatments.
Source: own.

If we compare the FTIR spectrum of the powdered raw materials in Figure 2 and the FTIR spectrum of the AAM composite materials in Figure 20, we can see that there is no induced chemical reaction at room temperature in cases of Mix 5 and Mix 7 while in the case of Mix 6, we can see that the change is occurred (even during the mixing of the APP with alkali the gases released).

The XRD pattern presented in Figure 21-23 shows that with increasing temperature in samples Mix 6 and Mix 7, there were changes in curves while in Mix 5 there were no changes.

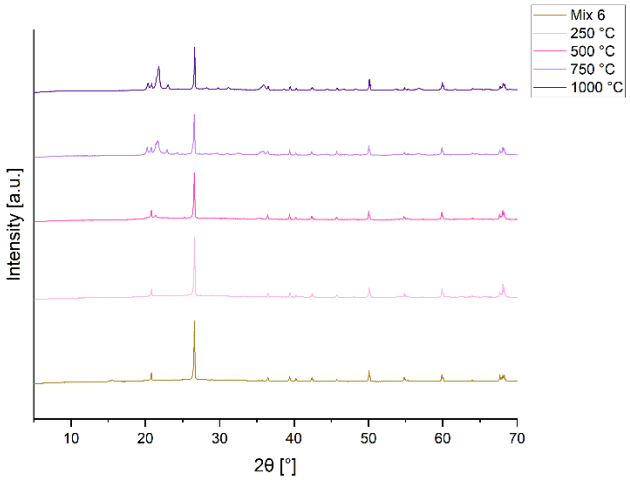

Figure 22: XRD pattern of the sample Mix 6 at different temperature treatments.
Source: own.

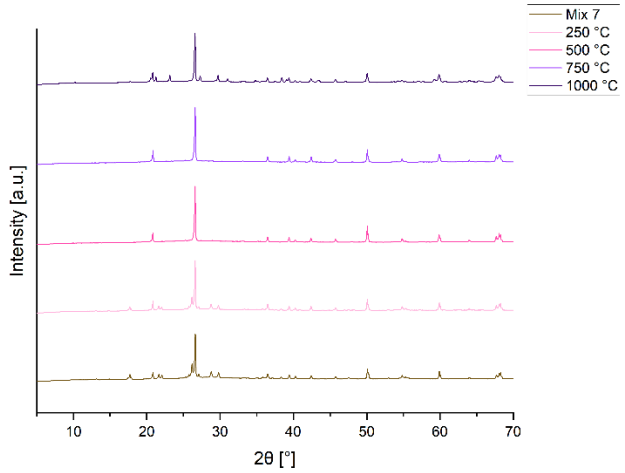

Figure 23. XRD pattern of the sample Mix 7 at different temperature treatments.
Source: own.

In Figure 21, the XRD pattern of Mix 5, it is seen that there are no changes up to 1000 °C and the material is very temperature stable. In Figure 22, the XRD pattern of Mix 6, it is seen that at temperatures T0 and 250 °C, we cannot see the presence of APP which was dissolved in an alkali solution. At 500 °C, we can see the beginning of the mineralogical changes in sample Mix6 which are even more visible at temperatures 750 °C and higher. In Figure 23, the XRD pattern of Mix 7, the presence of TATA is seen up to 500 °C. We can also see the appearance of new compounds at 750 °C and 1000 °C (similar to the pores size distribution behaviour).

5 Conclusions

In the present work, two polymer additives that are used as flame retardants are included in two completely different materials by chemistry, final properties, and the purpose of use. In PURs, which are used as insulating materials, fire-retardant properties were increased while in AAM materials which are non-flammable, fire-retardant material that does not react with alkali got well encapsulated in the ASN where it is permanently stored for the case of the fire in the surrounding materials.

Flame retardants reduced the strength and stress in the PUR polymer matrix. Additives APP and TATA still maintained satisfactory mechanical properties of PURs although the hardness of PUR 1 and PUR 2 weakened and both, TATA and APP, significantly reduced inflammation.

The mechanical properties of AAM composites with APP and TATA are inferior compared to pure AAM, especially for APP. The combinations of fire retardant powders and AAM reduce the density. Flame retardants have expectedly better and greater positive effects on PUR than AAM.

Acknowledgment

This work is part of the ARRS project of Barbara Horvat, Ph.D., and was financially supported by the Slovenian Research Agency under Grant No. J2-3035 and also by Slovenian Research Agency program group no. P2-0273.

References

Amran U.A., Salleh K.M., Zakaria S., Roslan R, Chia C.H., Jaafar S.N.S, Sajab M.S, Mostapha M., 2021, Production of Rigid Polyurethane Foams Using Polyol from Liquefied Oil Palm Biomass: Variation of Isocyanate Indexes. Polymers, 13, 3072.

Covaci A., Gerecke A.C., Law R.J., Voorspoels S., Kohler M., Heeb N.V., Leslie H., Allchin C.R., De Boer J., 2006, Hexabromocyclododecanes (HBCDs) in the environment and humans: a review. Environ Sci Technol, 40(12):3679-88. doi: 10.1021/es0602492.

Dyrud A.M., Polluting the Pristine: Using Mount Everest to Teach Environmental Ethics, < https://peer.asee.org/polluting-the-pristine-using-mount-everest-to-teach-environmental-ethics> accessed 14 September 2023.

EN 826:2013. Thermal insulating products for building applications – Determination of compression behaviour.

EN 12089:2013. Thermal insulating products for building applications - Determination of bending behaviour.

EVS-EN ISO 868:2004. Plastics and ebonite – Determination of indentation hardness by means of a durometer (Shore hardness).

Fink, J.K.,2018, Poly(Urethane)s. In Reactive Polymers: Fundamentals and Applications; Elsevier, pp. 71–138, Amsterdam, The Netherlands

HBCD use in EPS for Building Applications, ICL-IP Europe BV, 06/07/2014, https://www.psloop.eu/wp-content/uploads/2023/08/Guide-for-PS-Loop_collection-and-pretreatment-of-EPS-waste_english.pdf accessed 31 Maj 2023.

Horvat B., Mušič B., Pavlin M., Ducman V., 2023. Microwave Irradiation of Alkali-activated Metakaolin Slurry, in: 5th International Conference on Technologies & Business Models for Circular Economy: Conference Proceedings. Presented at the International Conference on Technologies & Business Models for Circular Economy, University of Maribor Press, pp. 9–24. https://doi.org/10.18690/um.fkkt.1.2023.2

Horvat B., Pavlin M., Ducman V., 2022c. Influence of microwaves in the early stage of alkali activation on the mechanical strength of alkali-activated materials. Ceramics International. https://doi.org/10.1016/j.ceramint.2022.12.133.

Horvat B., Mušič B., Pavlin M., Ducman V., 2022b. Microwave irradiation of alkali-activated metakaolin slurry. Presented at the 5th International Conference on Technologies & Business Models for Circular Economy. https://doi.org/10.18690/um.fkkt.6.2022.

Hejna A., Haponiuk J., Piszczyk Ł., Klein M., Formela K., 2017, Performance Properties of Rigid Polyurethane-Polyisocyanurate/Brewers' Spent Grain Foamed Composites as Function of Isocyanate Index. Polymers, 17, 427–437.

ISO 291:2008 Plastics — Standard atmospheres for conditioning and testing.

ISO 845:2006. Cellular plastics and rubbers - Determination of apparent density.

Laoutid F., Bonnaud L., Alexandre M., Lopez-Cuesta J-M., Dubois P., New prospects in flame retardant polymer materials: from fundamentals to nanocomposites, 2009, Mat. Sci. Eng. R, 63, 100-125., https://doi.org/10.1016/j.mser.2008.09.002.

Miller, N.,. 2023, The industry creating a third of the world's waste <https://www.bbc.com/future/article/20211215-the-buildings-made-from-rubbish> accessed 25.August 2023.

Mušič B., Knez N., Bernard J., 2022, Flame Retardant Behaviour and Physical-Mechanical Properties of Polymer Synergistic Systems in Rigid Polyurethane Foams. Polymers, 14, 4616. https://doi.org/10.3390/polym14214616.

Shaw S.D., Blum A., Weber R., Kannan K., Rich D., Lucas D., Koshland C.P., Dobraca D., Hanson S, Birnbaum L.S., 2010, Halogenated flame retardants: do the fire safety benefits justify the risks? Rev. Environ. Health 25, 261–305.

TECHNO-ECONOMIC MODEL OF MULTIMODAL TRANSPORT

DAVID POUL, JIŘÍ GREGOR, MARTIN PAVLAS,
YEE VAN FAN

Brno University of Technology, Faculty of Mechanical Engineering, Brno, Czech Republic
David.Poul@vutbr.cz, Jiri.Gregor@vutbr.cz, martin.pavlas@vutbr.cz, fan@fme.vutbr.cz

With the current effort to reduce transport emissions, the shift in the transport of goods from road to rail or combination is expected on a larger scale. For this shift to have the expected results, it needs to be supported by detailed project planning and calculation. The paper presents the techno-economic model of multimodal transport, focusing on road and rail transport. The model includes a vast database of transport systems for both types of transport. To complete the logistic chain, the model includes the calculation for transfer stations, handling equipment, and other needed parts. The model also includes an economic evaluation allowing analysis of the whole logistic chain of multimodal transport or performing the comparison of individual types of transport.

DOI
https://doi.org/10.18690/um.fkkt.1.2024.6

ISBN
978-961-286-829-1

Keywords:
techno-economic model,
multimodal transport,
rail transport,
road transport,
intermodal systems,
transfer station,
circular economy

University of Maribor Press

1 Introduction

The current state of computational support of multimodal transport is insufficient. Models are simplified and do not always include all important parts of the logistics chain. One can often come across models that are not connected to real infrastructure and using only parameter for distance without considering e.g. slope or different route class (Jiang J. et al 2020) or include only general types of transport systems (Jiang C. 2022) which is not possible to modify without changing the calculation. Many simplifications result in inaccuracies that affect the evaluation quality. It is also necessary to distinguish between models that focus on mathematical optimization versus models that focus on technical-economic evaluation. The first-mentioned models, i.e. models or modelling approaches focusing on mathematical optimization, can be found more often in the literature. Techno-economic models are difficult to find on the level that is detailed enough for the universal use case.

In terms of multimodal transport, the models very often focus on the evaluation of emission production, especially CO_2, when comparing individual types of transport (Kirschstein, Meisel 2015) and not cost evaluation. If the models consider cost evaluation, their frequent shortcoming is only a simplified calculation, i.e. consideration of constant values of transport costs for individual modes of transport independent of the route, often given in the unit [€/tkm] (Christensen, Labbé 2015). This is addressed (Gregor, Šomplák, Pavlas 2017), which considers individual factors (vehicle type, consumption, route, loaded weight, etc.). As a result, compared to the previous approach, transport costs are not constant, but a variable value defined by different parameters.

(Niérat 2022) deals with the comparison of road and intermodal transport from the Dutch ports of Dunkirk and Zeebrugge to Dusseldorf and follows on from article (Hintjens et al. 2020). The authors make a critical reflection on some decisions and assumptions - overestimation of the intensity of traffic, underestimation of the costs of the intermodal chain - which in the compared article leads to a more significant decrease in the costs of intermodal transport compared to road transport. On the contrary, in the following article, intermodal transport is only a few percent cheaper than the purely road variant - this is due to the inclusion of the costs of transshipment of containers in the port, the transfer from road to rail transport and, above all, the inclusion of costs for the last section of the journey - transfer from rail

to road transport and delivery of cargo to the destination within the urban agglomeration – this final transfer was completely omitted in the referenced article. Here it's noticeable how important it is not to neglect the individual steps of the logistics chain, which can subsequently lead to a significant advantage of a certain type of transport. In terms of the model, simplifications were considered in both articles – the costs were determined on an annual basis and for a specific transport system – so one cannot speak of the universality of the model.

As it follows, a minimum of articles, models, or tools are devoted to complex multimodal transportation from the point of view of cost and technical evaluation. Probably the most overlooked part of the models is the transportation system specification, which is mostly generic, with no possibility of variability for the needs of the user. This problem occurs especially in the case of rail transport, which is evaluated rarely in the mentioned models and, if so, its specification lacks more detailed parameters. A critical feature of the models is the inclusion of all parts of the logistics chain – if even small parts are omitted, the results may be distorted, which may favour a certain type of transport. Therefore, creating an advanced techno-economic model of multimodal transport, which can evaluate in detail the technical, economic, and environmental demands of a given logistic chain is required.

2 Techno-economic model

The work aims to create a universal techno-economical model of multimodal transport (i.e. "TE model") with a focus on road and rail transport. Other modes of transport can be added if needed. The model in main form is created for users with basic knowledge of logistics but it also supports going deeper into the details if users have the knowledge to set the model correctly. The model can evaluate the whole chain as well as individual parts of the logistics chain so it can also be used for comparing different scenarios or individual types of transport.

The research showed key areas which the model should consider. Those areas are:

- Wide database of transport systems for road and rail transport
- Inclusion of all key parts of the logistics chain

- Infrastructure network based on real infrastructure
- Determination of the theoretical consumption of the transport system
- Determination of relevant elements for the evaluation of emission production (CO_2, NO_X, solid particles, etc.)
- Detailed assessment of technical and economic parameters

The model supports the use of two main types of transport – intermodal transport where the goods are loaded in a single transport unit for a whole transport so there is no manipulation with goods as itself (e.g. intermodal container is used) and "classic" type of transport when it is necessary to handle the goods every time in case of changing the transport mode.

The user will be able to evaluate the current situation (e.g. the use of purely road transport) and the newly proposed one, where it will be, for example, the use of multimodal transport for transport from point A to point D. The example will be shown for waste transport. After collecting the waste in point A, the road transport will be used to point B, where the waste will be transferred into an intermodal unit and then loaded onto a railway wagon. Rail transport will be used from point B to point C. The last step will be to transfer it to a road vehicle again and from point C to point D road transport will be carried out. The transport scheme is in Figure 1.

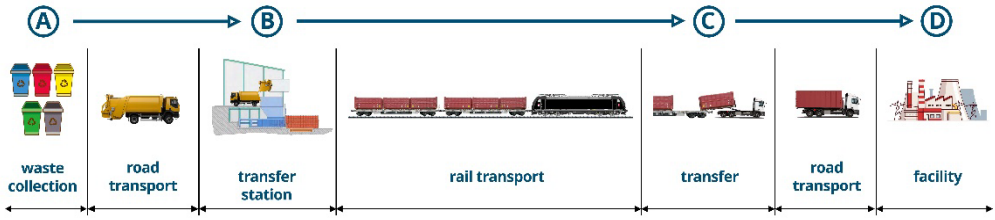

Figure 1: The example scheme of multimodal transport

Source: own

The model is composed of sub-models that include:

- Road transport
- Rail transport
- Transfer station
- Handling equipment

Transshipments between different modes of transport are a key part of the logistics chain. The transshipment can be done simply with the use of handling equipment on the paved area, e.g. next to the track at the railway station. When transferring a large volume of goods frequently with adjusted the entire system, it is worth using a stationary transfer station. Most often it's done for transshipment of intermodal containers.

A wide range of different transshipments can be encountered within the logistics chain. It is, therefore, necessary to focus on individual aspects that are important for the given transshipment. For example, the transfer of bulk materials using a wheel loader has significantly different technical specifications and costs than the transfer of liquid components from tanks or the use of a stationary transfer station for transferring containers.

Due to the scope of the article, the sub-models for transfer stations and handling equipment will not be analysed in detail in this article. The focus will be mainly on road and rail transport.

The main sub-models are the ones for road and rail transport. Both models are created with the same structure and layout so it's user-friendly. Both models are also designed with the same input and output parameters. This ensures the possibility of easy connection of both models and the possibility of easy comparison of both types of transport. The structure of both models is shown in Figure 2.

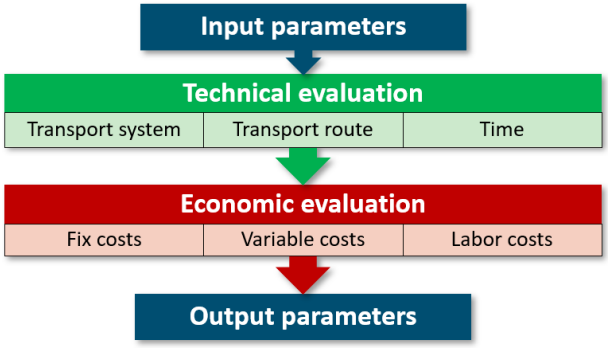

Figure 2: Structure of sub-models

Source: own

The models have numerous input parameters, e.g. the sub-model for road transport has 98 parameters and the one for rail transport more than 110. Many of those parameters are based on research and it's not necessary to change them often. But it's still possible because they affect evaluation. Also number of parameters is changed automatically based on a selection of the transport system or pre-set data or limits. The key input parameters are:

- Starting point
- Destination point
- Type of transport system
- Bulk density or transported weight per cycle [kg/m^3, t]
- Transported weight per year or weight which is needed to be transported [t/year, t]

Main output parameters are:

- Total annual costs [€/year]
- Cost of 1 ton [€/t]
- Costs per 1 tonne-kilometre [€/tkm]
- Number of cycles per year [-]
- Theoretical utilization of the transport system [%]
- Annual mileage [km/year]
- Reworked weight in one cycle (loaded weight) [t]

2.1 Integration to the optimization tools

The model can be integrated into optimization tools. It is possible to use it as a whole, i.e. with a complex detail, but this increases the computational requirements, which is not desirable in most cases. Otherwise, the model can be simplified by setting aside selected parameters that will change for the task and consider the rest of the parameters as constants. Subsequently, the entire model is reduced to one equation.

The model also be used for pre-processing or post-processing. The typical approach can be:

- pre-calculations by TE model (e.g., all routes combinations - price, time, etc.) – input to optimization task
- optimization task (e.g., position of transfer stations and necessary supply routes)
- refinement of the output from the optimization task with use of TE model

3 Database of transport systems

Defining the transport system is an important part of the model. Since the model is universal, the database for road or rail transport includes a variety of different elements from which the final transport system can be set up. An important note is also that users can add elements of the transport system to the database.

The database for road transport considers:

- Passenger car
- Van
- Semi-trailer tractor
- Rigid chassis
- Semi-trailer
- Trailer
- Container
- Custom rigid cargo bodies

The database for rail transport considers:

- Locomotives
  - Electric
  - Diesel
- Goods wagons
  - Flat/intermodal wagon
  - Open/covered wagon
  - Tank wagon
- Intermodal containers

Each of the parts listed above includes many different real types with technical parameters given by product lists or companies. For example, each of the locomotives in the database is not only defined by general parameters such as weight, number of axles, etc. but also has given a traction characteristic (Figure 3) with which the model calculates.

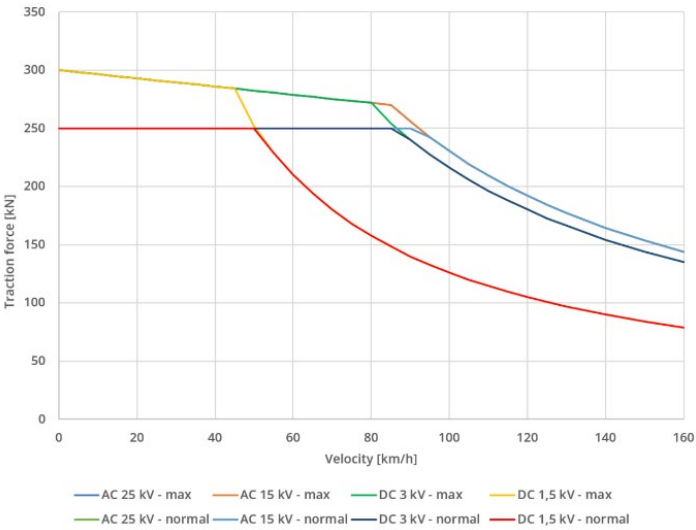

Figure 3: Traction characteristics of Siemens Vectron locomotive
Source: own based on Siemens's product list

The database makes it possible to select individual parts of the transport system and to assemble the final one in a modular way so it means that every different setup will have different parameters such as empty weight, different possible payload, each locomotive has different traction characteristics, power and so on. This guarantees that the model will calculate with accurate data. In terms of intermodal transport, i.e. intermodal containers, the database currently contains ISO containers, Innofreight system and ACTS system (Abroll Container Transport System).

4 Infrastructure network and route evaluation

Infrastructure is based on real data for both road and rail transport. Currently, the model includes infrastructure for the Czech Republic but it's possible to add other countries (and update the model with the specifics of operation in the given country).

However, since both types have their specifics, the next chapters will describe infrastructure in more detail.

4.1 Road transport

Road infrastructure is quite complex. Since the main focus of the model is for freight transport and not all roads are passable for trucks, it was possible to reduce the complexity of the network. All municipalities (6,254) can be considered as a benchmark. After proper evaluation, the smallest municipalities were taken out and the points of interest were added (Waste-To-Energy power plants, landfills, large production complexes outside the municipalities, etc.). With that, the database contains 1,132 points.

The real network was reduced with the condition that it's possible to connect all those points for different categories of vehicles. However, there are points where it's not possible to get by some categories of vehicles (large vehicle/truck) because there is some barrier (load capacity of the bridge, low underpass height). The categories were based on weight and size:

- Category 0: passenger car
- Category 1: max 3.5 t, max 2.5 m
- Category 2: max 10 t, max 3.2 m
- Category 3: max 26 t, max 4 m
- Category 4: max 48 t, max 4 m

The output network consists of 230,835 sections which respect intersections, turns, etc. Each section is defined with multiple parameters such as length, route class, slope, if there is tunnel or bridge, etc. As Figure 4 shows, the network is still quite complex and detailed.

Since the infrastructure considered in the model is not 1:1 with real infrastructure, the route evaluation in the model allows the user to add e.g. the last section from the destination point based on the network (the added section is defined only with length) and thus make the calculation more precise. The model also allows ignoring

included infrastructure and defining the transport route manually based on length for each route class.

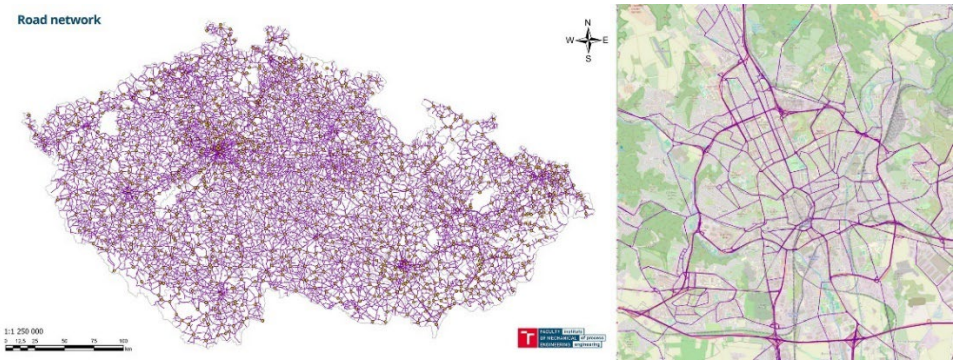

Figure 4: Road infrastructure

Source: own

A sample evaluation for different categories of vehicles is shown in Figure 5. It's noticeable that there are barriers for higher categories, and it is therefore necessary to use a different transport route, usually a longer one, which leads to different results in the overall evaluation.

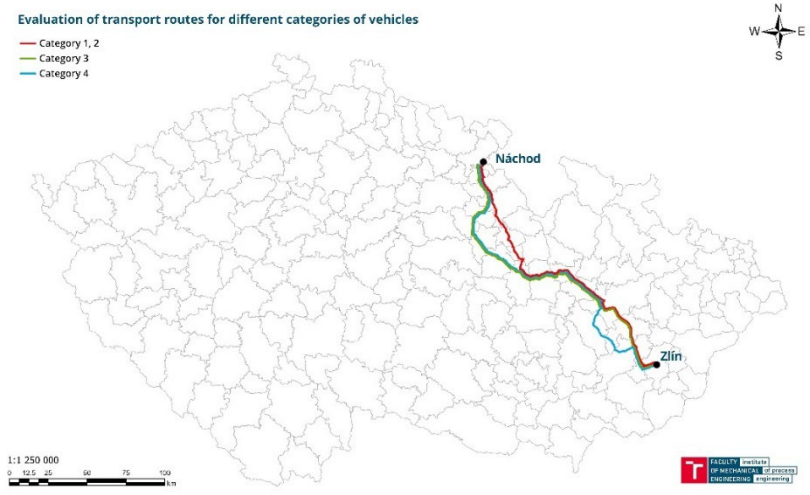

Figure 5: Evaluation of transport routes for different categories of vehicles

Source: own

It is also possible to evaluate route with multiple segments or circular route (Figure 6, Figure 7). The load factor can be different for each segment allowing to calculate loading/unloading at multiple stops.

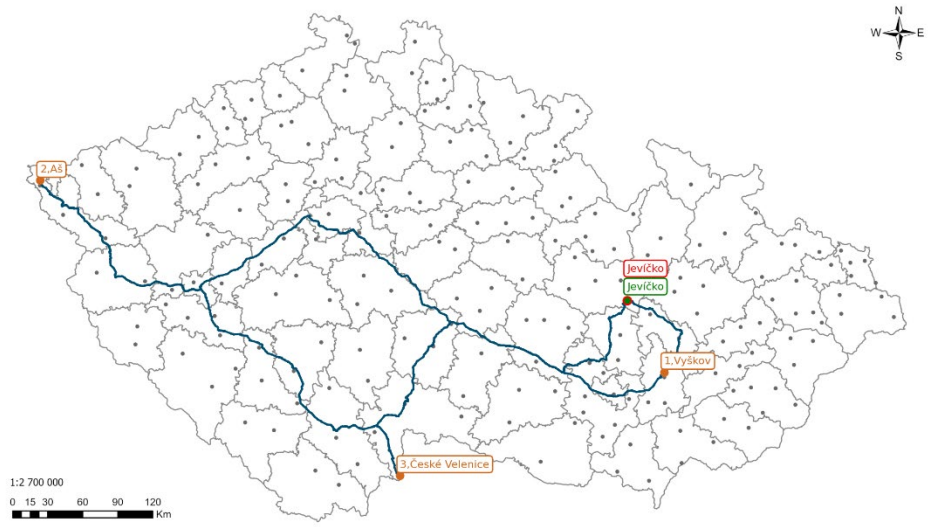

Figure 6: Circular route

Source: own

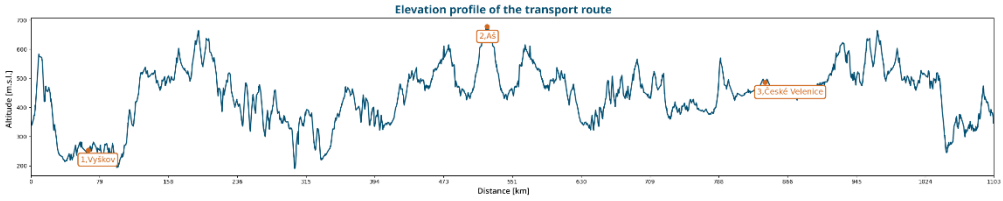

Figure 7: Elevation profile of the transport route

Source: own

4.2 Rail transport

Since the rail infrastructure is not as complex as the road one, the model incorporates full real infrastructure. The only limitation for now is that the double track is considered a single track. In some sections, this can make a difference in a different speed profile in the curves on each track. However, this should be addressed in the next update of rail infrastructure considered in the model.

The rail infrastructure includes 2,755 points with 4,118 sections. This apparently low number is due to the original division of the individual interstation sections with regard to the slope of the track, not the individual curves on the track. As it was mentioned before with a number of tracks, this should be addressed as well in the next update of infrastructure. Each section has 28 parameters that the model can use for the calculations, such as the length of the section, maximum speed, road class, normative length of the train, etc. Rail infrastructure is in Figure 8.

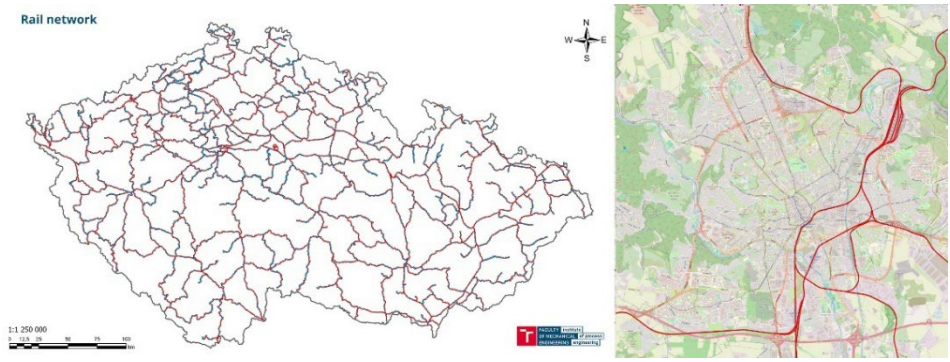

Figure 8: Rail infrastructure
Source: own

Based on the defined transport system, the model will evaluate the limiting parameters and conditions (length of the train, axle load, traction power of the locomotive, etc.). The user can also limit some sections of the infrastructure, for example, due to the closures. Then the model will find the best transport route based on the conditions.

Part of the evaluation is the calculation of speed profile and energy/fuel consumption. This calculation considers multiple parameters such as the traction characteristics of the locomotive, load of the train, slope of the track, multiple resistances of the train, etc. The calculation is quite complex and again, due to the scope of the article, it won't be described in detail. The sample evaluation of the speed profile is in Figure 9, force diagram in Figure 10. Calculated consumption is in kilowatt hours [kWh] or litres [l].

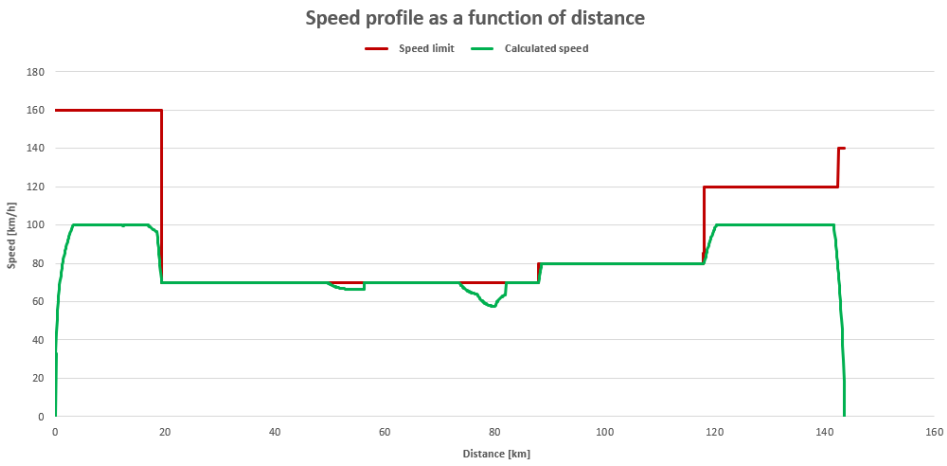

Figure 9: Speed profile as a function of distance
Source: own

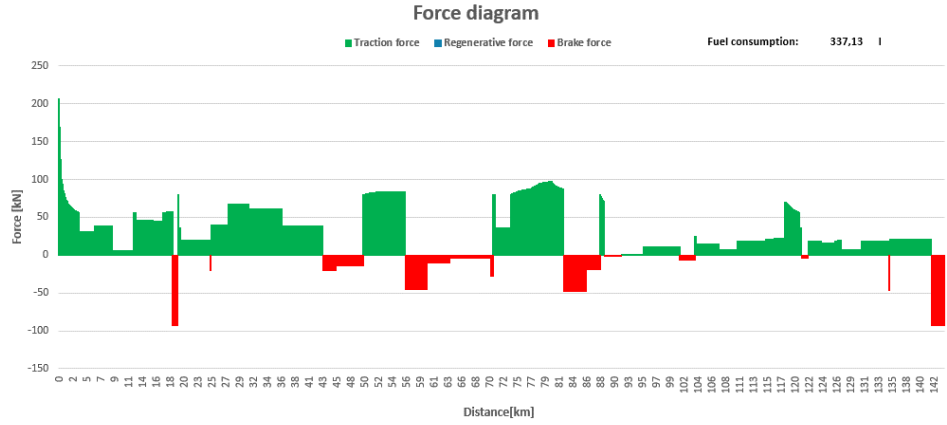

Figure 10: Force diagram, source: own
Source: own

Since the model and rail infrastructure do not consider curves on the track it's noticeable that in the speed profile, there are no drops in speed caused by lower maximum speed in curves (there are speed drop caused by slope of the track). It's going to be addressed in the next update of infrastructure with higher detail.

5 Emission production

The production of emissions is an often talked about topic these days. There is a significant effort to reduce produced emissions, as transport is a significant air polluter and there are many ways to calculate emissions production. The one which is used in the presented model is based on fuel/energy consumption calculated by the model and values of emission factors given by „EMEP/EEA air pollutant emission inventory guidebook 2023" published by the European Environment Agency (EEA), an agency of the European Union. An example of emission factors given by the guidebook is in Table 1 for NO_X and Particulate matter (PM). Emission production for CO_2 is given by the combustion equation, respectively the emission factor for the fuel.

Table 1: Emission factors for NO_X and PM

Vehicle category	Fuel	NO_X [g/kg fuel]			PM [g/kg fuel]		
		Mean	Min	Max	Mean	Min	Max
Passenger car	Petrol	8,73	4,48	28,89	0,03	0,02	0,04
	Diesel	12,96	11,20	13,88	1,10	0,80	2,64
	LPG	15,20	4,18	34,30	0,00	0,00	0,00
Light commercial truck < 3,5 t	Petrol	13,22	3,24	25,46	0,02	0,02	0,03
	Diesel	14,91	13,36	18,43	1,52	1,10	2,99
Heavy duty vehicle > 3,5 t	Diesel	33,37	28,34	38,29	0,94	0,61	1,57
	CNG	13,00	5,5	30,00	0,02	0,01	0,04
Motorcycle	Petrol	6,64	1,99	10,73	2,20	0,55	6,02

Source: https://www.eea.europa.eu/publications/emep-eea-guidebook-2023/part-b-sectoral-guidance-chapters/1-energy/1-a-combustion/1-a-3-b-i/view

6 Economic balance

Before describing the costs, it is important to mention the time component of the entire evaluation. Based on the evaluation of the transport route, the time that the given transport will take from start to finish is determined - loading, transport, transhipment, further transport, unloading, etc. This time can be compared with the working time of the entire transport system in one day or a whole year. Thanks to this, a percentage representation of the evaluated transport to the total working time is calculated. This parameter can be described as the theoretical utilization of the transport system and it's important for the calculation of economic balance.

Costs can be divided into fixed and variable costs. Labour costs are set aside. Fixed costs are mainly the costs of purchasing or renting transport systems, their maintenance (annual technical controls, regular and irregular maintenance) and insurance together with road tax. Maintenance costs are set at a fixed amount per year - assumed regular maintenance or they can be evaluated based on total mileage which is nowadays quite typical in rail transport.

The model also considers the lifespan of each part of the transport system. For example, the typical lifespan of a semi-trailer truck is around 6-7 years, locomotive around 30 years. During the expected lifespan of the project under consideration, e.g. 20 years, the company will need to buy a new truck three times. The locomotive only once with the possibility of doing larger modification at half of the lifespan. Those differences for each transport type are considered in the model and are evaluated for each part of the transport system.

Variable costs include tolls and fees, tire costs based on annual mileage and operating costs. The toll fee is determined based on road class and toll sections. The biggest part of variable costs are operating costs. These are mainly determined by the consumption of fuel or electricity (rail transport), oil and AdBlue liquid, which is necessary to reduce emissions from exhaust gases. In the case of rail transport, these are also the costs of the transport route (similar to a toll) but are paid on the entire railway network.

The last big part is labour costs. These are considered on a simplified approach. Labour costs for the crew play a primary role. The remaining labour costs (administrative and operational overheads) are considered constant but can be developed based on more detailed information.

The economic balance considers several other parameters. Costs can be evaluated for the purchase or rental of transportation systems and their use only for evaluated transportation. The second option is the evaluation of costs based on the theoretical utilization of the transport system, which enables the percentage expression of costs to be determined with regard to the time required for the evaluated transport. With this approach is possible to combine multiple evaluated transports for one transport system.

6 Case study

The output of this article is a conference poster describing the main characteristics of the model, its usage and incorporating the model into optimization tasks. Thus, the presented study case is described briefly.

The presented model was used to design and evaluate the logistics chain for supply of heating plant in Olomouc which aimed to switch from coal to a mixture of biomass (20 kt/year) and alternative solid fuel (RDF) (80 kt/year). As part of the evaluation, suitable transport systems were proposed, for which theoretical breakpoints were determined. Figure 11 shows a comparison of road and rail transport for the transport of 20 kt/year of biomass and 80 kt/year of RDF. Due to the significantly larger quantity (and also bulk density, thus higher weight) in the case of RDF, rail transport has a lower price than road transport from 280 km as opposed to 490 km in the case of biomass.

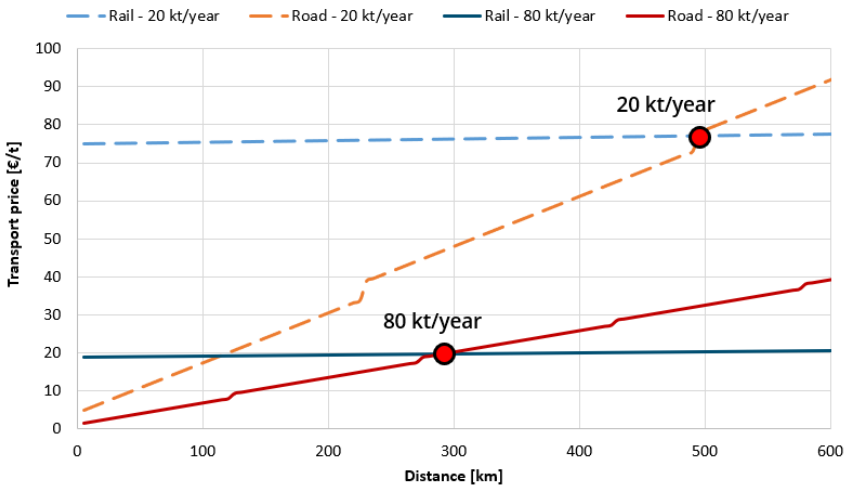

Figure 11: Theoretical breakpoints

Source: own.

Furthermore, localities with sufficient production of both commodities were selected and an evaluation was carried out for road and rail transport. Two main scenarios (1 – biomass from single location, 2 – biomass from 4 locations) were further divided into two variants in terms of locations of producers. Variant 1 was

carried out fully by rail transport, in variant 2 rail transport was used for RDF and road transport for biomass.

- 1a – RDF: Bielsko-Biala (Poland); biomass: Ždírec nad Doubravou
- 1b – RDF: Linz (Austria); biomass: Ždírec nad Doubravou
- 2a – RDF: Bielsko-Biala (Poland); biomass: Doloplazy, Bouzov, Vsetín, Otaslavice
- 2b – RDF: Linz (Austria biomass: Doloplazy, Bouzov, Vsetín, Otaslavice

Table 2 shows the resulting prices of the entire logistics chain for each variant. The cheapest option is option 2a, where RDF is transported from Bielsko-Biala (rail transport) and biomass is transported from 4 regional locations (road transport).

Table 2: Transport prices of individual variants

Variant	Price [€/t]
1a	20,2
1b	20,85
2a	19,83
2b	20,48

7 Conclusion

The techno-economic model presented in the article aims to focus on problematics in detail and addresses many areas which are insufficiently covered in models presented in current research. The model can be used to evaluate a wide range of transports, both from the point of view of the carrier and from the point of view of the contracting authority, which wants to know the costs of transport before starting negotiations with carriers.

Another use of models is in combination with optimization tools, where the techno-economic model can be used for pre-processing, or to refine the results of given optimizations. It can also be simplified and directly integrated into the optimization tool and help with the precision of optimization right away.

Acknowledgments

The authors gratefully acknowledge the financial support provided by the Technology Agency of the Czech Republic (TACR) as part of the Program Environment for Life, specifically through the project CEVOOH (SS02030008).

References

Jiang J., Zhang D., Meng Q., Liu Y. (2020). Regional multimodal logistics network design considering demand uncertainty and CO2 emission reduction target: A system-optimization approach, Journal of Cleaner Production, 248, doi: 10.1016/j.jclepro.2019.119304

Jiang C. (2022). Research on Optimizing Multimodal Transport Path under the Schedule Limitation Based on Genetic Algorithm, Journal of Physics: Conference Series, 2258, doi: 10.1088/1742-6596/2258/1/012014

Kirschstein T., Meisel F. (2015). GHG-emission models for assessing the eco-friendliness of road and rail freight transports, *Transportation Research Part B: Methodological, 73*, 13-33, doi: 10.1016/j.trb.2014.12.004

Christensen T. R. L., Labbé M. (2015). A branch-cut-and-price algorithm for the piecewise linear transportation problem, *European Journal of Operational Research, 245*, 645-655, doi: 10.1016/j.ejor.2015.03.039

Gregor J., Šomplák R., Pavlas M. (2017). Transportation Cost as an Integral Part of Supply Chain Optimisation in the Field of Waste Management, Chemical Engineering Transactions, 56, doi: 10.3303/CET1756322

Niérat P. (2022). Methodological shortcuts in intermodal freight transport: Critical review and proposals, *Journal of Transport Geography, 103*, doi: 10.1016/j.jtrangeo.2022.103396

Hintjens J., Van Hassel E., Vanelslander T, Van de Voorde E. (2020) Port Cooperation and Bundling: A Way to Reduce the External Costs of Hinterland Transport, *Transport Systems for Sustainability: Policy, Planning and Exploitation, 12*, doi: 10.3390/su12239983

Design and Manufacturing of Sustainable Industrial Packaging From Alternative Lignocellulosic Biomass

David Ravnjak,[1] Gregor Čepon,[2] Aleš Mihelič,[3] Tina Frangež,[4] Jawad Elomari[5]

[1] Pulp and paper institute, Ljubljana, Slovenia
david.ravnjak@icp-lj.si
[2] University of Ljubljana, Faculty of Mechanical Engineering, Ljubljana, Slovenia
gregor.cepon@fs.uni-lj.si
[3] Gorenje gospodinjski aparati d.o.o., R&D Laundry Care Competence Centre, Velenje, Slovenia
ales.mihelic@gorenje.com
[4] Surovina d.o.o., Maribor, Slovenia
tina.frangez@surovina.com
[5] SINTEF AS, Trondheim, Norway
jawad.elomari@sintef.no

DOI
https://doi.org/10.18690/um.fkkt.1.2024.7

ISBN
978-961-286-829-1

Due to high demand and increasing prices of wood-based cellulose, alternative sources of lignocellulosic biomass are gaining on their importance. Among them are invasive alien plants (IAP) that currently are being discarded (burned or composted) in spite the fact that they can be converted to useful products. For packaging of large home appliances, currently expanded polystyrene (EPS) is used. By exchanging EPS with cellulose-based (from IAP biomass) packaging, the circular nature of the packaging will be improved. Within the first stage of the LEAP project the potential of IAP biomass for conversion to cellulose and its use for production of foam formed packaging materials is being studied – various IAP have been evaluated in terms of their potential use for cellulose production, cellulose quality and key mechanical parameters. The data gathered is being used in computer assisted design and construction of packaging for large home appliances. A preliminary LCA analysis on the use of alternative raw materials as a source for cellulose production has also been performed.

Keywords:
cellulose,
invasive alien plants,
biomass,
alternative raw materials,
packaging design

University of Maribor Press

1 Introduction

For the industrial packaging of heavier products such as big home appliances, most often the protective elements, made of expanded polystyrene (EPS), are being used. The main role of this protective packaging is to provide mechanical protection of the packed product including shock absorption during transport and handling. Having good shock absorption properties and being a lightweight material EPS has proven itself as a good solution for this purpose. However, in terms of material itself there are some drawbacks using EPS based packaging – its non-biobased origin, its poor recyclability and non-biodegradability. According to EUMEPS the recycling rate of EPS in Europe is around 32 %, making EPS packaging a challenge in terms of circular economy, so solutions for its exchange with more sustainable materials are being developed.

One of possible solutions is the use of cellulose fibre based packaging for production of foam formed protective elements. Compared with EPS based packaging the protective properties of cellulose based packaging are not as good as those of EPS packaging, so additional research of material properties and packaging design is needed.

In terms of material sources for cellulose production invasive alien plants (IAP) represent a good alternative to wood. While there is generally a shortage of wood-based cellulose on the global scale, raw material from IAP is widely available as according to EU Regulation 1143/2014 it must be removed from the environment in order to protect the biodiversity. Currently this biomass after cutting is being discarded by burning or composting, hence losing significant quantities of valuable cellulosic fibre material. By converting IAP into cellulosic fibre material new alternative source of cellulose from currently unused biomass will be gained, opening additional possibilities for its use in fibre-based packaging.

Within the LEAP research project various types of IAP are being studied in terms of their potential use for cellulose production, cellulose quality and key mechanical parameters for production of foam formed packaging. By exchanging EPS-based packaging with cellulose-based packaging from IAP biomass, the circular nature of the packaging will be improved while using the raw material from alternative, not wood-based source.

2 Materials and methods

2.1 Data on collection process for IAP

The data on existing processes for collection of IAP was gathered via questionnaire sent to the providers of public services. The questionnaire contained questions on frequency of IAP collection, type of collection process and treatment of IAP biomass after collection. Data was statistically evaluated and a general process scheme of collection process was designed. Furthermore a proposal for an improved collection process was made and comparison in terms of environmental impact was performed using the SIMAPRO software tool.

2.2 Evaluation of IAP potential for cellulose production

For the evaluation of IAP potential for cellulose production the IAP biomass was subjected to the kraft pulping process where after solubilizing extractives, lignin and hemicellulose, cellulose fibre materials were isolated by filtration, according to the procedure described in work by Kapun *et. al.* The chemical structure, mechanical, optical and morphological properties of were determined and compared to those of bleached eucalyptus pulp and unbleached softwood pulp. For the first series of evaluations, biomass originating from the stems of Japanese knotweed (*Fallopia japonica*) was selected.

2.3 Preparation of samples / prototypes

Cellulose pulp obtained by the kraft pulping process was used for preparation of standard test specimens that will be used for the performing the compression test of cellulose based protective packaging. The specimens were prepared by wet moulding process using pulp dispersion with 1 % solids content, where the solids composition was: 26 % commercial softwood pulp, 26 % commercial hardwood pulp, 35 % IAP pulp, 9 % inorganic fillers, 3 % cationic starch and 1 % sizing agent. The same pulp with addition of foaming agent was used for preparation of foam formed prototypes.

3 Results and discussion

3.1 Collection systems for IAP

Based on the results of the questionnaire it has been established that 72 % of public service providers have an established system for collection and removal of IAP. For removal process to be effective also the correct seasonal timing is crucial – only 44 % of public service providers collect and remove the IAP regularly (more than three times a year), while about one third performs the removal once a year and 22 % on request only.

After the IAP are removed from the environment proper handling of this biomass is extremely important. By using proper handling methods (such as incineration in incineration facility or burning on collecting site) potential spreading of IAP is prevented, while using improper handling (e.g. landfilling or composting) can potentially facilitate the spreading (Invasive Species Council of BC, 2021). In terms of handling methods one third of public service providers incinerate the collected IAP biomass, while one third handover the IAP biomass to landfill and 26 % use composting as IAP biomass treatment.

For potential industrial use of IAP biomass also the purity (in terms of material type) of collected biomass is important. It is desired that IAP are collected separately from other (native) plants and in case of areas where IAP are already the predominant species a separation by IAP species would be preferrable. Currently slightly more than a half of public service providers is removing and collecting IAP separately from native plants. However separate collection of individual IAP species is not performed by any of them as there is not enough data (including cost benefit analysis) on utilisation of IAP biomass for production of useful products such as pulp and paper or fibre-based packaging.

Within the evaluation of collection systems also a new system for collection of IAP has been proposed. Compared to existing collecting systems, where all streams are being collected centrally in one facility and then discarded by incineration or composting, in the new system the separation of IAP is done already on site during harvesting, followed by individual treatment of IAP material streams consisting of separation of wooden parts (stalks) from other residues (roots, leaves) and grinding

the wooden parts into wood chips which are being used as raw material for production of cellulose pulp.

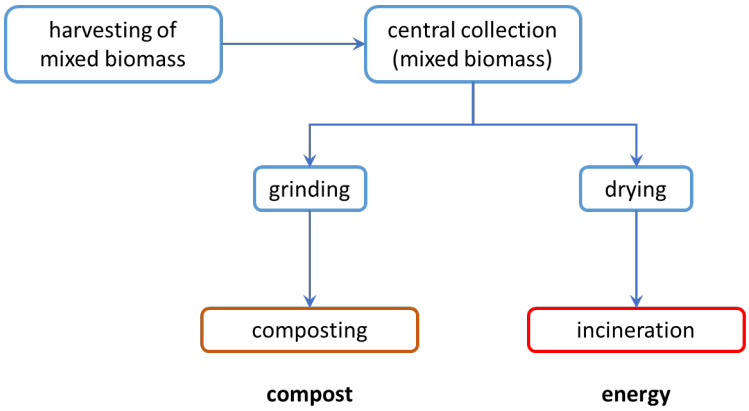

Figure 1: Process scheme of existing IAP collecting system

Source: own.

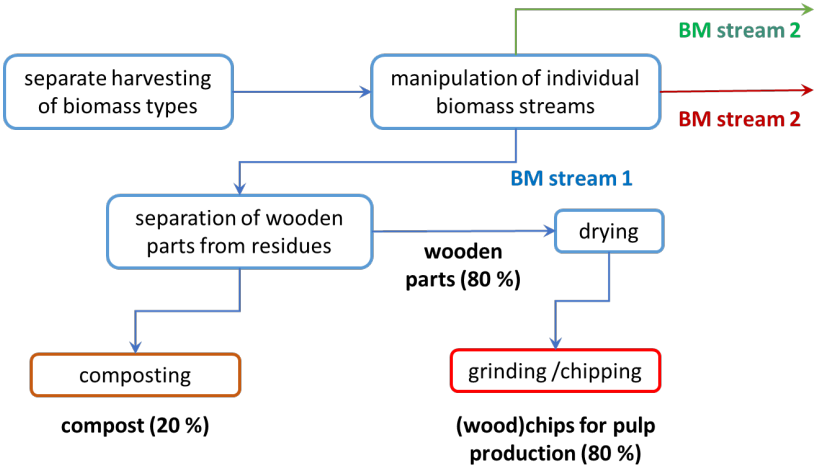

Figure 2: Process scheme of proposed new IAP collecting system

Source: own.

For both processes presented in figures 1 and 2 an LCA evaluation has been made by the SIMAPRO software using the ReCipe calculation method. The results show relative improvement (reduction) of environmental impact when using the new

(modified) collecting system for IAP. Main improvements of environmental impact are seen in terms of reduced CO_2 and SO_2 emissions, reduced use of fossil energy, reduced water eutrophication and improved biodiversity. However it should be noted that, compared to the original process, the new process is giving intermediate products intended for further use and does not generate energy.

3.2 Potential of IAP for cellulose production

By using the kraft pulping process for treatment of wood chips from Japanese knotweed a fractionation of the IAP biomass into five main components (cellulose, hemicellulose, lignin, wood extractives and ash) has been performed. This was followed by determination of fibre morphology and main mechanical properties of obtained pulp. The results and a comparison to bleached eucalyptus pulp and unbleached softwood pulp are presented in tables 1 and 2.

Table 1: Composition of biomass from Japanese knotweed in comparison to eucalyptus and softwood

	Japanese knotweed	Eucalyptus	Softwood
cellulose (%)	35	54	57
hemicelluloses (%)	37	21	25
lignin (%)	27	26	26
extractives (%)	1,5	5	5
ash (%)	2,5	0,9	0,9

Table 2: Fibre and pulp properties of pulp from Japanese knotweed in comparison to bleached eucalyptus pulp and unbleached softwood pulp

	Japanese knotweed	Eucalyptus (bleached)	Softwood (unbleached)
fibre length (mm)	0,670	0,876	2,07
fibre diameter (µm)	19,7	14,88	27,74
cell wall thickness (µm)	6,86	3,77	4,95
fines (%)	6,58	4,41	4,13
fibrillation (%)	1,58	1,33	1,04
drainability (°SR)	17,5	14,5	12,5
tensile index (Nm/g)	33,91	19,24	20,51
tear index (mNm^2/g)	4,05	1,8	7,55
burst index ($kPam^2/g$)	1,68	0,67	1,04
stiffness (mN)	70,6	80,3	70,9

In terms of material composition Japanese knotweed contains similar portion of lignin as eucalyptus or softwood. The cellulose content is 35 %, however the difference (compared to eucalyptus or softwood) is compensated by significantly higher hemicelluloses content. Along with lower extractives content the ash content is more than double compared to eucalyptus or softwood.

In terms of fibre and pulp properties cellulose from Japanese knotweed can be positioned between the eucalyptus and softwood cellulose. Fibre length, diameter and fibrillation are more similar to those of eucalyptus, while the mechanical properties of pulp are more like those of softwood pulp.

In spite lower cellulose yield after pulping, it is viable to use Japanese knotweed for pulp production, considering the properties of pulp that are comparable to those of standard pulp used for paper production.

3.2 Samples and protypes

For the second stage of the research various samples for compression testing of cellulose based packaging products have been produced by the wet moulding process. The results of compression tests will be used for material modelling and design of protective packaging. Additionally, the production process for foam forming has been tested with samples of foam formed packaging material being produced. These samples will also be tested for their performance as potential packaging material for protective packaging.

Figure 3: Samples of wet moulded and foam formed packaging materials

Source: own.

Acknowledgments

The LEAP project is funded by Slovenian Ministry of Cohesion and Regional Development and by Norway Grants.

References

EUMEPS https://eumeps-powerparts.eu/recycling/recycling-in-europe
Invasive Species Council of BC (2021). Healthy landscapes and communities free of invasive species.
Department of Environmental Conservation (2019). Guidelines for disposing of invasive plant material: Proper disposing of invasive plants can help limit their spread.
Regulation (EU) No. 1143/2014 of the European parliament and of the Council on the prevention and management of the introduction and spread of invasive alien species
Kapun, T., Zule, J., Fabjan, E. et al. Engineered invasive plant cellulose fibers as resources for papermaking. Eur. J. Wood Prod. 80, 501–514 (2022). https://doi.org/10.1007/s00107-021-01779-y

The Influence of Different Operation Atmospheres on the Produced Biochar Quality

Marjana Simonič,[1] Christoph Hochenauer,[2]
Nika Fekonja,[1] Darko Goričanec,[1]
Danijela Urbancl[1]

[1] University of Maribor, Faculty of Chemistry and Chemical Engineering, Maribor, Slovenia
marjana.simonic@um.si, nika.fekonja@student.um.si, darko.goricanec@um.si, danijela.urbancl@um.si
[2] Graz University of Technology, Institute of Thermal Engineering, Graz, Austria
christoph.hochenauer@tugraz.at

Biological wastewater treatment plants are used to purify water, but they also generate large quantities of sewage sludge and other solid residues. Sewage sludge and the residues on screens have a promising energy content. The article deals with the characterization of two different samples from small wastewater treatment plants, the dewatered sewage sludge and the material remaining on a fine screen after the removal of sand particles and mineral oils. The added value of the waste produced is studied using the torrefaction process. To establish torrefaction, a pilot process was developed in which various waste materials were processed and the effects of different process parameters, such as the influence of different atmospheres and temperatures on the quality of the biofuel, were studied. The raw samples and the solid products of the thermal treatment were analyzed.

DOI
https://doi.org/10.18690/um.fkkt.1.2024.8

ISBN
978-961-286-829-1

Keywords:
torrefaction, wastewater treatment plant, sewage sludge, CO_2 atmosphere, N_2 atmosphere, biofuel

University of Maribor Press

1 Introduction

Wastewater treatment is a major challenge, and it is important that wastewater treatment plants function properly in order to reduce water pollution. Biological treatment of wastewater also produces a by-product, namely sewage sludge and residues on screens. Sewage sludge and screen residues have a promising energy content (Petrovič et al. 2023).

Nowadays, the question often arises as to how this sludge can be treated efficiently. One promising method is torrefaction, a low-temperature pyrolysis process that produces products with a higher energy density that can be used for energy purposes. The process of torrefaction is one of the thermochemical conversion routes that improves the properties of the feedstock, eliminates pathogenic organisms and produces an environmentally acceptable energy source with similar properties to coal (Ivanovski et al. 2022).

Therefore, torrefaction of activated sludge (SS2) and cellulosic material (RS) was performed. Mass and energy yield (MY, EY), energy density (EF), energy- mass co-benefit index (EMCI) and high heating value (HHV) were determined.

2 Methodology

Two samples were analyzed during the torrefaction process. The sewage sludge sample (SS2) was taken after the dewatering process. The second sample (RS) is waste collected with fine rakes and contains mainly cellulosic and biological waste. This waste is collected in a special container and separated from the sludge. The sample of sludge and cellulosic waste was dried in a dryer at 50 °C to a constant mass before starting the experimental work. The dried samples were then grinded in a water-cooled MultiDrive basic M 20 mill from IKA to achieve homogeneity of the samples.

The torrefaction analyses were carried out in a Carbolite tube furnace (Figure 1a) with a tube diameter of 90 mm. The sample was weighed and placed on a special tray as shown in Figure 1b. The tray has four zones separated by perforated metal. Torrefaction was performed at 250 °C and 350 °C under N_2 atmosphere with a flow rate of 1 l/min. The inert gas was previously heated to 50 °C. The temperature was

measured in four zones during the experiment. The concentrations of the exhaust gases, such as methane, carbon dioxide, carbon monoxide and oxygen, were measured at the exit of the furnace. After torrefaction, the samples were cooled and weighed. The experimental calorific value of the raw and processed samples was determined using an IKA C 6000 calorimeter.

Figure 1: a) Carbolite tube furnace b) The tray with material
Source: own.

The torrefication efficiency (MY, %) was calculated by Eq. 1:

$$\text{MY}\ (\%) = \frac{m_t}{m_0} \cdot 100 \tag{1}$$

m_t–torrefied sample mass (kg)
m_o– non torrefied sample mass (kg)

Energy yield (EY, %), energy efficiency (EF) and energy co-benefit index (EMCI) were determined by Eq. 2-4:

$$\text{EY}\ (\%) = \left(\text{MY} \cdot \frac{\text{HHV}_t}{\text{HHV}_o}\right) \tag{2}$$

HHV_t–torrefied sample (MJ/kg)
HHV_o– non torrefied sample (MJ/kg)

$$\text{EF} = \frac{\text{HHV}_t}{\text{HHV}_o} \tag{3}$$

$$\text{EMCI} = \text{EY} - \text{MY} \tag{4}$$

3 Results

Samples SS2 and RS are shown in Figure 2. From left to right are the samples SS2 in N_2 atmosphere torrefied at two different temperatures (250 °C and 350°) and the raw sample (Figure 2a). The same order applies to the RS samples (Figure 2b). Sample SS2 is dark after treatment as well as the raw dewatered sludge, while samples RS have a light color as well as the raw sample (Figure 2b), due to cellulose residues content.

The temperature is a very important parameter in the torrefaction process as it influences the mass and energy yield as well as the energy efficiency. When the torrefaction temperature was increased from 250 °C to 350 °C, the mass and energy yields decreased for all samples. It follows that the higher the torrefaction temperature, the lower the MY and EY. In terms of energy efficiency, however, better results were obtained for the RS samples.

a) b)

Figure 2: a) SS_2 and b) RS after treatment and raw material
Source: own.

Figure 3 shows the changes in temperature and gas composition during torrefaction. The temperature was constant during the experiment and fluctuated slightly around 250 °C and around 350 °C. It was found that the SS2 samples extracted the most CO_2 in N_2 atmosphere. This suggests that the fluctuations in CO_2 concentration are a measure of the progress of torrefaction, while the time between the increase and decrease in CO_2 concentration corresponds to the time during which the torrefaction process takes place in the material. The extraction of the individual gases from the sample was not affected by the temperature fluctuations. However, the RS sample showed that temperature affects the extraction of organics, with more CO and CO_2 extracted at higher temperatures. The oxygen contained in the material is released during torrefaction in the form of volatiles and other organic compounds

(Doddapaneni et al., 2022), which explains the high content of CO_2 in the gas phase. The content of other gases was negligible.

The mass yield was influenced by the temperature in such a way that a better torrefaction yield was achieved at lower temperatures than at higher temperatures.

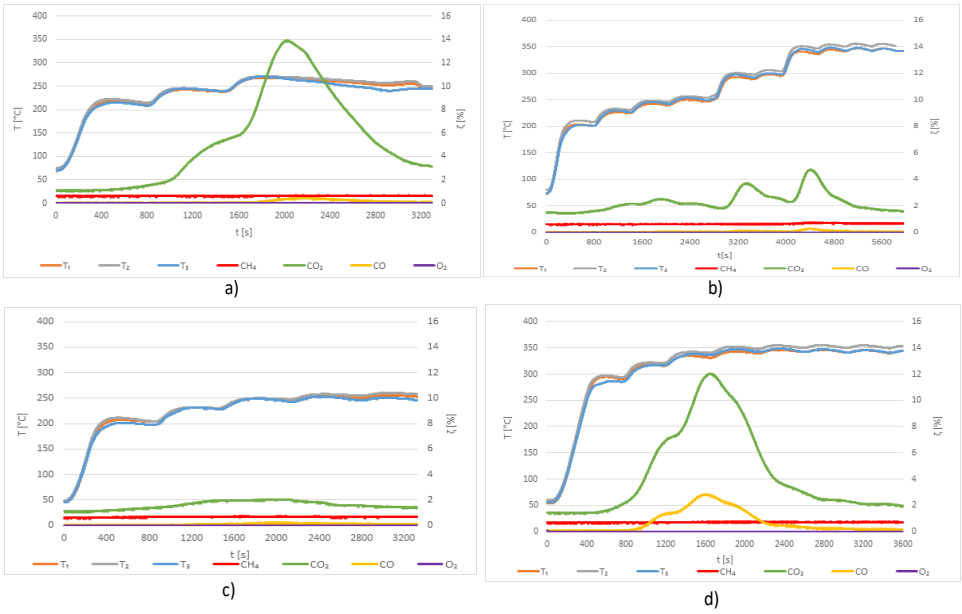

Figure 3: Measurements of temperature and exhaust gas composition during the torrefaction for sample a) SS2 at 250 °C, b) SS2 at 350 °C, c) RS at 250 °C and d) RS at 350 °C

Source: own.

Table 1 shows all calculated indexes. The highest MY and EY were achieved at 250°C, while EMCI was higher at 350°C for both samples. Other studies have reported a wide range of mass yields up to 80 %, depending on feedstock type, composition, and operating conditions (Huang et al., 2017).

Table 1: Calculations for mass yield, energy yield, energy efficiency and factor EMCI

	sample, atmospehere, T, volumne flow	MY [%]	EY [%]	EF [/]	EMCI [%]
1	SS_2			1.00	
2	SS_2, N_2, 250 °C, 1 L/min	75.33	92.24	11.79	16.91
3	SS_2, N_2, 350 °C, 3 L/min	57.44	85.04	10.86	27.60
4	RS			10.00	
5	RS, N_2, 250°C, 1 L/min	80.95	92.30	11.40	11.35
6	RS, N_2, 350 °C, 1 L/min	35.44	47.93	13.52	12.49

Figure 4 shows that the highest mass yield was calaculated at 80.95 % at 250 ºC with 1 L/min flow for RS samples treated in N_2 atmosphere.

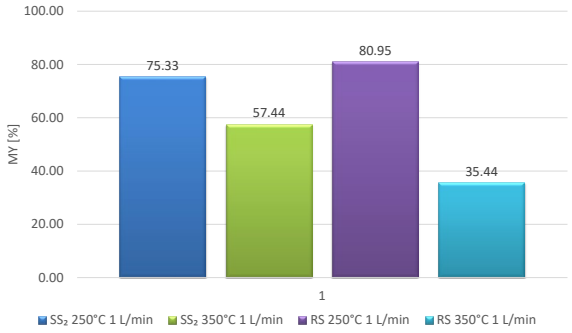

Figure 4: Mass yield (%) for SS2 and RS in N_2 atmosphere
Source: own.

Figure 5 shows the calculated values for all treated SS2 and RS samples. Regarding HHV the highest HHV was calculated at 23.32 MJ/kg for RS sample in N_2 atmosphere at 350º C and 1 L/min flow and 17.81 MJ/kg for SS2 sample.

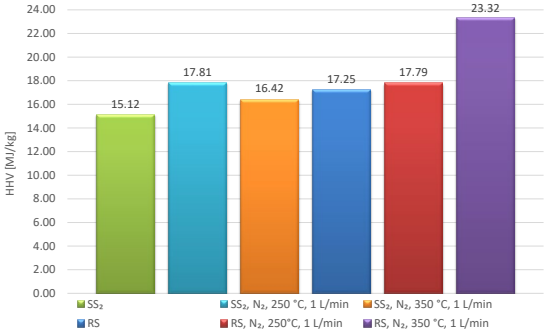

Figure 5: High heating values for SS2 and RS samples
Source: own.

4 Conclusions

Based on the results obtained on the heating values, we concluded that sludge and RS are suitable for combustion and could be used as biofuel. Both samples have high HHV values, but the cellulosic material has even higher values.

This is an important finding as more sludge and waste are produced each year and are simply disposed of in landfills. It is important that the resulting products are properly used as a secondary resource in wastewater treatment. Given the problems, these resources are underused and demand more attention.

References

Clewlow, R. R. Carsharing and sustainable travel behavior: Results from the San Francisco Bay Area. Ivanovski M., Goricanec D., Krope J., Urbancl D. Torrefaction pretreatment of lignocellulosic biomass for sustainable solid biofuel production. Energy. 2022, vol. 240. doi: 10.1016/j.energy.2021.122483

Doddapaneni T.R.K.C., Pärn L., Kikas T., Torrefaction of Pulp Industry Sludge to Enhance Its Fuel Characteristics, Energies. 15(17), 6175, 2022, doi.org/10.3390/en15176175

Huang M., Chang C.-C., Yuan M.-H., Chang C.-Y., Wu C.-H., Shie J.-L., Chen Y.-H., Chen Y.-H., Ho C., Chang W.-R., Yang T.-Y., Lin F.-C., 2017, Production of Torrefied Solid Bio-Fuel from Pulp Industry Waste, Energies, 10(7), 910. doi.org/10.3390/en10070910

Petrovič A., Stergar J., Škodič L., Rašl N., Cenčič, T., Čuček L., Goričanec D., Urbancl D., 2023, Thermo-kinetic analysis of pyrolysis of thermally pre-treated sewage sludge from the food industry, Thermal science and engineering progress, 42, DOI: 10.1016/j.tsep.2023.101863.

Simonič M., Goričanec D., Urbancl D. Impact of torrefaction on biomass properties depending on temperature and operation time. Science of the total environment. 2020, vol. 740, doi: 10.1016/j.scitotenv.2020.140086.

Donatello S, Cheeseman CR. Recycling and recovery routes for incinerated sewage sludge ash (ISSA): A review. Waste Manag. 1. november 2013;33(11):2328–40. doi: 10.1016/j.wasman.2013.05.024.

Cahyanti MN, Doddapaneni TRKC, Kikas T. Biomass torrefaction: An overview on process parameters, economic and environmental aspects and recent advancements. Bioresour Technol. 1. april 2020;301:122737.*Transport Policy, 51*, 158-164. doi:10.1016/j.tranpol.2016.01.013

Energy Management of Buildings With a Focus on Municipalities

Karolína Smutková,[1] Jiří Gregor,[1]
Petar Sabev Varbanov,[2] Petr Stehlík[1]

[1] Brno University of Technology, Faculty of Mechanical Engineering, Institute of Process Engineering, Brno, Czech Republic
karolina.smutkova@vut.cz, jiri.gregor@vutbr.cz, stehlik@fme.vutbr.cz
[2] NETME Centre, Sustainable Process Integration Laboratory, Brno, Czech Republic
varbanov@fme.vutbr.cz

Due to the climate situation, the EU policy, the impact of the coronavirus pandemic and the war in Ukraine, it is necessary for municipalities to take a conceptual approach to their energy sector. A big topic of this issue and also the subject of this paper is the energy optimization of municipal buildings. The reality in the Czech Republic is that municipalities, with a few exceptions, do not combine data on energy and water consumption with the actual technical condition of the buildings concerned, so they have no basis for decision-making and individual projects are often dealt with in an unconceptual and ad-hoc manner. The methodology is based on an analysis of the situation in the South Moravian Region and a questionnaire survey of the Union of Towns and Municipalities of the Czech Republic. This article identifies the key areas that affect the energy efficiency of buildings and therefore specific data should be collected from these areas to form the basis for setting up the energy management of the city.

DOI
https://doi.org/10.18690/um.fkkt.1.2024.9

ISBN
978-961-286-829-1

Keywords:
energy management,
municipality,
renewable energy,
measurement,
regulation,
green deal

University of Maribor Press

1 Introduction

This article deals with energy optimization of municipalities, specifically in the field of buildings. The European Union policy [1, 3] gave a sign of gradual pressure to reduce the energy intensity of the operations. However, the coronavirus pandemic and the war in Ukraine have accelerated the issue - these incidents have brought to light how the current European concept of energy is tied to fossil resources. The need to secure transitional fossil gas from countries other than the current majority Russia [2], to rebuild the energy mix in favour of renewables, and to decentralise previously robustly centralised sources of electricity has inevitably caused energy supply prices to jump. In addition, from 2025 onwards, the tariff structure in the Czech Republic is expected to be rebuilt to better reflect the impact of renewables on the resulting balance of the electricity system. These influences are forcing municipalities to rebuild from the base the current approach to their energy system. By making energy carrier payments a minority share of municipal budgets until recently, municipalities have not been motivated to optimise their buildings conceptually. By this is meant the implementation of energy management in accordance with ČSN EN 500001 and the renovation of buildings based on techno-economic grounds. For buildings, the heat loss through the building envelope and the performance and type of heat and cooling source are very closely related. For this reason, insulation with a constant thickness of polystyrene cannot be applied uniformly to all buildings, which is the idea of many municipal representatives of a sufficient energy solution.

Therefore, this article discusses the data sets that cities should track. This is a first step in the energy optimization of cities, because any further strategies need to be based on data that cities do not normally collect. These are data describing the building envelope and the technologies used that have an impact on energetics. Such datasets should provide a robust basis for municipalities to make energy optimisation decisions.

An important note is that the term "energy production and consumption" will be used here. While it is clear that energy is only converted, this terminology is used here because of its familiarity and not its factual correctness.

2 Methodology

The information on the current state of municipal energetics is obtained from the experience in the regional and district level municipalities of the South Moravian Region and from the questionnaire survey of the Union of Towns and Municipalities of the Czech Republic [4]. The South Moravian Region is a good reference region because on the one hand it contains very prosperous localities close to Brno, which is the second largest city in the Czech Republic. On the other hand, this region also includes relatively undeveloped areas in the south of the Czech Republic.

The analysis covered the current situation in the field of building energy management in municipalities of 5,000 - 30,000 inhabitants. The lower limit of 5,000 inhabitants was set because the smaller municipalities have a minimum of buildings under management - usually a municipal office, a fire station, a school and a kindergarten in the maximum version. This minimum of buildings can usually be secured by a more responsible mayor without extensive record keeping. Municipalities over 30,000 inhabitants have a contributory organisation that conceptually manages their energy. For municipalities in the range of 5,000- 30,000 inhabitants, existing practices were examined, both in terms of collecting and handling data on energy and water consumption and the technical condition of buildings. Based on these analyses, key datasets and practices were proposed to begin effective energy management.

The result of the research was that the majority of municipalities of the surveyed size do not systematically keep energy-related data. In most cases, knowledge of municipal assets is dispersed among a relatively large number of people in different departments (investment, finance, property, planning). Also, municipalities do not have professional management. If municipalities have their own energy manager, in most cases he/she is of very low professional level. Thus, the data is not approached conceptually and no linkage between them is observed (e.g. correlation between energy consumption and heat leakage). This article therefore provides a list of areas that municipalities should track in order to lay the basis for energy management.

3 Data collection areas

3.1 Energy consumption

Municipalities should register the consumption of energy in their utilities and subsidiary organisations. This includes consumption of electricity, gas and heat from central heating supply. These data should be recorded at least five years back and for average years - i.e. years not affected by the coronavirus pandemic or the war in Ukraine, as these events had a significant impact on energy consumption. Furthermore, it is advisable to register consumption at the finest granularity appropriate to the type of measurement used. Unfortunately, in the Czech Republic, quarter-hourly measurement is not yet commonplace.

This evidence plays a key role for a number of reasons:

3.1.1 Invoice control

Although it may not be obvious at first look, the value of the meter and the invoice do not always match. It is therefore necessary to compare the two values.

3.1.2 Monitoring the impact of the actions implemented

If any changes are made to the buildings (e.g. reduction of heat transfer through the structure or removal of thermal bridges), the impact of the changes can be accurately quantified through the energy consumption records. These savings can then provide an motivation to continue such actions.

3.1.3 Influencing the consumption profile

If the installation of renewable energy sources is intended, then in the case of the majority of photovoltaics in the Czech Republic it is possible to predict the production trend of this source quite accurately. In order to maximise the economic and environmental impact, it is necessary to ensure as far as possible that the production of the source and the consumption of the energy are coeval. Therefore, in these situations, it is necessary to take the consumption profile of the planned consumption points (community energy), identify the possibilities of influencing it

in favour of the photovoltaic production curve and design the sizes and locations of photovoltaic plants accordingly. In the Czech Republic it is uneconomical to oversize photovoltaic power plants. Firstly, it increases the purchase price and secondly, the market is not interested in unused energy. In many cases, the distribution system is overloaded and does not even have the technical capacity to transfer the energy. These phenomena occur because the Czech electricity grid is already relatively saturated with photovoltaics and there is an excess of such energy in the grid during sunny periods, which has a number of other effects.

3.2 Envelope of the building

3.2.1 Energy efficiency of the building (Energy class)

To identify the energy efficiency of a building, a specialized technician performs a physical inspection of the building - factors such as insulation, windows, heating, ventilation, and more are measured and evaluated. In addition, the building's annual heating and cooling energy consumption is determined. Based on the calculations and measurements, the building is assigned to an energy class from A (low energy consumption, high energy efficiency) to G (high energy consumption, low energy efficiency). The result is presented on the energy label in the form of a graphic symbol with a letter indicating the class. This visual presentation facilitates a quick look at the energy efficiency of the building.The energy performance certificate also usually contains recommendations for improving the energy efficiency of the building. These can be specific suggestions for insulation, window replacement, heating upgrades, etc.

3.2.2 Thermal bridges

A thermal bridge is an area in a building structure where the thermal resistance of the material is lower than in surrounding areas. This means that heat can more easily leak or enter the building through this area. The most common places where thermal bridges occur are the connections of walls to the floor, ceiling or other walls, the connections of windows and doors, where pipes or electrical lines pass through insulation, and the corners of the building. Consequences of thermal bridges include increased energy consumption, condensation that promotes mould growth and lack of comfort due to uneven interior temperatures.

3.2.3 Heat transfer through the envelope

Assessing heat loss through the building envelope involves monitoring several key parameters for each part of the structure (walls, floors, roofs).

- **Walls, floors, ceilings**

The thermal conductivity of the material affects how quickly heat passes through the wall. The thickness and type of insulation is also analysed, as well as its potential compatibility with the building - taking into account the risk of moisture gain.
*Green roofs and walls - Vegetated surfaces on roofs and walls that can help with insulation and reducing heat loss.

- **Building envelope penetrations**

For the energy optimization of window and door frames, glass and sealing quality, various values and parameters are monitored that can affect the energy efficiency of a building. Here are the key values and parameters that should be monitored:

Heat transfer coefficient

This parameter indicates the thermal transmittance of a window or door system. A lower value means better insulation properties.

Seals

The quality of the sealing of window and door frames is a key element in preventing air leakage and minimising leakage.

Dimensions and positioning

Dimensions and placement can affect the amount of sunlight and natural lighting, which impacts overall energy efficiency.

3.3 Technologies

The technologies influencing municipal building energy can be diverse and depend on the specific conditions and strategies of each city. These technologies are mostly related to heating, ventilation, domestic hot water and energy production and management. It is important for the city to record their type, performance, scheduled revision dates and date of acquisition.

3.3.1 Air exchange

Air exchange in buildings can take place in a variety of ways, some of which include:

- **Native ventilation**

Takes advantage of temperature differences between the outside and inside environment to move air.

- **Mechanical ventilation**

Involves the use of fans and fan systems to actively exhaust air and bring in fresh air. It can be implemented using heat recovery systems to reuse the thermal energy from the exhaust air**.**

- **Hybrid or combined systems**

The combination of natural and mechanical ventilation allows optimised air exchange depending on the outdoor conditions and the requirements inside the building.

- **Underpressure or overpressure conditions**

Creating negative pressure or positive pressure conditions in designated areas of the building can control the direction of air exchange.

3.3.2 Use of renewable energy sources

The use of renewable energy sources is also a big topic in the energy optimisation of municipal buildings. This strategy relies in particular on the installation of solar photovoltaic panels, solar thermal systems and heat pumps. In this way, urban buildings contribute to environmental protection, reduce greenhouse gas emissions and increase their energy self-sufficiency. The implementation of these renewable technologies and innovative solutions brings economic savings, promotes innovation and contributes to the sustainable development of the urban environment. Municipalities should therefore register:

- Type of system and their consumption.
- The amount of energy produced by these technologies.
- Elements of smart technologies and automation - systems that control energy consumption according to predicted production, temperature settings, heating settings, etc.
- Storage elements - batteries, water storage.

3.3.3 Heating and hot water production

This subchapter achieves a slight overlap with the chapter about renewables. This is largely due to the fact that this chapter deals with the largest energy consumers in buildings and there is an attempt to replace them with renewable options. Municipalities should again register the input power, type, age and revision requirements for heat sources, for example:

- heat pumps
- gas-fired boilers
- solid fuel boilers
- central heating supply
- technologies using electricity (boilers, electric boilers, foils)
- cogeneration units
- waste heat recycling - waste heat exchangers

3.4 Lighting

Municipal lighting can be divided into indoor lighting and public lighting, which is evaluated according to energy consumption per 1 light point. Municipalities should register the technical condition of lighting and target the use of LED technology. The interesting thing is that cities can provide their public lighting for power balance services - in case of surplus energy in the network, this lighting would be lit even in the daytime and it would be one of the financial revenues for the city.

4 Conclusion

In the context of increasing pressure on municipal energy efficiency in the European Union, triggered not only by the coronavirus pandemic and the conflict in Ukraine, but also by the drive to gradually shift to renewable energy sources, it is becoming a key step for cities to rethink their approach to energy. This paper highlights that the current lack of procedures and the absence of systematic data management related to energy in municipal buildings hinders effective energy management. In the first part of the paper, the necessity of collecting and reporting data related to energy consumption and energy performance of buildings was presented. The information obtained will not only allow for an informed and conceptual planning of urban energy renewal, but also for controlling the effectiveness of implemented actions and the adequacy of energy expenditure. The next part of the paper focuses on specific areas of data collection on the building envelope, focusing on energy performance, thermal bridges and heat transfer through the envelope. Identifying and monitoring these factors are key to developing an effective building energy optimization strategy that leads to savings and improved energy efficiency. Finally, the technologies responsible for hot water, lighting, heat, electricity, heat recovery and air exchange were discussed. Proper inventory of system types, their performance and smart technologies allows municipalities to plan strategically and use available resources efficiently. Overall, effective data collection and use are key tools for municipal energy management. Municipalities that systematically register and analyse their energy indicators are better equipped to make informed decisions and successfully transition to a more sustainable energy model in line with current European guidelines and requirements.

Acknowledgments

The research leading to these results has was supported by funds from GA BUT within research project FSI-S-23-8173.

References

Adger, W. N., Huq, S., Brown, K., Conway, D., & Hulme, M. (2003). Adaptation to climate change in the developing world. Progress in Development Studies, 3(3), 179–195. https://doi.org/10.1191/1464993403ps060oa

EUROSTAT. EU trade with Russia - latest developments. Online. Dostupné z: https://ec.europa.eu/eurostat/statisticsexplained/index.php?title=EU_trade_with_Russia_-_latest_developments. [cit. 2023-12-08]. Clewlow, R. R. (2016). Carsharing and sustainable travel behavior: Results from the San Francisco Bay Area. Transport Policy, 51, 158-164. doi:10.1016/j.tranpol.2016.01.013

AKHMAT, Ghulam, Khalid ZAMAN, Tan SHUKUI a Faiza SAJJAD. Does energy consumption contribute to climate change? Evidence from major regions of the world. Renewable and Sustainable Energy Reviews. 2014, 36, 123-134. ISSN 13640321. Dostupné z: doi:10.1016/j.rser.2014.04.044

Společně hájíme zájmy měst a obcí!

Odpovědi dle **obc**

SVAZ MĚST A OBCÍ ČESKÉ REPUBLIKY

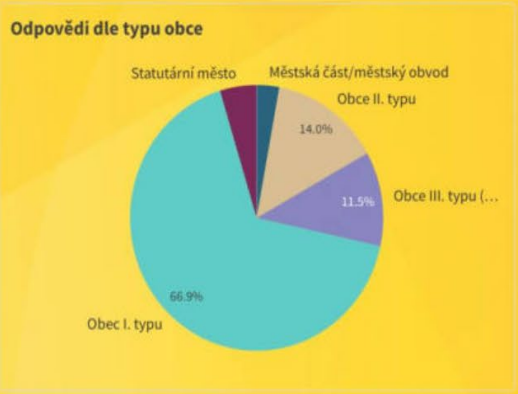

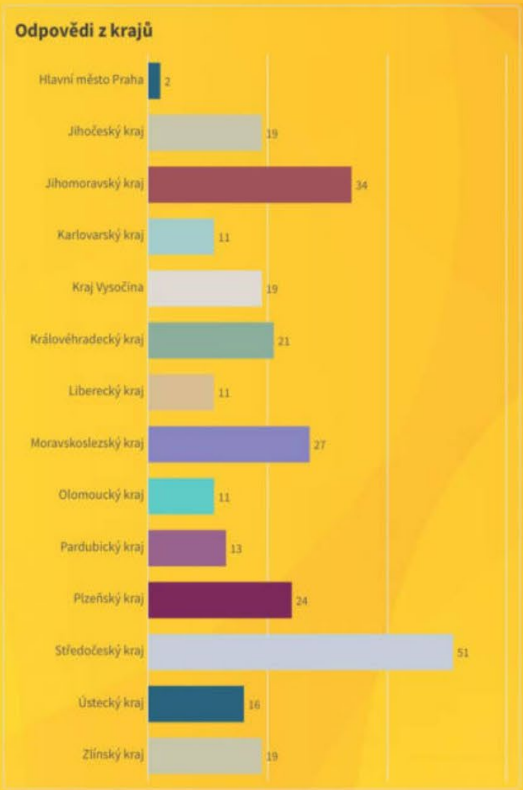

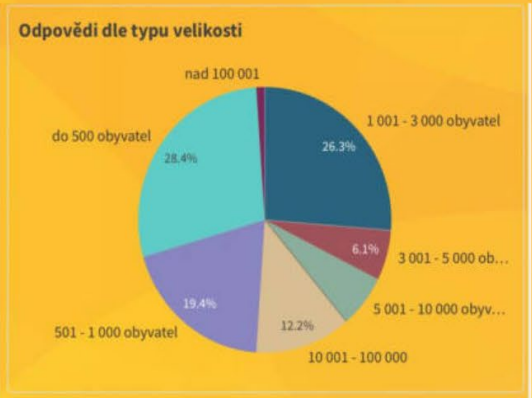

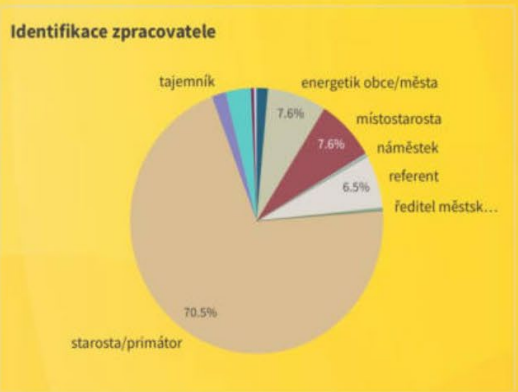

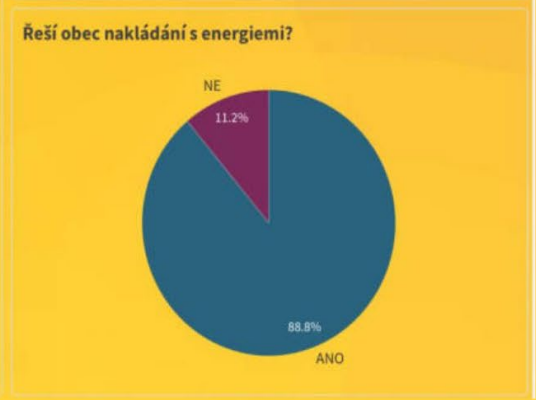

Kdo **řeší** energetiku

SVAZ MĚST A OBCÍ ČESKÉ REPUBLIKY

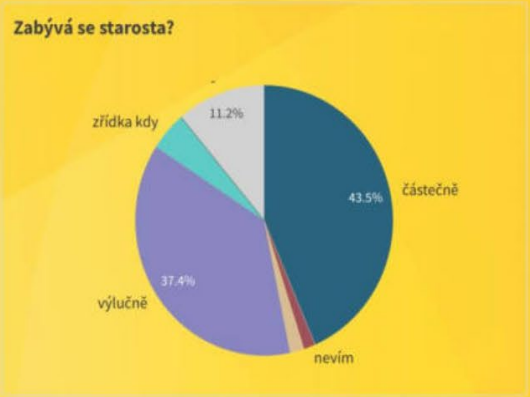

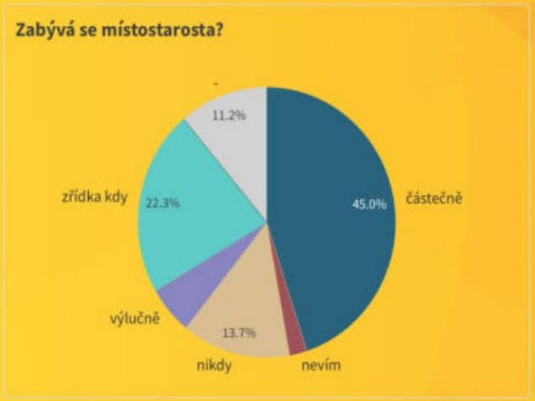

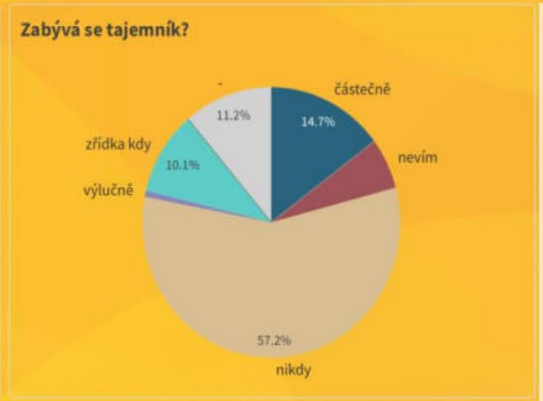

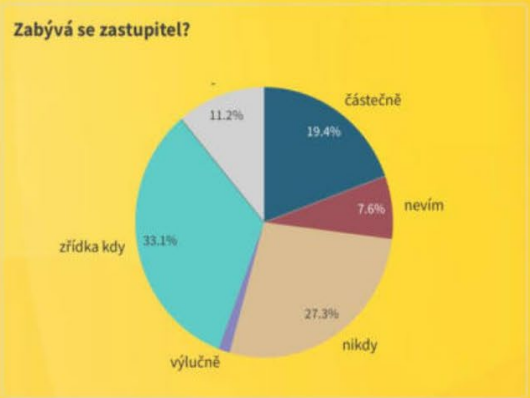

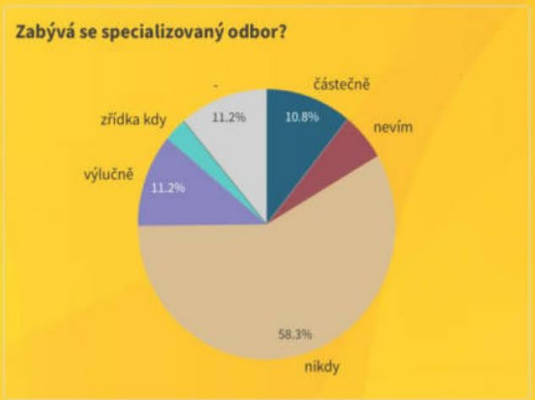

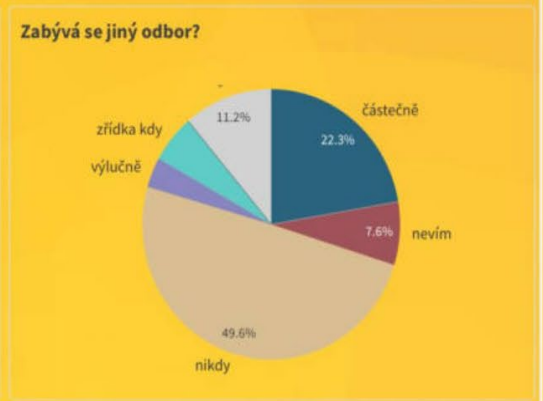

Energetické řešení

SVAZ MĚST A OBCÍ ČESKÉ REPUBLIKY

Řeší obecní energetická společnost?

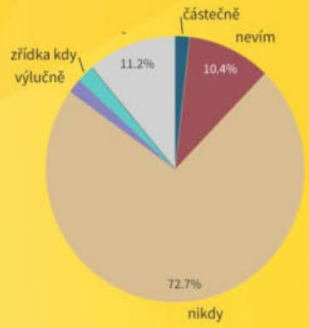

Řeší externí odborná společnost?

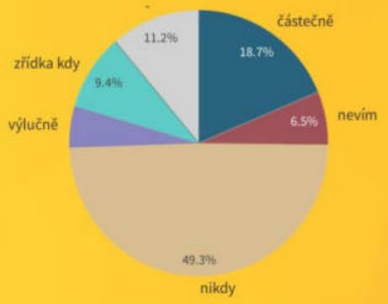

Řeší externí poradce?

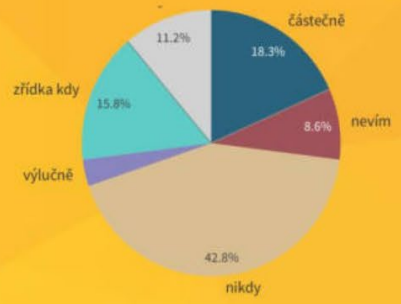

Řeší někdo jiný

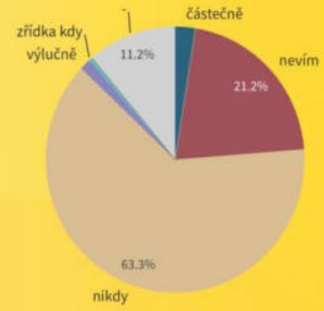

Pokud je někdo jiný:

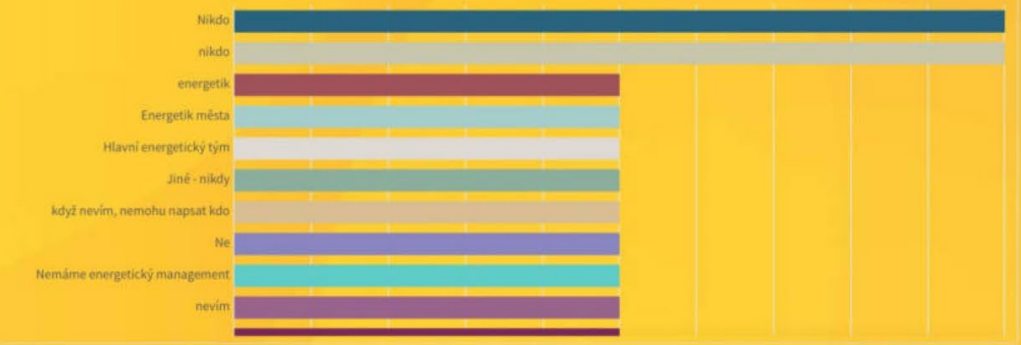

Správce energií

SVAZ MĚST A OBCÍ ČESKÉ REPUBLIKY

Interní správa energií

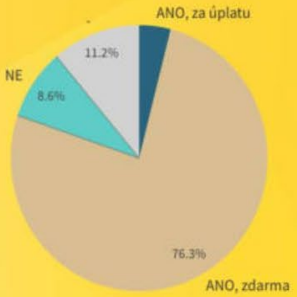

Obecní energetická společnost

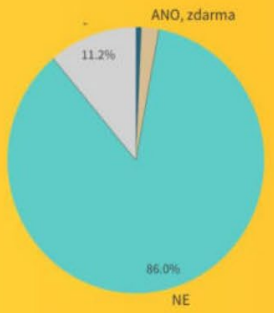

Externí odborný poradce

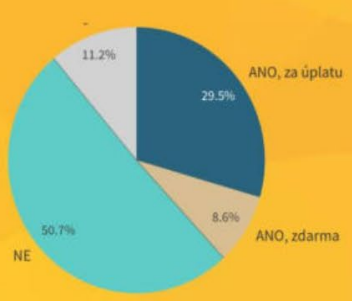

Jiný správce

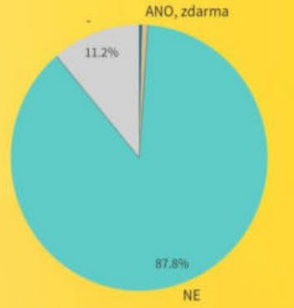

Kdo jiný:

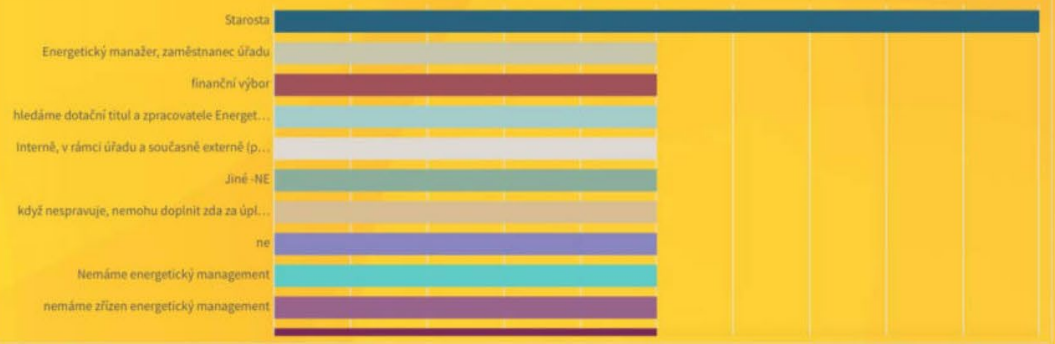

Energetický audit

SVAZ MĚST A OBCÍ ČESKÉ REPUBLIKY

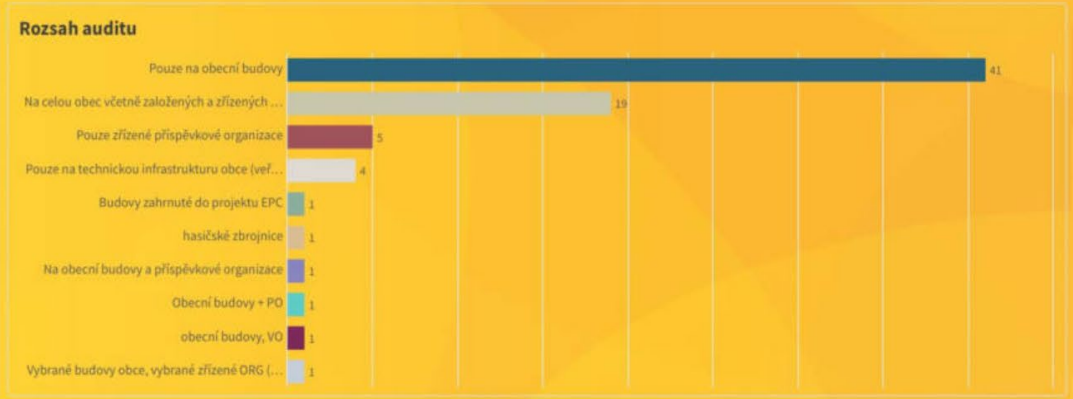

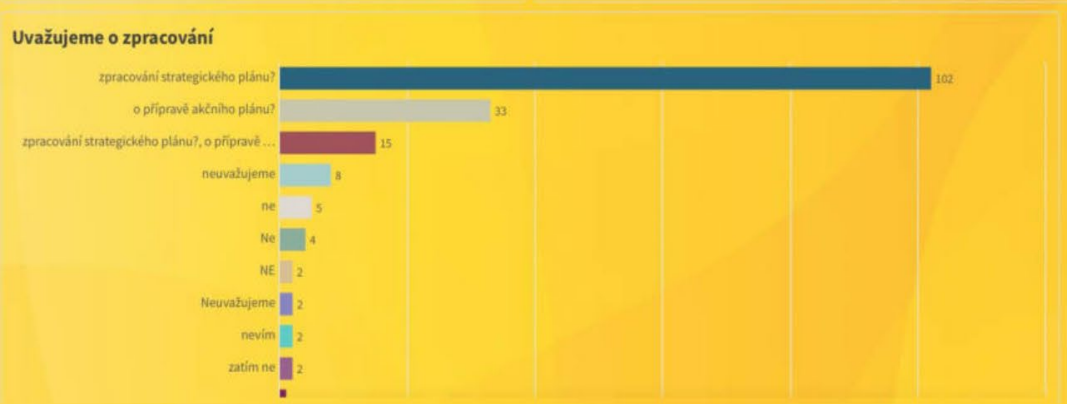

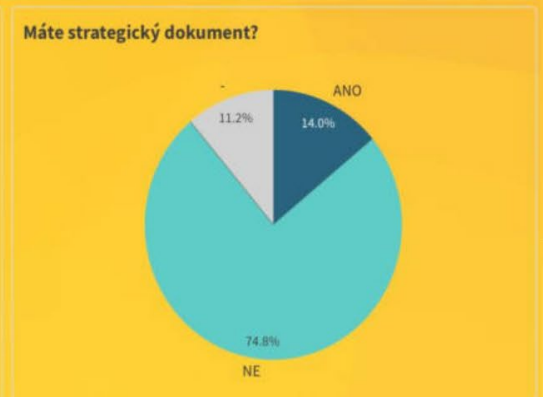

Opatření a strategie

SVAZ MĚST A OBCÍ ČESKÉ REPUBLIKY

Opatření pro spotřebu

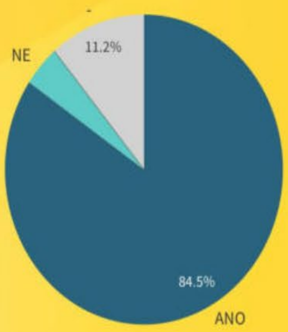

Obecní úřad - celkem budov

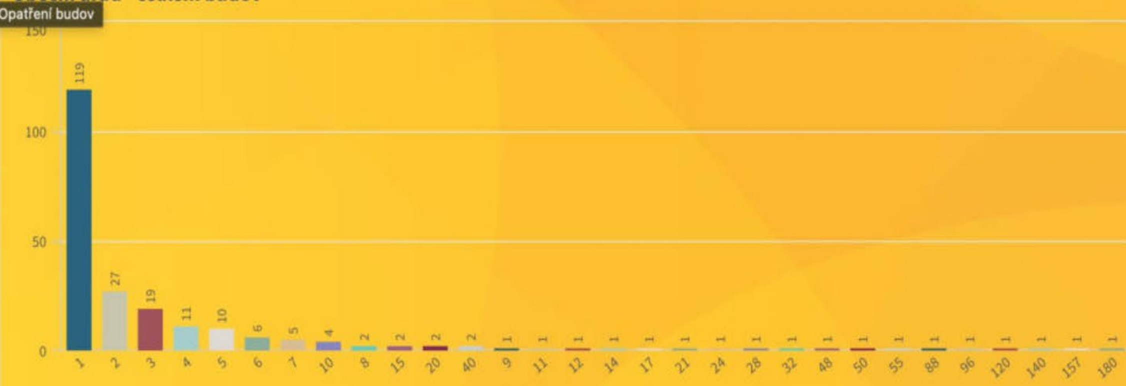

Kolika proces budov se opatření týká?

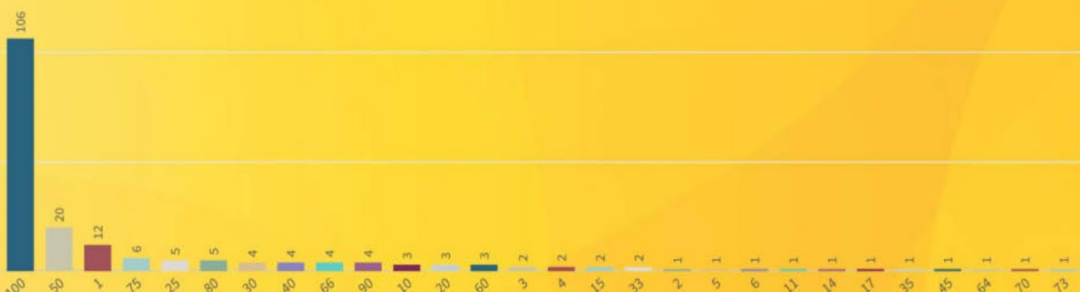

Máte strategický dokument?

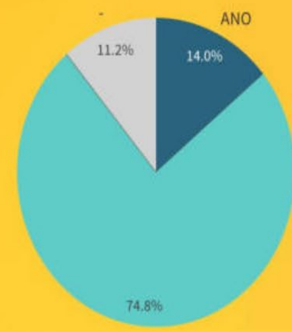

Školy

SVAZ MĚST A OBCÍ ČESKÉ REPUBLIKY

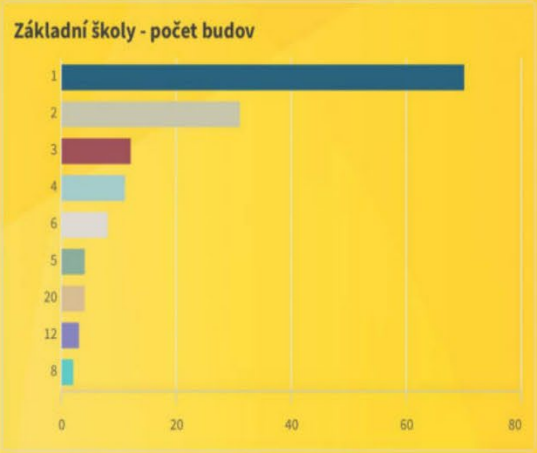

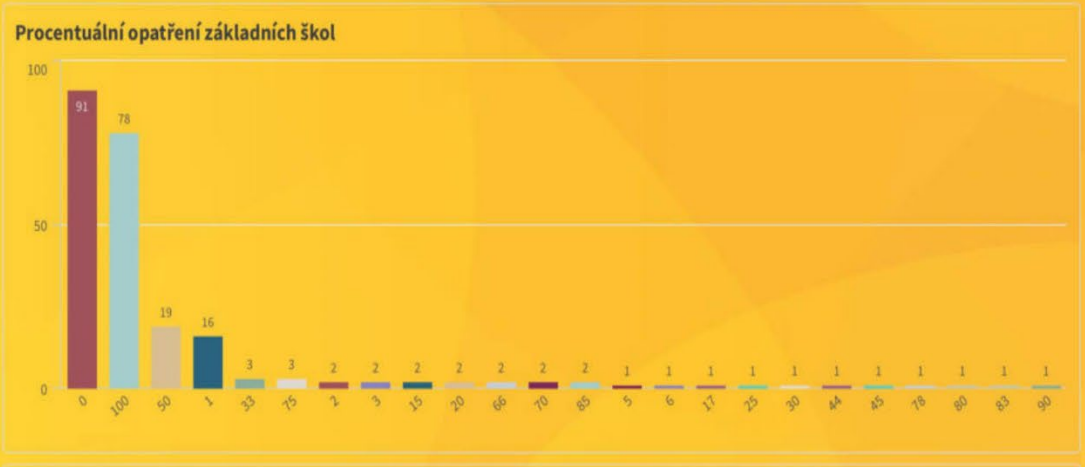

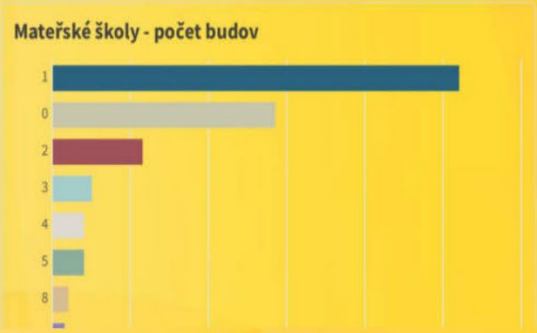

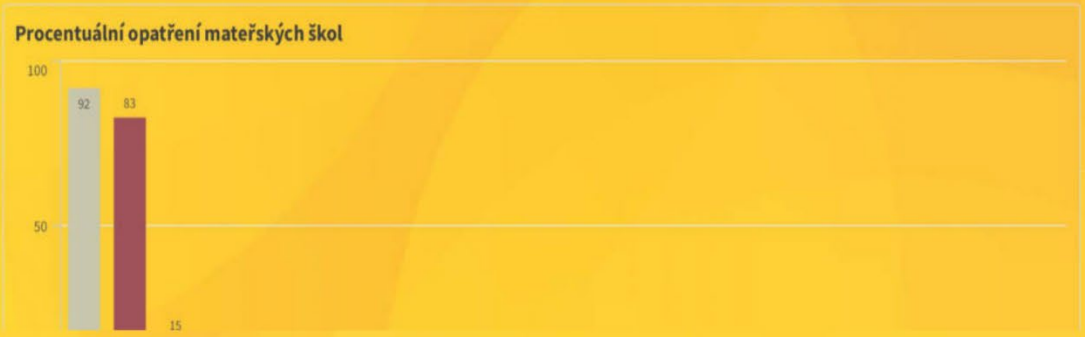

Kultura s sport

SVAZ MĚST A OBCÍ ČESKÉ REPUBLIKY

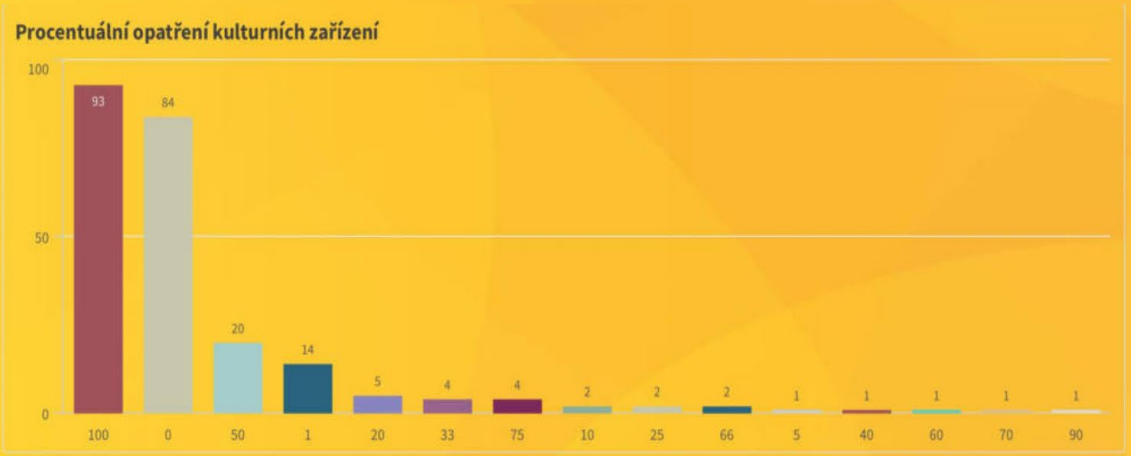

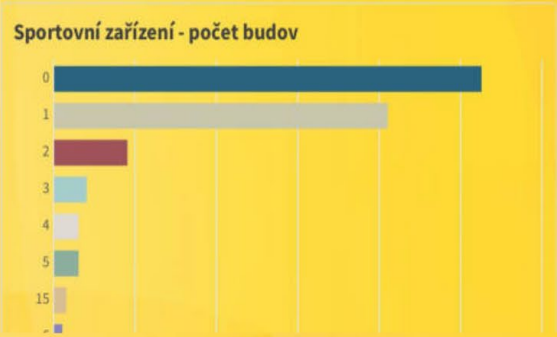

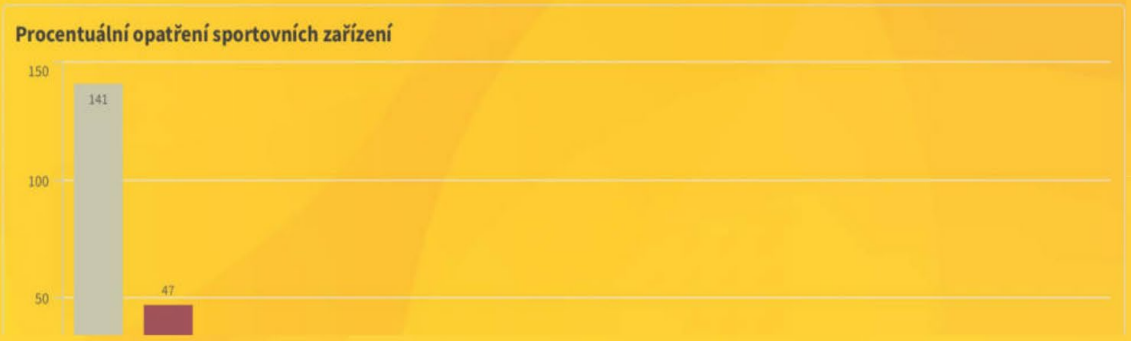

ČOV a byty

SVAZ MĚST A OBCÍ ČESKÉ REPUBLIKY

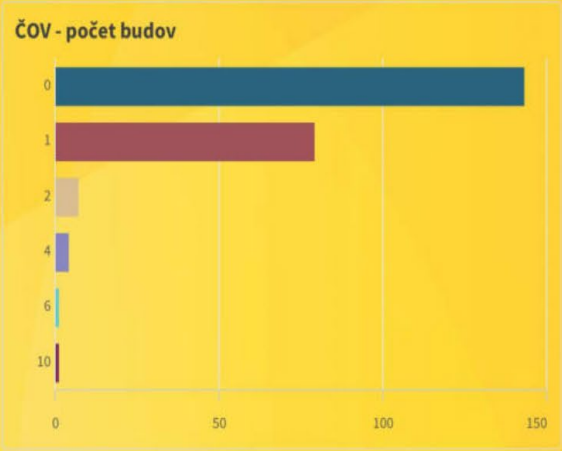

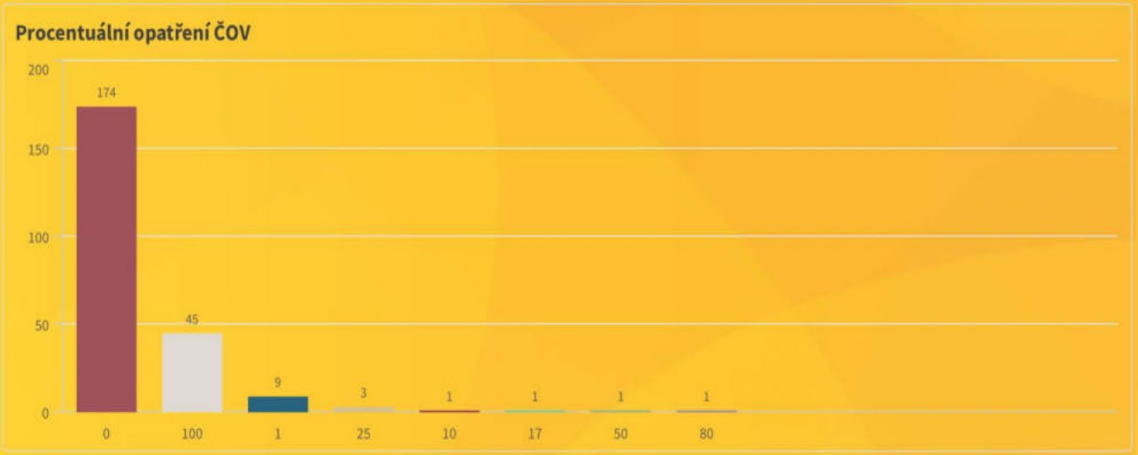

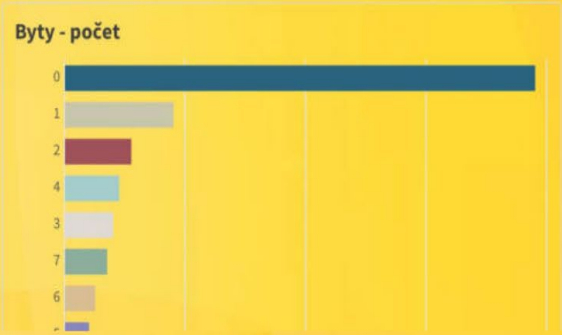

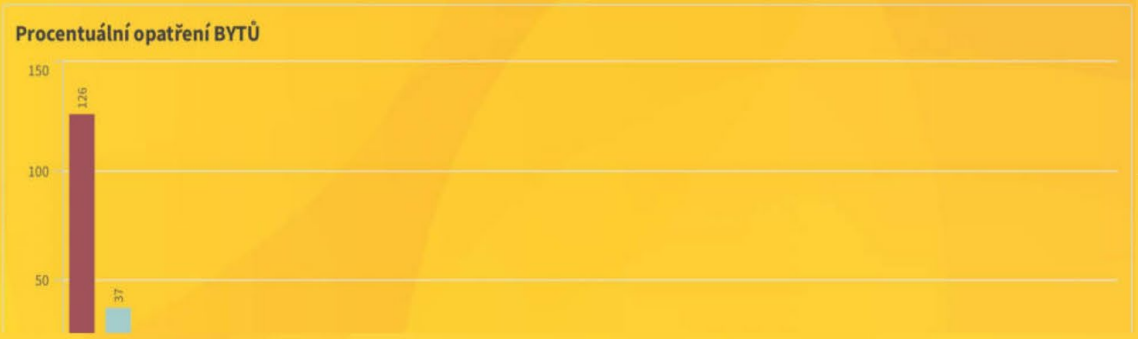

Ostatní zdroj

SMO
SVAZ MĚST A OBCÍ ČESKÉ REPUBLIKY

Veřejné osvětlení

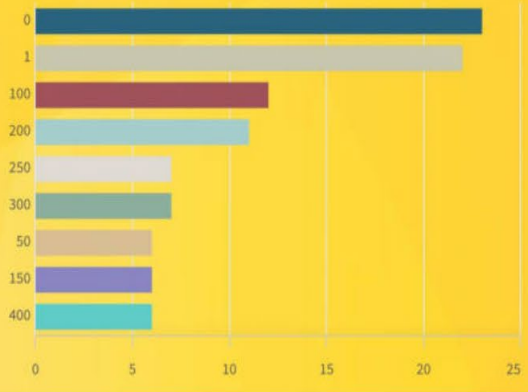

Procentuální opatření osvětlení

Jiné aktivity

0	-	Budova regionálního centra = 1 = 100% Budova městsk…	energetické zpracování plastů	hasičská zbrojnice, obecní knihovna, dům s pečovatelskou…	kontejnerová bioplynová stanice, FVE elektrárna na s…	ne	příprava FVE na budovu OÚ a MŠ	sídlo Správy zeleně a veřejnách ploch MČ Brno-Židenice	Úpravna vody, Zdravotní středisko	Vodárna - FW	Všechny budovy máme zateplené, okna vyměně…	výměna systému vytápění v ZŠ	Výměna za účinnější kotle v tepelném hospodař-ení města
	Aktivní energetický management, Fotovoltaika	budova technických služeb	fotovoltaická elektrárna obecní úřad, škola, škola tepelná čerpadla,	Hasičská zbrojnice, zateplení stropu + FVE, Rodný d…	Koupaliště, hotel, sportovní areál	obecní vodojem	Realizace geotermálního projektu, spolupráce s m…	Sociální služby - 3 budovy - 50% Zdravotní střediska - 2 bu…	veřejné osvětlení je nové LED, na ČOV bude obce napojena v roc…	Výstavba budovy pro obecní techniku, na této budově je uva…	Využívání studniční vody na zálivku	zateplení hotelu, vybudování kogenerační jednotky	
	Aktuálně řešíme pouze FVE na 3 budovách. Využíváme tepl…	Budovy se sociálním účelem, 2, 50%	hasičárna 100%, zdravotní středisko 100%,	instalace FVE	Lampy VO jsou vyměňovány průběžně, na střechu MŠ plá…	Objekt hasičské zbrojnice,	řízení energií - flowbox	solární osvětlení v rekreační oblasti	Veřejné osvětlení, zateplení bytů	Výše uvedená čísla jsou relativně malá, protože řada budo…	zbudování společenství obnovitelné energie	zhasínání v noci	
	Budova prodejny, plánujeme osazení FVE.	Domovy pro seniory p.o., počet jednotek 8, procenta 13	Hasičská zbrojnice Dobrovolných Hasičů (1 ks - 1…	Kino - FVE, Městská knihovna - FVE, loděnice - FVE	MŠ a ZŠ jsou v jedné budově - nelze rozdělit	pouze FVE zdroj, všechna svítidla LED	sběrný dvůr - fotovoltaika	technická budova	VO na místních komunikacích s FVE svítidly prozatím 16, př…	Vytápění úřadu a 2 DPS z bioplynové stanice ZD			

Obnovitelné zdroje

SVAZ MĚST A OBCÍ ČESKÉ REPUBLIKY

Uvažujete o obnovitelných zdrojích?

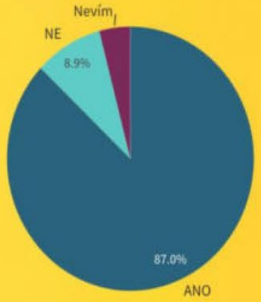

Uvažujete o vlastních zdrojích?

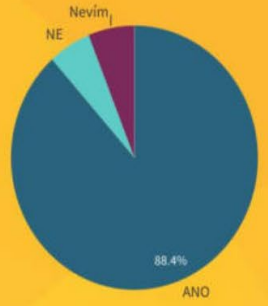

Spolupráce s jinými obcemi?

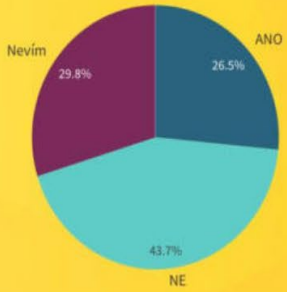

Kombinace více způsobů?

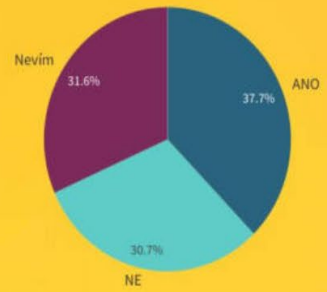

Fotovoltaiky

SVAZ MĚST A OBCÍ ČESKÉ REPUBLIKY

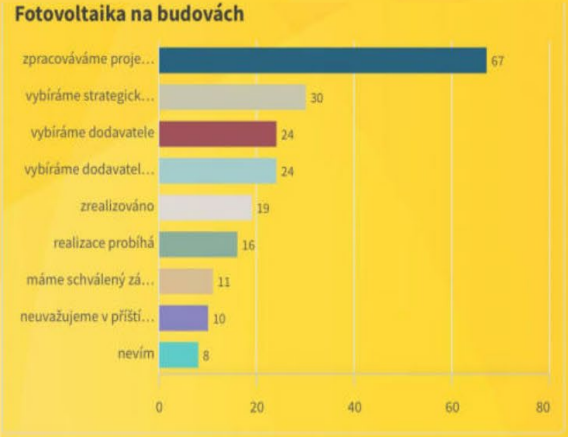

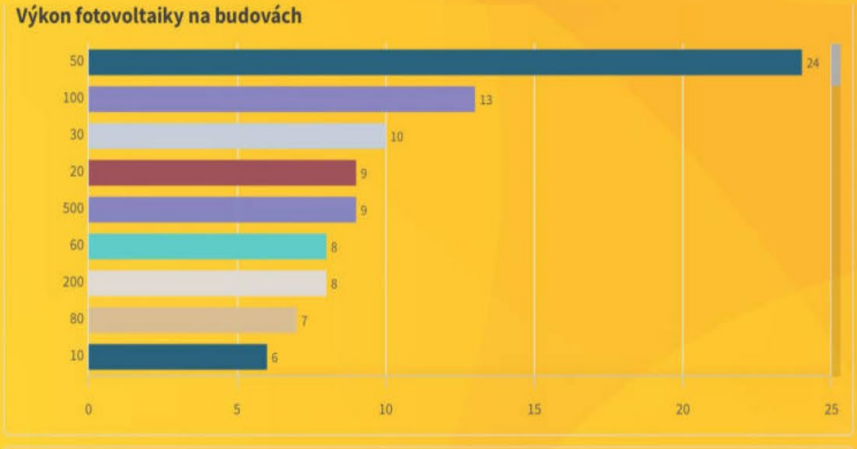

Celkem výkon

1 586 258

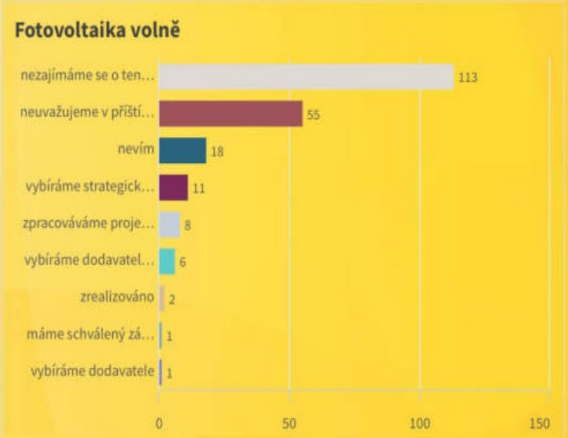

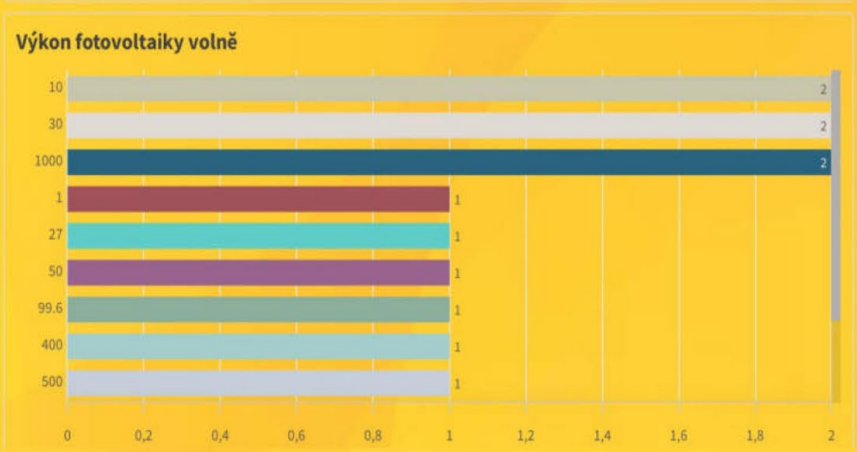

Celkem výkon

6 347

Agro + **čerpadla**

SVAZ MĚST A OBCÍ ČESKÉ REPUBLIKY

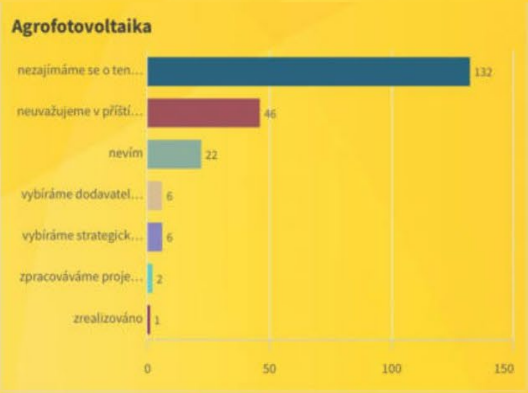

Celkem výkon

11 530

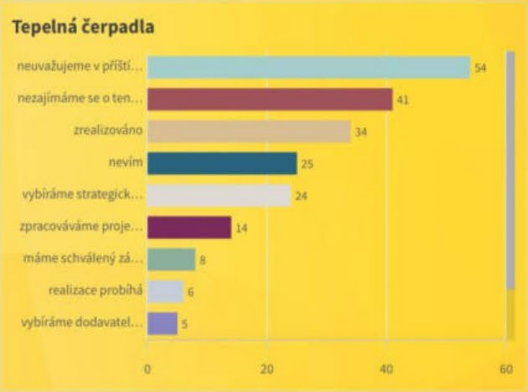

Celkem výkon

11 447

Bioplyn + **větrné**

SVAZ MĚST A OBCÍ ČESKÉ REPUBLIKY

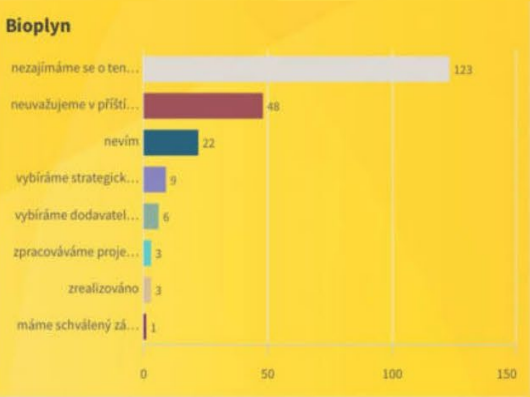

Celkem výkon

12 450

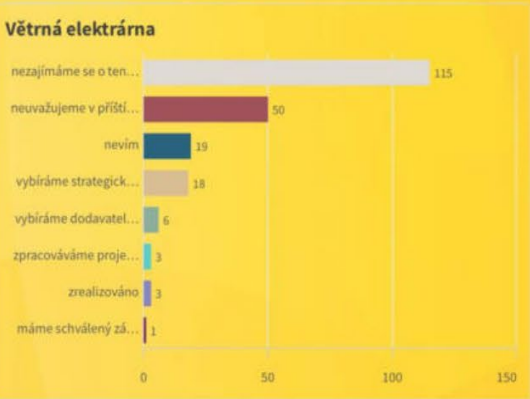

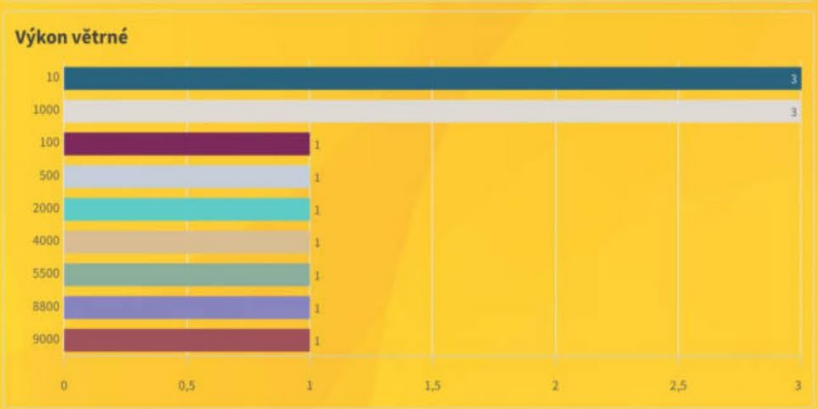

Celkem výkon

32 930

Vodní a **celkové** zdroje

SVAZ MĚST A OBCÍ ČESKÉ REPUBLIKY

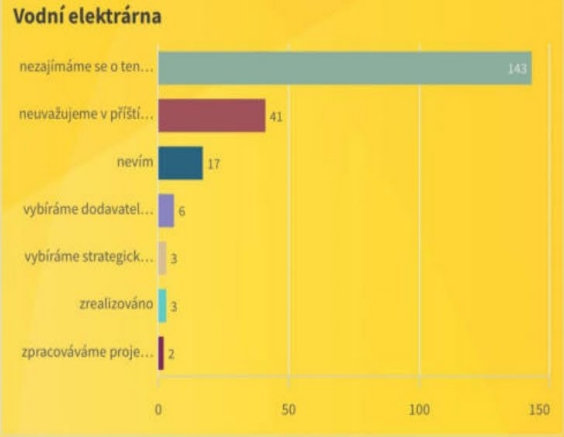

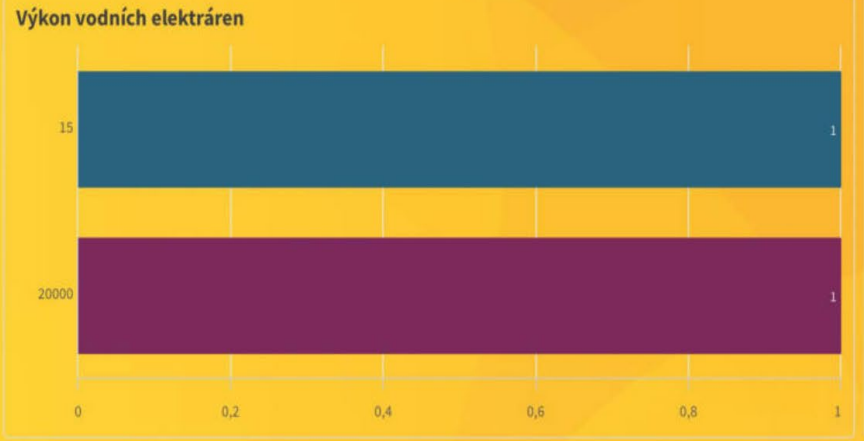

Celkem výkon

20,01k

Počet všech nových zdrojů

294

Výkon nových zdrojů celkem

1 680 977

Investice a zdroje

SVAZ MĚST A OBCÍ ČESKÉ REPUBLIKY

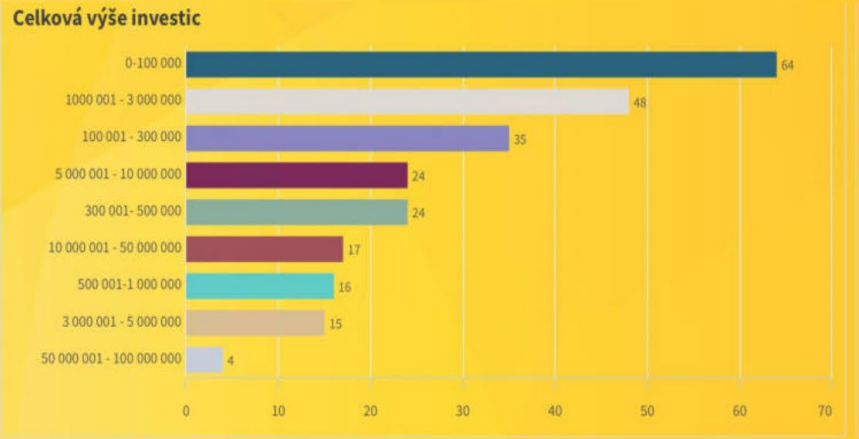

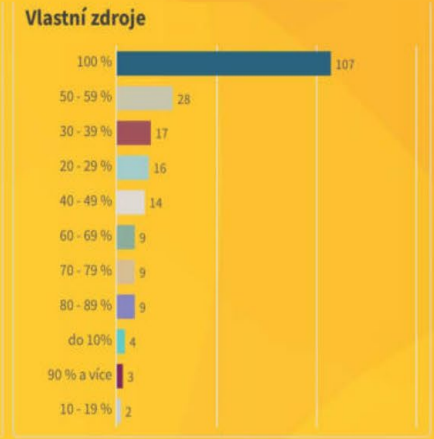

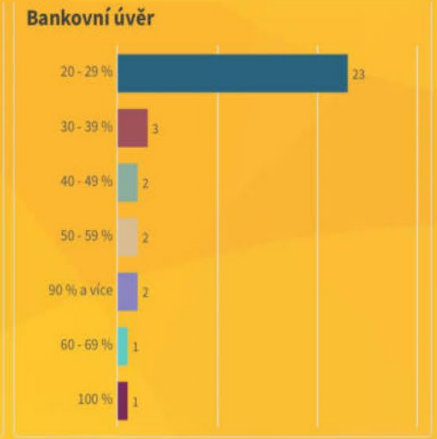

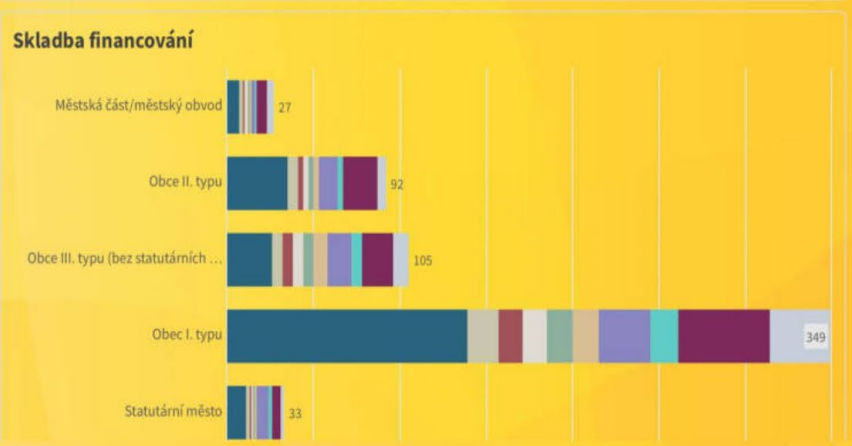

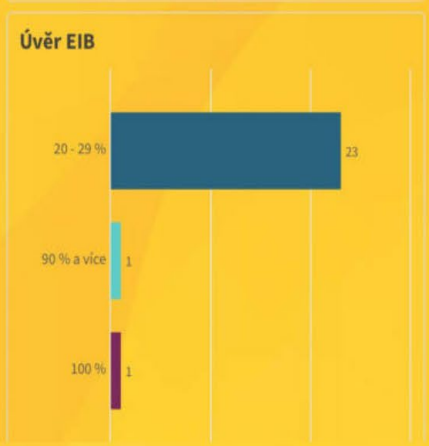

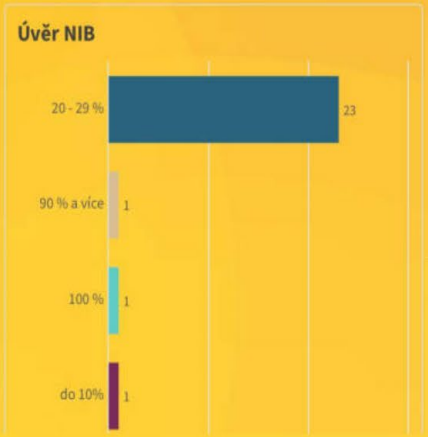

Podpora

SVAZ MĚST A OBCÍ ČESKÉ REPUBLIKY

Bude obec soběstačná

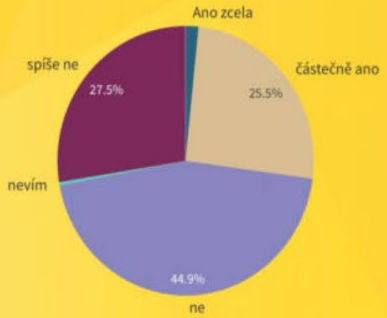

Je trh předvídatelný?

Jsou nároky na výpočet dopadů vysoké?

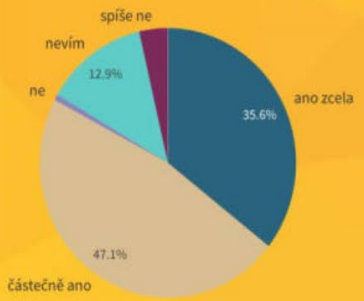

Uvítáte metodickou podporu státu?

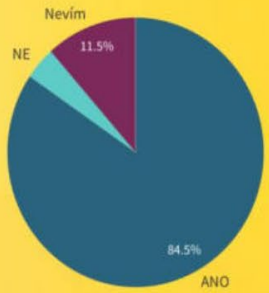

Uvítáte poradenství SMO?

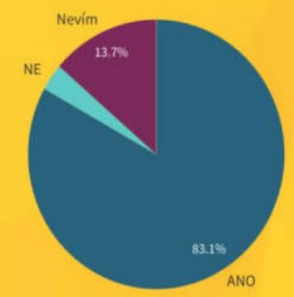

Řešíte požadavky občanů v energii?

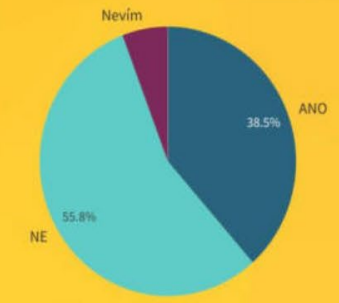

Zdroje **informací**

SVAZ MĚST A OBCÍ ČESKÉ REPUBLIKY

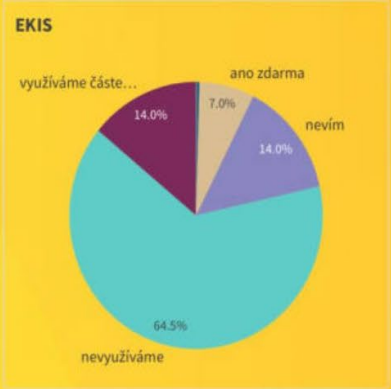

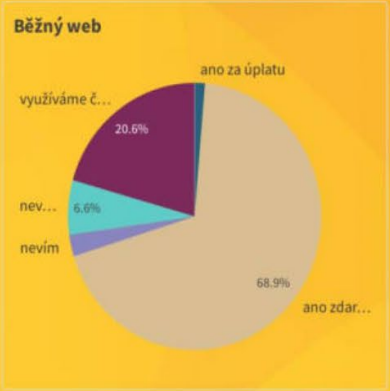

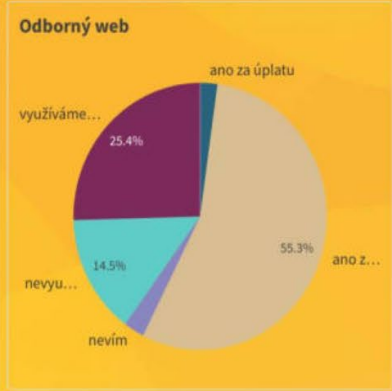

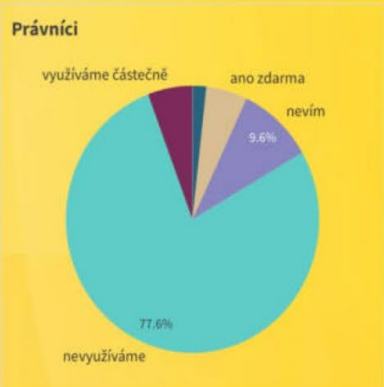

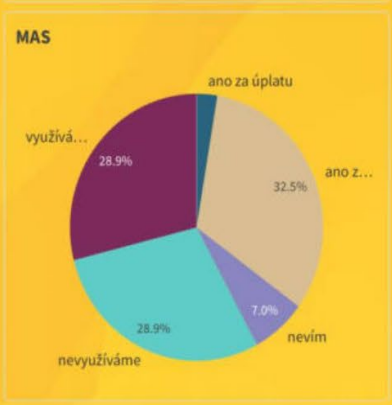

Komunitní energetika

Budoucnost

SVAZ MĚST A OBCÍ ČESKÉ REPUBLIKY

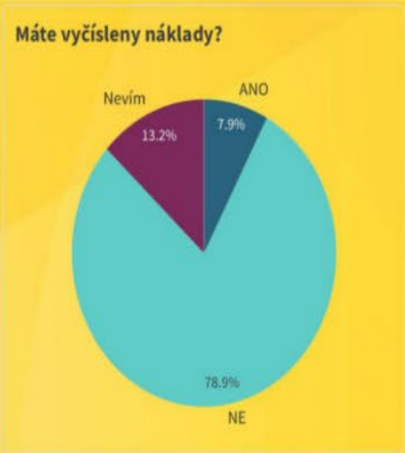

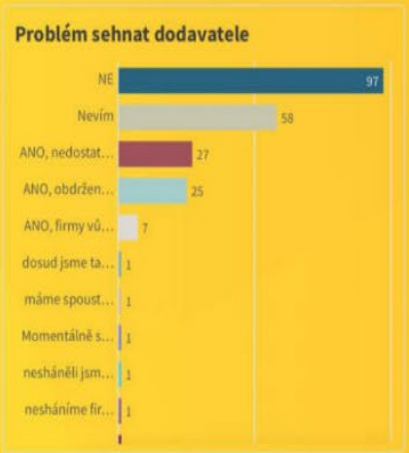

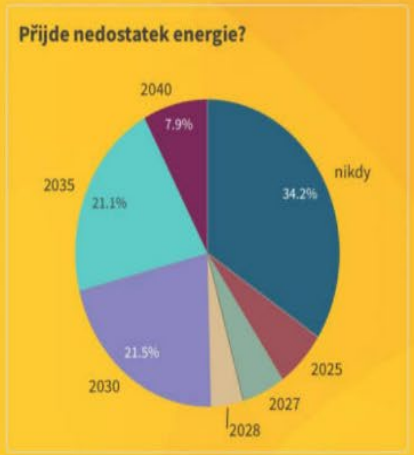

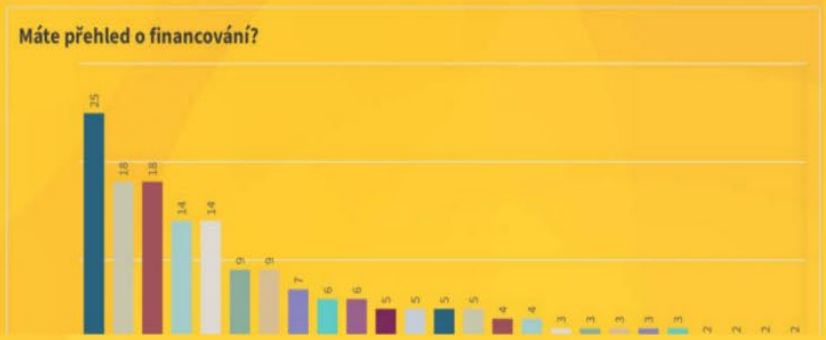

Začátek komunitní energetiky

SVAZ MĚST A OBCÍ ČESKÉ REPUBLIKY

Uvítáte pomoc se založením komunity?

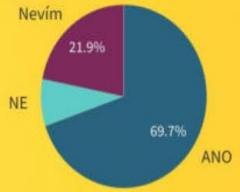

Uvítali byste spolupráci se zahraničními partnery?

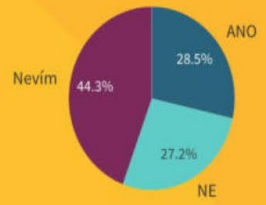

Jak diskutujete komunitu s občany??

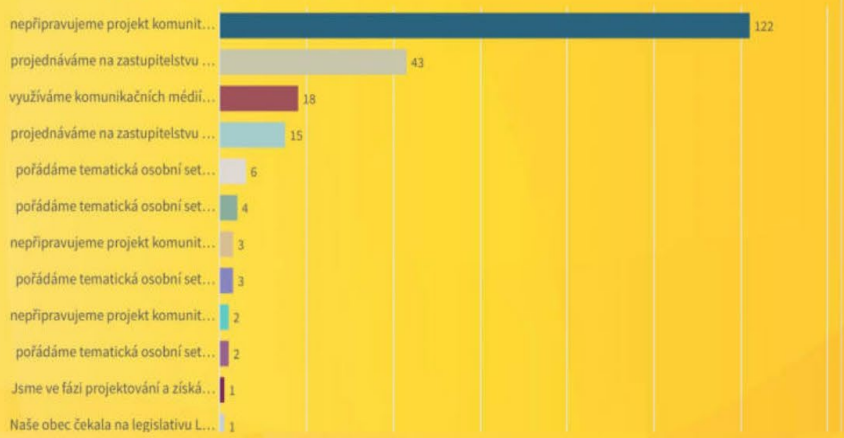

CHARACTERIZATION AND MECHANICAL PROPERTIES OF SINTERED CLAY MINERALS

SARA TOMINC,[1] VILMA DUCMAN,[1] JAKOB KÖNIG,[2] SREČO ŠKAPIN,[2] MATJAŽ SPREITZER[2]

[1] Slovenian National Building and Civil Engineering Institute, Ljubljana, Slovenia
sara.tominc@zag.si, vilma.ducman@zag.si
[2] Jožef Stefan Institute, Ljubljana, Slovenia
jakob.konig@ijs.si, sreco.skapin@ijs.si, matjaz.spreitzer@ijs.si

The need to reduce energy consumption and the carbon footprint generated by firing ceramics has stimulated research to develop sintering processes carried out at lower temperatures (ideally not above 300 °C) and high pressures (up to 600 MPa), the so-called cold sintering process (CSP) (Grasso et al., 2020, Maria et al., 2017). To evaluate the applicability of CSP to clays, we focused on two representative clay minerals, kaolinite and illite, and on the natural clay material obtained from a Slovenian brick manufacturer. The selected clay materials were characterized on the basis of mineralogical-chemical composition (XRD, XRF) and particle size distribution (SEM analysis, PSD, BET). The powders of clay minerals and natural clay material were first sintered in a heating microscope to determine the sintering conditions and then in a laboratory furnace at 1100 °C for 2 hours and additionally at 1300 °C for kaolinites. The effect of compression of the initial powders on their final properties was also investigated.

DOI
https://doi.org/10.18690/um.fkkt.1.2024.10

ISBN
978-961-286-829-1

Keywords:
conventional sintering,
cold sintering,
clay minerals,
characterization,
mechanical properties

University of Maribor Press

1 Introduction

The cold sintering process (CSP) is a process in which an inorganic powder is densified in the presence of a transient liquid phase as a phase fraction between 1-10% by volume (Maria et al., 2017). The main goal of this process is to reduce the energy consumption, processing time, cost and carbon footprint generated by conventional sintering processes (Galotta et al., 2021, Grasso et al., 2020). CSP was developed at Pennsylvania State University by Prof. Clive Randall and his research team (also known as the Randall`s method) and first applied for a patent in 2015 (Galotta et al., 2021, Grasso et al., 2020).

The low temperature (< 300 °) C and high pressure (up to 600 MPa) of CSP enable a considerable reduction in the energy and costs required for the consolidation of ceramic powder. The low temperature is not only advantageous from an energy point of view, but also because it drastically reduces the possibility of unwanted phase transformation during the sintering process (Galotta et al., 2021, Grasso et al., 2020, Guo et al., 2016). The synergy between the externally applied pressure, the limited temperature and the added liquid phase enables the successful production of dense materials in a short time with a large energy saving compared to other sintering techniques. Although cold sintering is already widely used, the densification mechanisms are not yet clearly understood (Galotta et al., 2021).

In order to compare the CSP approach with clays, a reference study was first carried out on the conventional sintering of kaolinite, illite and natural clay material so that the success of the samples produced with CSP could be evaluated later. Kaolinite and illite are common clay minerals found in nature and used for various applications (Gianni et al., 2020, Zhang et al., 2022). Kaolinite is of particular interest as it undergoes dehydroxylation to an amorphous state (forming metakaolin), which is stable over a wide temperature range (Michot et al., 2008). The natural clay material used for the production of clay bricks was taken from the production line just before the molding stage to ensure an industrially suitable clay sample.

2 Materials and methods

Representative clay mineral kaolinite-low defect (Kl) (Warren Country Georgia USA, KGa-1b, 125 grams/unit), kaolinite-high defect (Kh) (Warren Country Georgia USA, KGa-2, 125 grams/unit), illite (Il) (ilite-smectite mixed layer (70/30 ordered), Slovakia ISSCz-1, 50 grams/unit) and representative natural clay material (Cl) from the Slovenian brick manufacturer were selected.

For chemical analysis, samples were sieved below 125 μm and dried at 105 °C. The loss on ignition (LOI) was determined at 950 °C. A fused bead was then prepared with a mixture of sample and flux (50% lithium tetraborate/50% lithium metaborate) at a ratio of 1:10 (0.947 g: 9.47 g) and heated at 1100 °C. The chemical composition was determined using an ARL PERFORM'X wavelength dispersive X-ray fluorescence spectrometer (WDXRF; Thermo Fischer Scientific Inc., Ecublens, Switzerland) with a Rh-target X-ray tube and UniQuant 5 software (Thermo Fisher Scientific Inc., Waltham, MA, USA). Mineralogical analyses were performed using a Bruker AXS D4 Endeavor (Bruker, Bilelrica, MA) X-ray diffractometer equipped with Cu Kα radiation with a step size of 0.04° from angles 5-70°. The XRD patterns were solved using EVA software.

The specific surface area was determined by the Brunauer–Emmett–Teller (BET) method using a Micromeritics ASAP-2020 analyzer (Micromeritics, Norcross, GA, USA). The shape and size of the clay mineral particles were determined by field emission scanning electron microscopy (FE-SEM, Carl Zeiss ULTRA Plus, Oberkochen, Germany). The particle size distribution (PSD) of the samples was measured by laser diffraction granulometry using a Sync + FlowSync laser grain size analyzer (Microtrack MRB) in wet dispersion (dH_2O) measurement mode.

Prior to sintering, the densification characteristics of the samples were recorded using a heating microscope (Hesse Instruments, Osterode am Harz, Germany). The densification curves were recorded up to 1200 °C for Cl, 1280 °C for Il and 1400 °C for Kh and Kl with a heating rate of 10 °C/min. Kaolinite, illite and natural clay material were then ground to a grain size below 63 μm and pressed uniaxially at a pressure of 150 MPa to form 10 mm thick pellets with a diameter of 10 mm. The samples were sintered in a laboratory furnace PLF 160/9 (Protherm, Ankara, Turkey) at 1100 °C and 1300 °C for 2 hours with heating/cooling rates of 150 °C/h.

The open porosity of the sintered clay materials was determined by mercury intrusion porosimetry (MIP). Small representative pellets with a diameter and height of 10 mm were analysed immediately after sintering using the Micromeritics® Autopore IV 9500 instrument (Micromeritics, Norcross, GA, USA). The compressive strength was measured using a ToniTROL compressive strength testing machine (ToniTechnik, Berlin, Germany) at a force rate of 1.2 kN/s.

XRadia CT-400 tomography (XRadia, Concord, California, USA) was used to determine the pellets produced with CSP. The spatial resolution per pixel was 22.5 μm, equipped with a 0.39x optical objective. The voltage and current were set to 80kV and 87 μA respectively. 1600 projection images with an exposure time of 1 second per projection were captured through the charge-coupled device (CCD) camera. Avizo software (Thermo Fisher) was used for density-based segmentation and 3D reconstruction.

3 Results and Discussion

3.1 Characterization

XRF analysis of the clay minerals and natural clay material showed that they are mainly composed of Al_2O_3, SiO_2 and Fe_2O_3, with minor contents of CaO, MgO, K_2O and TiO_2. The average values of the primary oxides measured by XRF, LOI at 950 °C (Figure 1) and BET are given in Table 1.

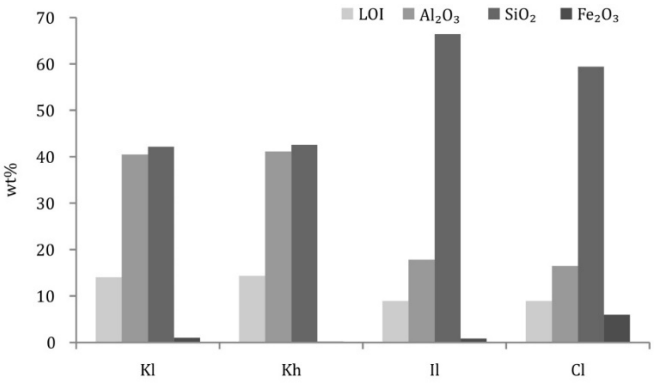

Figure 1: Comparison of LOI and primary oxides by XRF analysis
Source: own.

Table 1: BET, LOI at 950 °C and chemical composition of the clays in terms of primary oxides (wt%), measured using XRF.

Sample	BET (m^2/g)	LOI (950 °C)	Al_2O_3	SiO_2	Fe_2O_3	CaO	MgO	K_2O	TiO_2
Kl	19.85	14.05	40.48	42.15	0.98	0.02	0.06	0.04	1.92
Kh	11.15	14.31	41.13	42.58	0.19	0.03	/	0.01	1.44
Il	38.55	8.95	17.84	66.44	0.83	0.20	1.56	3.81	0.10
Cl	26.88	9.94	16.46	59.38	5.97	3.21	1.67	2.34	0.03

The phase composition of the samples was analyzed using powder XRD. Figure 2 shows that the kaolinites Kl and Kh have a XRD pattern typical of kaolinite. However, Kl has more pronounced reflections in the range 2 Θ =19-24° than Kh, indicating a higher degree of crystalline order. The Hinckley index for Kl is 0.98, while for Kl it is 0.41. XRD analysis of Il and Cl showed that the clay also contains quartz (Q), while Cl also contains zeolite (Z), illite (I), muscovite (M), kaolinite (K) and calcite (C).

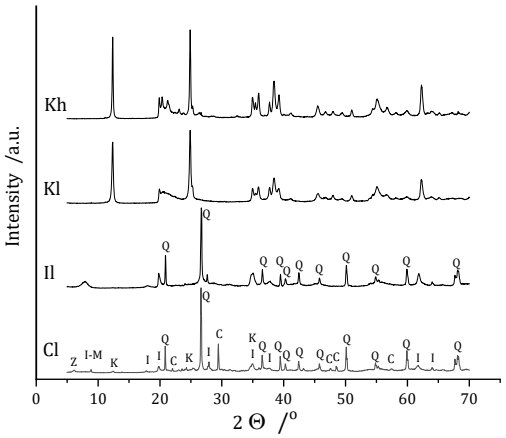

Figure 2: X-ray diffraction patterns of selected samples

Source: own.

In the next step, we examined the microstructural features of the samples using the SEM. We observed the presence of kaolinite "booklets", i.e. micron-sized morphological structures composed of numerous platelets typical of the mineral kaolinite (Balan et al., 2014), as well as fine kaolinite particles (Figure 3a, b), curled illite leaves (Figure 3c) and large particles of natural clay material (Figure 3d).

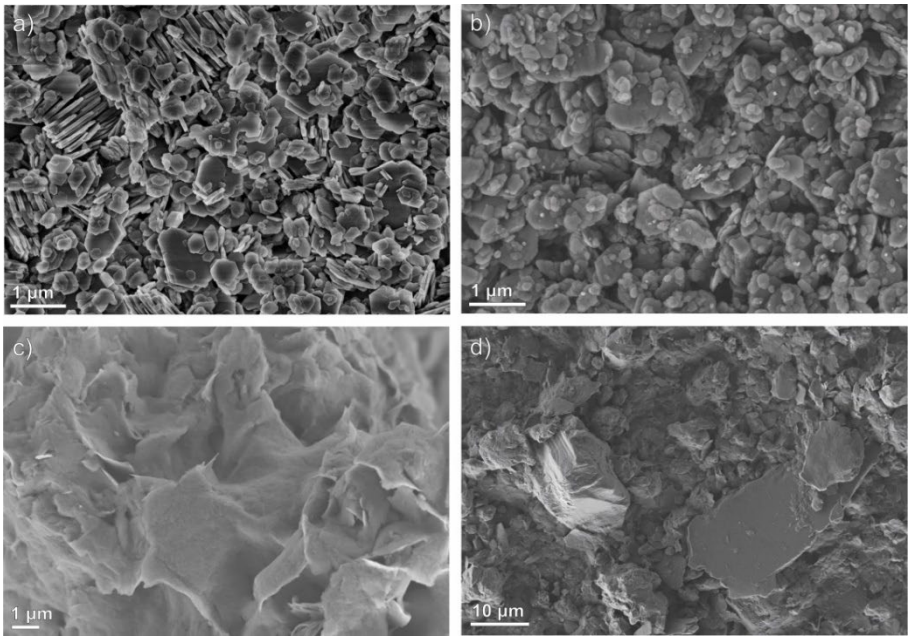

Figure 3: SEM images of a) Kl, b) Kh, c) Il and d) Cl
Source: own.

In addition, the measurement of PSD showed that the fineness of the clay minerals was greater in Kl and Kh than in Il and Cl (Figure 4).

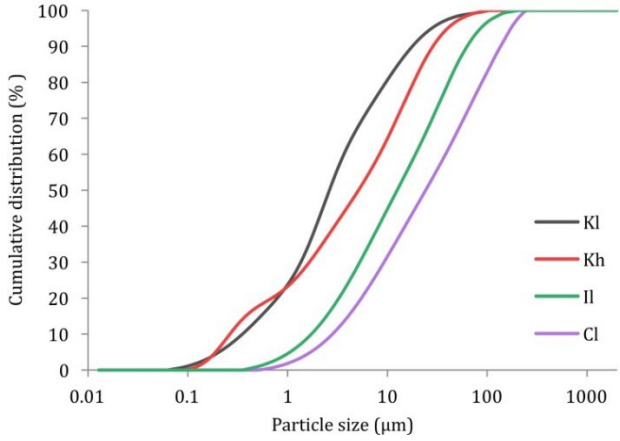

Figure 4: Cumulative distribution (% passing, based on volume) of selected samples
Source: own.

In order to determine the optimum sintering temperature, the densification behavior of our samples was measured using a heating- stage microscope. The relative shrinkage (%) of the samples as a function of temperature is shown in Figure 5. Cl reaches the peak of the densification rate at 1160 °C, Il at 1250 °C, while the onset of densification of Kl and Kh occurs at higher temperatures and the maximum rate is reached at 1320 °C for Kh and 1400 °C for Kl. In accordance with the densification behavior, the sintering temperature was set at 1100 °C for all samples and at 1300 °C for Kl and Kh.

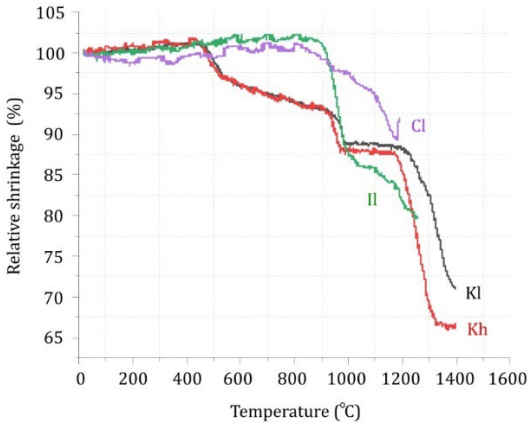

Figure 5: Relative shrinkage of the Kl, Kh, Il and Cl as a function of temperature
Source: own.

3.2 Mechanical properties

In the last step, we addressed the mechanical properties of the sintered clay minerals. At a sintering temperature of 1100 °C, the densification of Cl and Il is intensive, while a higher temperature was required for Kh and Kl. The compressive strength was measured on five pellets of each sample after sintering at 1100 °C and at 1300 °C for Kl and Kh. The results are shown in Table 2 and Figure 6.

The total porosity of the samples sintered at 1100 °C was between 11 and 40%. The porosity of the kaolinites was significantly lower with increasing sintering temperature up to 1300 °C. At 1300 °C, Kh and Kl showed significantly lower porosity (~4-5%), which is consistent with the higher mechanical strength and density of these samples.

Table 2: Geometric density, bulk density and porosity, measured with MIP, and compressive strength of selected samples, sintered at 1100 and 1300 °C.

Sample	Temp. (°C)	Bulk density (g/cm³)	Geom. density (g/cm³)	Porosity (%)	Compressive strength (MPa)
Kl	1100	1.66	1.45	39.5	5.6 ± 2.0
	1300	2.58	2.57	4.6	340.9 ± 36.8
Kh	1100	1.81	1.75	31.1	35.5 ± 8.0
	1300	2.68	2.68	4.3	74.0 ± 36.8
Il	1100	2.21	2.19	13.9	160.5 ± 6.2
Cl	1100	2.26	2.27	11.0	303.3 ± 31.9

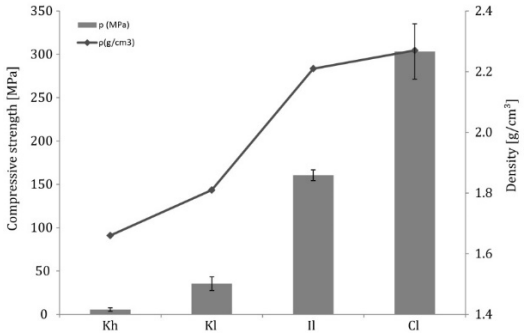

Figure 6: Compressive strengths and bulk densities of clay materials after conventional sintering at 1100 °C for 2 hours

Source: own.

The porosity values and the bulk density of the samples, measured with the MIP, are listed in Table 2. The pore size distribution ranged from 0.01 to 100 µm, as shown in Figure 7.

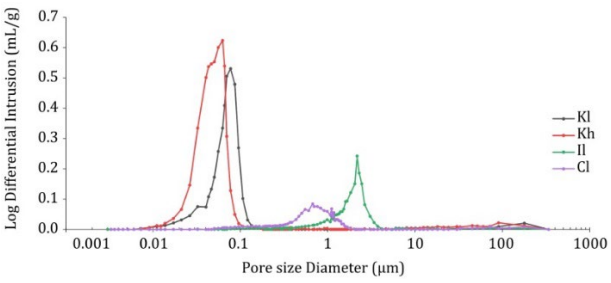

Figure 7: Differential mercury intrusion porosimetry of sintered clay minerals

Source: own.

In addition, a series of samples will be prepared using CSP under different conditions in the typical range of CSP. Preliminary results show that the Cl pellet was successfully prepared using CSP at a temperature of 240 C, a pressure of 500 MPa and a processing time of 3 minutes (Figure 8).

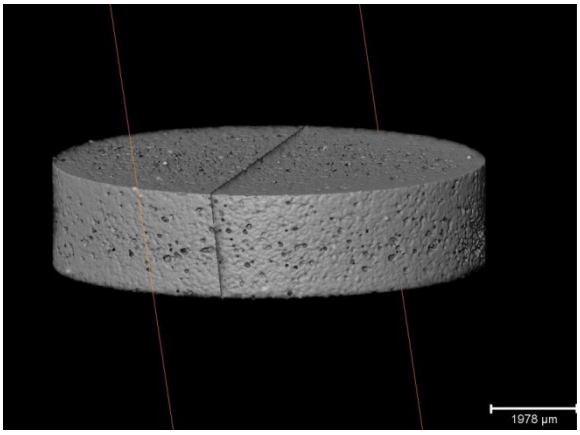

Figure 8: 3D view with cross-section of the Cl pellet prepared using CSP at a temperature of 240°C, a pressure of 500 MPa and a processing time of 3 minutes

Source: own.

4 Conclusions

In this study, selected clay minerals and the natural clay material were characterized and then conventionally sintered at 1100 and 1300 °C for 2 hours to compare their mechanical properties with those of clays prepared with CSP. After sintering at 1100 °C, the highest compressive strength was obtained with Cl, which also had the highest density (2.27 g/cm^3) and the lowest porosity (~11%). Illite with comparable density (2.21 g/cm^3) and porosity (~14 %) achieved a twice lower compressive strength (161 MPa), while kaolinite showed significantly lower compressive strengths with values from 6 to 36 MPa. The lower values for the compressive strength of kaolinite can be attributed to the fact that the optimum sintering temperature was not reached at this temperature. After sintering at 1300 °C, the low-defect kaolinite achieved the highest compressive strength (341 MPa) with low porosity (4.6 %) and high density (2.58 g/cm^3). In a preliminary analysis, we have also shown the promising results of CSP.

Acknowledgments

The authors thank Dr. Lea Žibret for the particle size distribution measurements, Dušica Tauzes for the XRF measurements and Dr. Lidija Korat and Roman Maček for microXCT images and 3D reconstructions (all from the Laboratory for Cements, Mortars and Ceramics, ZAG). This work was supported by the Slovenian Research Agency through the project No. J1-3026 »Applicability of the cold sintering process to clay minerals«.

References

Balan, E., Calas, G., Bish, D.L. (2014). Kaolin-Group Minerals: From Hydrogen-Bonded Layers to Environmental Recorders, Elements, 10(3), 183–188. doi: 10.2113/gselements.10.3.183

Galotta, A., Sglavo, V.M. (2021). The cold sintering process: A review on processing features, densification mechanisms and perspectives, Journal of the European Ceramic Society, 41(16), 1-17. doi: 10.1016/j.jeurceramsoc.2021.09.024.

Gianni, E., Avgoustakis, K., Papoulis, D. (2020). Kaolinite group minerals: Applications in cancer diagnosis and treatment, European Journal of Pharmaceutics and Biopharmaceutics,154, 359-376. doi: 10.1016/j.ejpb.2020.07.030.

Grasso, S., Biesuz, M., Zoli, L., Taveri, G., Duff, A.I., Ke, D., Jiang, A., Reece, M.J. (2020). A review of cold sintering processes, Advances in Applied Ceramics, 119(3), 115-143. doi: 10.1080/17436753.2019.1706825.

Guo, H., Baker, A., Guo, J., Randal, C.A. (2016). Cold Sintering Process: A Novel Technique for Low-Temperature Ceramic Processing of Ferroelectrics, Journal of the American Ceramic Society, 99(11), 3489-3507. doi: 10.1111/jace.14554.

Maria, J.P, Kang, X., Floyd, R.D., Dickley, E.C., Guo, H., Guo, J., Baker, A., Funihashi, S., Randall C.A. (2017). Cold sintering: Current status and prospects, Journal of Materials Research, 32(17), 3205–3218. doi:10.1557/jmr.2017.262.

Michot, A., Smith, D.S., Degot, S., Gault, C. (2008). Thermal conductivity and specific heat of kaolinite: Evolution with thermal treatment, Journal of the European Ceramic Society, 28(14), 2639-2644. doi: 10.1016/j.jeurceramsoc.2008.04.007.

Zhang, S., Sutejo, I.A., Kim, J., Choi, Y.-J., Park, H., Yun, H.-S. (2022). Three-dimensional complex construct fabrication of illite by digital light processing-based additive manufacturing technology, Journal of the American Ceramic Society, 105(6), 3827–3837. doi: 10.1111/jace.18369.

Magnetic Field as a Tool for Enhancing β -Lactamase Activity

Katja Vasić,[1] Mateja Primožič,[1] Mislav Trbušić,[2] Viktor Goričan,[2] Marko Jesenik,[2] Anton Hamler,[2] Željko Knez,[1] Yilmaz Yürekli,[3] Maja Leitgeb[1]

[1] University of Maribor, Faculty of Chemistry and Chemical Engineering, Maribor, Slovenia
katja.vasic@um.si, mateja.primozic@um.si, zeljko.knez@um.si, maja.leitgeb@um.si
[2] University of Maribor, Faculty of Electrical Engineering and Computer Science, Maribor Slovenia
mislav.trbusic@um.si, viktor.gorican@um.si, marko.jesenik@um.si, anton.hamler@um.si
[3] Manisa Celal Bayar University, Yunusemre, Manisa, Turkey
yilmaz.yurekli@cbu.edu.tr

DOI
https://doi.org/10.18690/um.fkkt.1.2024.11

ISBN
978-961-286-829-1

β-Lactam antibiotics have been extensively employed in bacterial treatment ever since penicillin's groundbreaking discovery. Despite the proliferation of antibiotics in the pharmaceutical sector today, bacteria often evolve defense mechanisms. Chief among these is the production of β-lactamase enzymes, which degrade β-lactam antibiotics, representing a prevalent form of antibiotic resistance. Additionally, these antibiotics exhibit limited biodegradability, with only 20% breaking down naturally. Hence, finding effective methods to mitigate the presence of β-lactam antibiotics is crucial in combating antibiotic pollution.

Keywords:
ß-lactamase, magnetic field, enzyme activity, hyperactivation, secondary structure

University of Maribor Press

1 Introduction

Numerous industries use enzymatic processes as opposed to conventional chemical catalysts, because they are specific in chemical transformations, rapid and save reagents and energy (Becker et al. 2021; Choi et al. 2015). Enzymes are used to catalyze highly selective and effective chemical reactions in terms of saving energy. Despite free enzymes possessing some drawbacks, regarding poor operational stability and low resistance to process conditions, they are highly applicable in industrial processes on a large scale. To overcome such limitations, the main research is focused on protein engineering solutions. However, the most common technique widely used for enhancing enzyme activity and operational stability is immobilization onto various supports. Immobilized enzymes are more resistant for harsh and unfavorable reactions conditions due to the interactions between enzymes and their carrier structure. Such conditions as pH, high temperature and ionic strength can destabilize and alter molecular structure and performance of a certain biocatalyst. Additionally, posing as an interesting alternative is the use of physical factors, such as magnetic field, which could stimulate and affect enzyme activity with its catalytic properties. With a potential effect of magnetic field on the enzyme reaction catalysis can change and alter enzyme's kinetics. When external magnetic field is applied in a reaction catalysis, it can affect molecular structure of the enzyme, thus modifying its catalytic properties. Furthermore, exposing enzymes to magnetic field can also affect kinetic energy of unpaired electrons, that are being released in catalysis, which can impact biological processes and chemical reactions (Emamdadi et al. 2021; Wasak et al. 2019; Magazù and Calabrò 2011; Liu et al. 2010).

ß-Lactamic antibiotics are one of the most common drugs used in treating bacterial infections, since their efficiency is in their ability to inhibit important reactions, which are involved in cell wall formation. Penicillin (PEN) is an antibacterial agent, that belongs to the β-lactam antibiotics, which have strong antimicrobial activities. Hence, it is extremely used in clinical practices worldwide. The use of PEN can also cause allergic reactions and lead to death, even more it can lead to development of PEN-resistant bacterial strains. Since PEN antibiotics are widely used in the dairy industry for treating various bacterial infections, the continual abuse of PEN has been reported and documented. PEN antibiotics show limited stability in hydrolysis and can therefore cause formation of different degradation products (Li et al. 2014). As such degradation products can cause allergic reactions as well, some enzymes

can catalyze and degrade antibiotics with the advantage of excellent catalytic features, high biocompatibility and eco-friendly performance (Yang et al. 2021). Such enzymes are ß-lactamases, which are produced by bacteria that play an important role in their resistance to ß-lactam antibiotics due to their hydrolyzation of ß-lactam ring (Wang et al. 2021).

With increasing antibiotic pollution and consequently avoiding bacteria developing defense mechanisms, the urge for developing methods for successful antibiotic removal are in place (Feng et al. 2021; Wang et al. 2021; Yang et al. 2021). Therefore, any new methods for enhancing enzymatic activity, operational stability and tolerance to pH and temperature of ß-lactamase are being investigated. In our study, we investigated the PEN degradation ability of free β-lactamase. As the PEN degradation study showed promising results, the enzyme was also treated with magnetic field to achieve improved catalytic activity and stability.

2 Materials and Methods

2.1 Enzyme preparation

Enzyme β-lactamase was studied in solution and powder form. When investigating the effect of magnetic field on its activity in powder form, 1 g of β-lactamase was used. When investigating the effect of magnetic field on its activity in a solution, 1 g of β-lactamase was dissolved in 1 mL of deionized water.

2.2 Degradation of PEN with β-lactamase

The degradation process was performed in batch reactor containing PEN solution with 0.1 mg/mL concentration. When β-lactamase was added, the reaction was performed at room temperature for 24 hours. The remaining PEN concentrations were monitored via HPLC (Agilent) with an Eclipse XDB C18 column, consisting of parameters: column temperature 30 °C, flow rate 1.0 mL/min, mobile phase consisting of methanol and phosphate, injection volume was 20 µL. The degradation was detected at a wavelength of 225 nm.

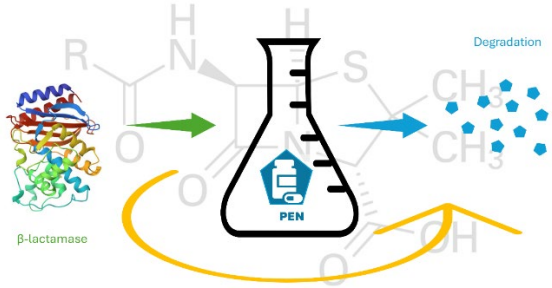

Figure 1: Schematic illustration of PEN degradation in a batch reactor using β-lactamase
Source: own.

2.3 Effect of magnetic field on β-lactamase activity

The effect of treatment with constant magnetic field with 50 mHz frequency was studied on the activity of enzyme β-lactamase. The activity of β-lactamase was investigated in forms of a solution and powder, while the effect of exposed time (2 and 20 min) was studied, as well.

2.4 β-lactamase activity assay

β-Lactamase activity was assessed spectrophotometrically. The reaction that contained 570 µL of β-lactamase enzyme in 50 mM HEPES buffer was initiated with 30 µL of substrate nitrocefin. β-Lactamase activity was monitored by measuring the increase in absorbance at 482 nm for 1 min at room temperature.

3 Results

3.1 Enzymatic degradation of PEN with β-lactamase

The catalytic performance of β-lactamase for degradation of PEN was determined in water solution at room temperature. As shown in **Figure 2**, PEN degradation with β-lactamase was determined using enzyme concentration of 0.01 mg/mL. PEN concentration was 0.1 mg/mL. From the results shown in **Figure 2** we can observe that the degradation of PEN with enzyme β-lactamase was slowly improving. After 10 min 10% of PEN degraded and after 6 and 24 hours 18% and 22% degradation of PEN was observed, respectively.

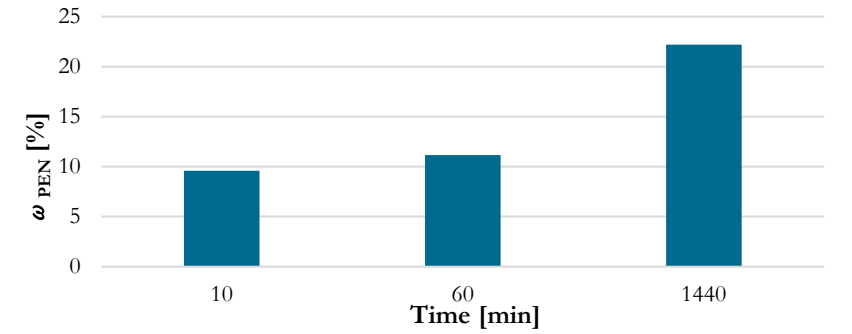

Figure 2: PEN degradation by enzyme β-lactamase after incubation for 24 hours.
Source: own.

3.2 Effect of magnetic field on β-lactamase activity

As the enzyme shows great promises in degradation studies, it will be immobilized onto nanostructured carriers and used for applications, where it can easily be separated with the use of an external magnetic field. Hence, we investigated the impact of a continuous magnetic field on the activity of β-lactamase in both solution and powdered forms. Our analysis revealed that magnetic treatment did not deactivate the enzyme; instead, it preserved its activity with only minimal loss compared to the non-exposed enzyme. The peak activity of the treated enzyme in powdered form under a constant magnetic field was attained after 20 minutes, resulting in a 96% retention rate, while for the enzyme in solution form, the highest activity was achieved after the same duration, with a retention rate of 99% (**Figure 3**).

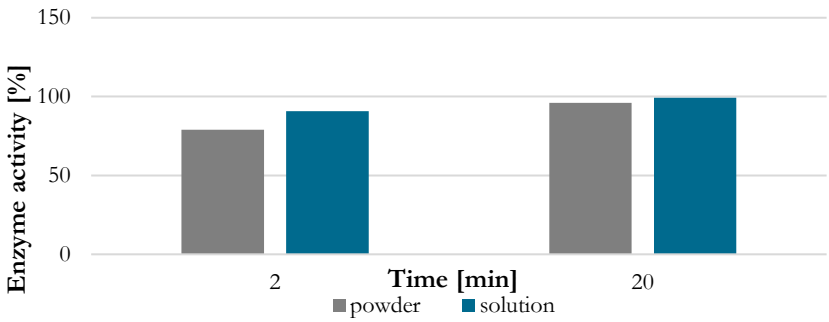

Figure 3: Enzyme activities of β-lactamase in powder form and in solution after constant magnetic field treatment.
Source: own.

Based on the findings, it can be concluded that the enzyme's activity is influenced by the frequency of exposure, potentially leading to alterations in its structure when subjected to a magnetic field. It is widely acknowledged that electromagnetic fields have the capacity to dynamically impact proteins and the ions within their composition (Wasak et al. 2019; Liu et al. 2010). The observed outcomes could stem from the distinctive structural characteristics of the enzyme and its catalytic function. The magnetic field's ability to modify physiochemical properties, such as conductivity or dielectric constant, may contribute to changes in the enzyme's structure. This factor is crucial for maintaining the stability of the enzyme's three-dimensional structure and its catalytic efficacy. The interaction between an external magnetic field and the enzyme's three-dimensional arrangement could trigger structural adjustments, thereby influencing the geometry of the enzyme's active sites.

4 Conclusions

Utilizing magnetic fields to regulate enzymatic activity appears to hold significant promise for enhancing the catalytic performance of enzymes. This approach not only boosts the enzymatic efficiency but also enhances the operational stability of the enzymes. Our research demonstrates that exposing β-lactamase to an external magnetic field can effectively modify its activity, maintaining its functionality without any adverse effects on enzyme performance.

Acknowledgments

This research was supported by the Slovenian Research Agency (ARRS) within the frame of program P2-0046 (Separation Processes and Production Design), program P2-0114 (Applied electromagnetics), project No. J2-3037 (Bionanotechnology as a tool for stabilization and applications of bioactive substances from natural sources), project No. L2-4430 (Production, Isolation and Formulation of Health Beneficial Substances from *Helichrysum italicum* for Applications in Cosmetic Industry), project BI-TR/22-24-04 "Enzyme immobilization techniques for efficient removal of antibiotics in wastewater" and project No. Z2-4431.

References

Becker, M., Lütz, S., and Rosenthal, K. (2021). Environmental Assessment of Enzyme Production and Purification. *Molecules* 26 (3):573. doi:10.3390/molecules26030573.

Choi, J.-M., Han, S.-S., and Kim, H.-S. (2015). Industrial applications of enzyme biocatalysis: Current status and future aspects. *Biotechnology Advances, Industrial Biotechnology: Tools and Applications* 33 (7):1443–1454. doi:10.1016/j.biotechadv.2015.02.014.

Emamdadi, N., Gholizadeh, M., and Housaindokht, M.R. (2021). Investigation of static magnetic field effect on horseradish peroxidase enzyme activity and stability in enzymatic oxidation

process. *International Journal of Biological Macromolecules* 170:189–195. doi:10.1016/j.ijbiomac.2020.12.034.

Feng, S., Hao Ngo, H., Guo, W., Woong Chang, S., Duc Nguyen, D., Cheng, D., Varjani, S., Lei, Z., and Liu, Y. (2021). Roles and applications of enzymes for resistant pollutants removal in wastewater treatment. *Bioresource Technology* 335:125278. doi:10.1016/j.biortech.2021.125278.

Li, L., Guo, C., Ai, L., Dou, C., Wang, G., and Sun, H. (2014). Research on degradation of penicillins in milk by β-lactamase using ultra-performance liquid chromatography coupled with time-of-flight mass spectrometry. *Journal of Dairy Science* 97 (7):4052–4061. doi:10.3168/jds.2014-7952.

Liu, Y., Jia, S., Ran, J., and Wu, S. (2010). Effects of static magnetic field on activity and stability of immobilized α-amylase in chitosan bead. *Catalysis Communications* 11 (5):364–367. doi:10.1016/j.catcom.2009.11.002.

Magazù, S. and Calabrò, E. (2011). Studying the Electromagnetic-Induced Changes of the Secondary Structure of Bovine Serum Albumin and the Bioprotective Effectiveness of Trehalose by Fourier Transform Infrared Spectroscopy. *J. Phys. Chem. B* 115 (21):6818–6826. doi:10.1021/jp110188k.

Wang, P., Shen, C., Cong, Q., Xu, K., and Lu, J. (2021). Enzyme-catalyzed biodegradation of penicillin fermentation residues by β-lactamase OtLac from Ochrobactrum tritici. *Microbial Cell Factories* 20 (1):117. doi:10.1186/s12934-021-01606-2.

Wasak, A., Drozd, R., Jankowiak, D., and Rakoczy, R. (2019). Rotating magnetic field as tool for enhancing enzymes properties - laccase case study. *Sci Rep* 9 (1):3707. doi:10.1038/s41598-019-39198-y.

Yang, L., Hu, D., Liu, H., Wang, X., Liu, Y., Xia, Q., Deng, S., Hao, Y., Jin, Y., and Xie, M. (2021). Biodegradation pathway of penicillins by β-lactamase encapsulated in metal-organic frameworks. *Journal of Hazardous Materials* 414:125549. doi:10.1016/j.jhazmat.2021.125549.

6TH INTERNATIONAL CONFERENCE ON TECHNOLOGIES & BUSINESS MODELS FOR CIRCULAR ECONOMY: CONFERENCE PROCEEDINGS

SANJA POTRČ, MILOŠ BOGATAJ, ZDRAVKO KRAVANJA, ZORKA NOVAK PINTARIČ (EDS.)

University of Maribor, Faculty of Chemistry and Chemical Engineering, Maribor, Slovenia
sanja.potrc@um.si, milos.bogataj@um.si, zdravko.kravanja@um.si, zorka.novak@um.si

The 6th International Conference on Technologies & Business Models for Circular Economy (TBMCE) was organized by the Faculty of Chemistry and Chemical Engineering of the University of Maribor in cooperation with Strategic Research and Innovation Partnership – Networks for the transition into circular economy (SRIP – Circular economy), managed by the Chamber of Commerce and Industry of the Štajerska. The conference was held in Portorož, Slovenia, at the Grand Hotel Bernardin from September 6th to September 8th, 2023. TBMCE 2023 was devoted to presentations of circular economy concepts, technologies and methodologies that contribute to the shift of business entities and society as a whole to a more responsible, circular management of resources. The conference program included a round table Standardization for circular economy – more secure and less complicated closing of material loops, 6 panel discussions, 1 plenary and 3 keynote lectures, oral and poster presentations. The event was under the patronage of Ministry of the Economy, Tourism and Sport and Ministry of Cohesion and Regional Development. The Netherlands joined us as a partner country.

DOI
https://doi.org/10.18690/um.fkkt.1.2024

ISBN
978-961-286-829-1

Keywords:
circular economy, sustainable development, processes and technologies, circular business models, research and development

University of Maribor Press

University of Maribor

Faculty of Chemistry and Chemical Engineering

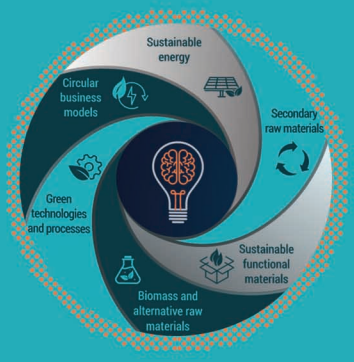

September 6 - 8

Grand Hotel Bernardin
Portorož, Slovenia